Author:
Waggett, Jonathan

Title:
The study of inorganic semiconductor quantum dots for solar cell applications

The Study of Inorganic Semiconductor Quantum Dots for Solar Cell Applications

Jonathan Waggett

A dissertation submitted to the University of Bristol in accordance with the requirements of the degree of Doctor of Philosophy in the chemistry department of the Faculty of Science.

Abstract

It has been determined that inorganic semiconductor nanoparticles could potentially be used as a replacement for organic dyes in solar cells. A number of different candidate sensitisers have been prepared and characterised.

Bi_2S_3 nanoparticles have been synthesised and deposited on tin oxide electrodes using an arrested precipitation technique, involving the reaction of bismuth iodide and H_2S in the presence of a stabiliser. The size of the particles was found to decrease with increasing concentration of stabiliser. However, the size of the particles was determined to have little effect on the band gap and low incident photon to photocurrent efficiencies were observed in the photocurrent spectra.

The heating of a heavy metal source with sulfur in oleylamine was used to prepare cadmium sulfide, ruthenium sulfide and copper sulfide. After dip coating the particles onto tin oxide electrodes, no photocurrent was observed.

CdSe particles on tin oxide electrodes have been prepared *in situ* using the reaction between cadmium perchlorate and bis(trimethylsilyl)selenide. These particles were found to decrease in size with increasing reaction time in solution, which is the opposite of the expected outcome of this type of reaction.

A 'hot injection' technique was utilised in order to prepare PbS nanoparticles. These particles where then heated in pyridine to produce pyridine coated particles. A decrease in size was observed upon pyridine exchange. PbS before and after pyridine exchange were drop coated on to TiO_2 coated

tin oxide electrodes and their photoelectrochemical properties were studied. It was found that the pyridine exchanged particles exhibited an enhanced photocurrent compared to the non-exchanged particles.

The above particles have been characterised using a variety of techniques, including UV-Vis absorption spectroscopy, transmission electron microscopy and photocurrent spectroscopy. The incident photon to current conversion efficiency has been discussed in terms of the factors that affect the electron transfer from the conduction band of the nanoparticles to the electrode. The suitability of these particles as sensitisers in solar cells has been determined.

Acknowledgements

First and foremost I would like to thank my supervisor, Dr Jason Riley, for all his patience, guidance and encouragement over the last three years.

Thanks must also go to Liz Tull for answering my many questions at the start of my Ph.D. and Dan Marsh for his help with SEM and sorting out computer software.

I would like to acknowledge Dr Sean Davis and Jon Jones for their assistance with TEM and Dr Keith Hallam for the XPS results.

Many thanks go to my brother, Christopher Waggett, for allowing me to live in his house while I was writing and my parents for helping me keep going whenever I got stuck.

Finally I would like to thank Dem, Rachel, Elodie, Min and the other members of the Electrochemistry Group for making my stay in Bristol an exciting and enjoyable time.

Author's Declaration

I declare that the work in this dissertation was carried out in accordance with the regulations of the University of Bristol. The work is original except where indicated by special reference in the text and no part of the dissertation has been submitted for any other degree.

Any views expressed in the dissertation are those of the author and in no way represent those of the University of Bristol.

The dissertation has not been presented to any other University for examination either in the United Kingdom or overseas.

Signed: ...J.P.Waggett.....Date: 17th June 2005

Contents

List of Figures

List of Tables

List of Chemicals

Chemical	Supplier	Quality
Titanium (IV)isopropoxide	Aldrich	99.999 %
Isopropanol	Rathburn	HPLC
Glacial acetic acid	Fisher Scientific	99 %
Carbowax	BDH	-
Na_2SO_3	Lancaster	98+ %
NaOH	Fisher Scientific	97 %
$NaHPO_4$	M & B	99 %
KOH	Fisher Scientific	85 %
Ethanol	Rathburn	HPLC
BiI_3	Aldrich	99 %
H_2S	Aldrich	99.5 %
3-mercaptopropionic acid	Aldrich	99+ %
Triphenylbismuth	Aldrich	99 %
Tetrahydrofuran (THF)	Rathburn	HPLC
Oleylamine	Acros	97 %
Sulfur powder	Aldrich	99.98 %
$CdNO_3 \cdot 4H_2O$	BDH	99 %
$RuCl_3$	Aldrich	-
CuI	Acros	98 %
Hexane	Rathburn	HPLC

List of Chemicals Continued

Chemical	Supplier	Quality
3-mercaptopropyltrimethyl silane	Lancaster	95 %
$Cd(ClO_4)_2$	Aldrich	99.999 %
bis(trimethylsilyl)selenide	Acros	98 %
Trioctyl phosphine	Fluka	90 %
PbO	Aldrich	99.999 %
1-octadecene	Aldrich	90 %
Oleic acid	Aldrich	90 %
Chloroform	Rathburn	HPLC
Methanol	Rathburn	HPLC
Pyridine	Aldrich	99.8 %

Chapter 1

Introduction

This thesis is concerned with the sensitisation of TiO_2 with semiconductor quantum dots and the use of the resultant sensitised TiO_2 in Grätzel Cells. Grätzel Cells and their mode of operation are discussed below. This is followed by an introduction to semiconductor quantum dots, with a discussion of how the particle size influences their properties. The advantages of using quantum dots over dyes, typically used as sensitisers in Grätzel Cells, are outlined. Factors that may influence the utilisation of quantum dots in Grätzel Cells are discussed, particularly electron transfer between the quantum dot and the TiO_2.

1.1 The Grätzel Cell

The first assembly and characterisation of a dye sensitised solar cell with a significant light to energy conversion efficiency was reported by Grätzel and O'Regan in 1991[1]. The device, shown schematically in Fig.1.1, consisted of

a tin oxide coated glass electrode (1), covered with a high surface area semiconductor film (2), typically TiO_2, which is sensitised with a monolayer of an organometallic dye (3), a redox electrolyte (4) and a tin oxide conducting glass counter electrode (5). This type of device is commonly referred to as a Grätzel Cell.

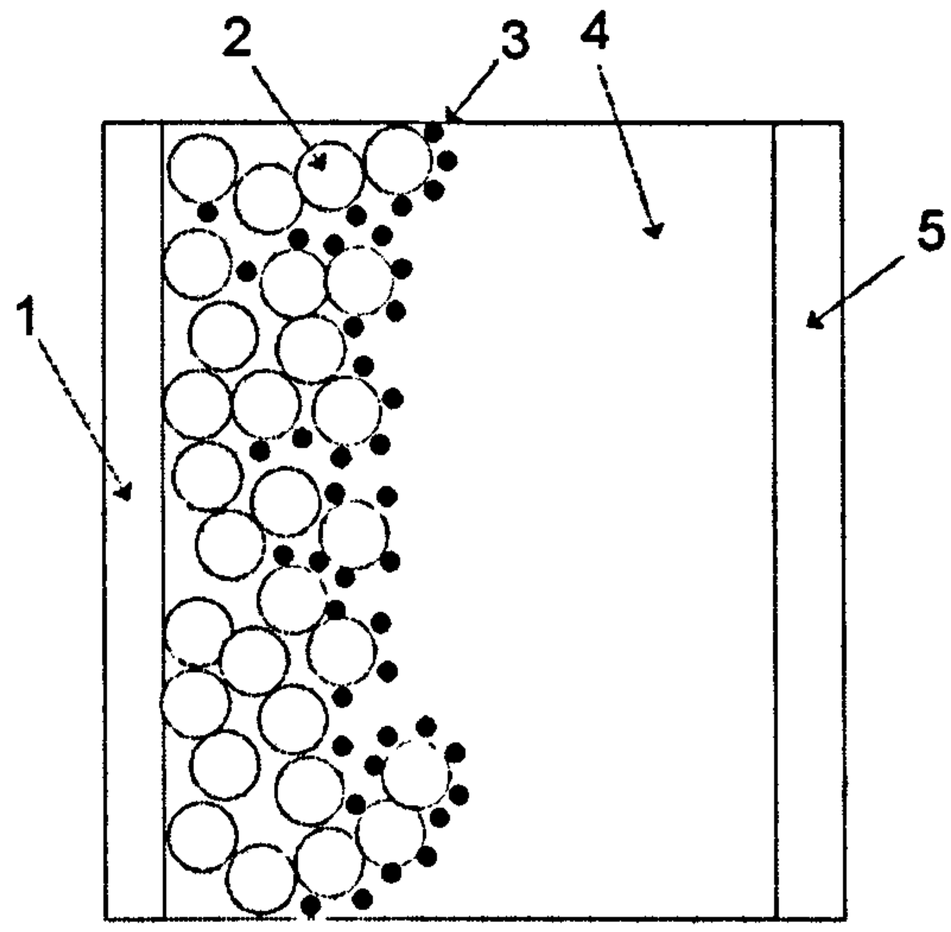

Figure 1.1: Schematic of the dye sensitised solar cell. (1) tin oxide electrode, (2) high surface area semiconductor film, (3) organometallic dye, (4) redox electrolyte and (5) counter electrode.

When the cell is exposed to light, a photon is absorbed by the dye, producing an electronically excited dye molecule, D^*, which then injects an electron from the dye into the conduction band of the TiO_2, resulting in the formation of an oxidised dye species, D^+. The electron is then passed round an external circuit and reduces a redox species, R, at the counter electrode to form the reduced species, R^-. The redox species then regenerates the dye via an electron transfer, thus completing the circuit and returning the dye

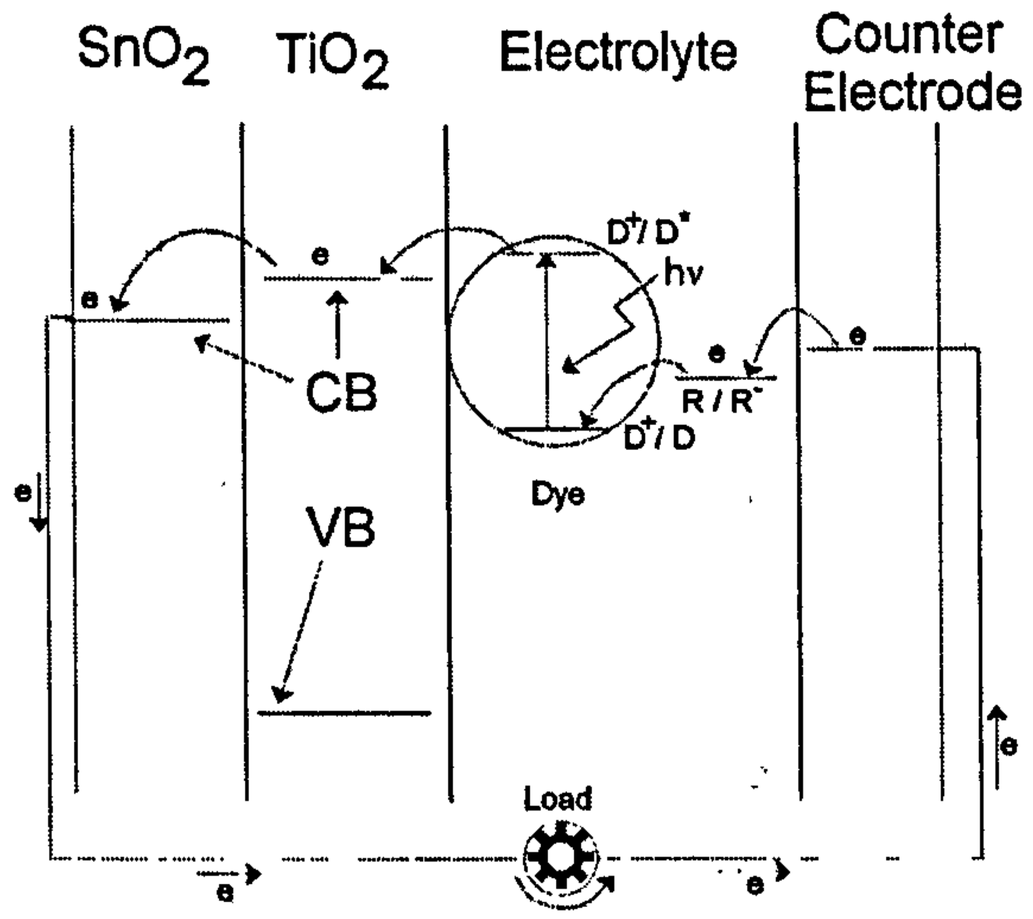

Figure 1.2: Schematic of the electron transfer processes involved in the Grätzel solar cell. Key:D=Dye, D*=electronically excited dye, D^+=oxidised dye, R/R^-=redox couple.

and the redox species to their original states. These processes are shown diagrammatically in Fig.1.2. Electrons can be lost by recombination in the dye and back electron transfer from the TiO_2 film to the dye or the electrolyte. These losses are minimised if the rate of electron transfer from the dye to the electrode is faster than the rate of the electron loss mechanisms. The role of the individual components are discussed in more detail below.

1.1.1 The electrodes

Light must be able to travel through the cell in order for it to be absorbed by the dye. This requires the use of at least one transparent electrode, which precludes the use of metal electrodes. A conducting tin oxide glass electrode is typically used as it is optically transparent to near infra-red and visible light.

1.1.2 The dye

The dye in the Grätzel Cell is used to absorb light. When an organometallic dye is exposed to light, the dye absorbs a photon to become electronically excited by the promotion of an electron from an occupied molecular orbital to an unoccupied molecular orbital as shown in Fig.1.3. As the solar spectrum

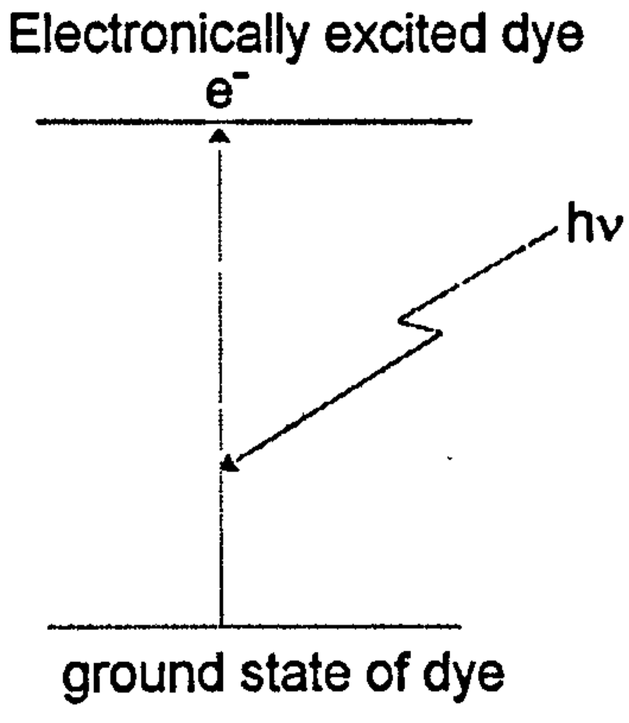

Figure 1.3: Excitation of an electron in the dye by the absorption of light.

covers the range of wavelengths between 300 nm and 885 nm, the dye used must have good absorption properties over this range. A number of dyes have been developed for use in solar cells. The absorption edge, the wavelength at which a material starts to absorb, for a few efficient dyes is shown in Table.1.1[2–8]. The black ruthenium dye and its homologues are currently used to produce the most efficient dye sensitised solar cells with an efficiency under sunlight (AM 1.5) of 10.4 %. These dyes are generally produced by complex multistage syntheses involving refluxing in a number of stages over

Name of dye	Absorption edge / nm
Ru(2,2'-bipyridyl-4,4'-dicarboxylic acid)$_2$(μ-(CN)Ru(CN)(2,2'-bipyridine)$_2$)$_2$	750
cis-Di(thiocyanato)-N,N-bis(2,2'-bipyridyl-4,4'-dicarboxylic acid)-ruthenium(II) dihydrate or N3 dye	780
tri(thiocyanato)-(2,2',2"-terpyridyl-4,4',4"-tricarboxylate) Ru(II) or black ruthenium dye	900
Coumarin based dye NKX-2677	800

Table 1.1: Absorption edge of example dyes.

several days, rotary evaporation, sublimation under vacuum, precipitation of precursors at low temperature and reaction under argon. The absorption edge of the dye is determined by its chemical structure. A new dye has to be synthesised in order to change the absorption properties of the system. The chemical structures of the examples tabulated are shown in Fig.1.4. These dyes degrade upon prolonged exposure to light reducing the efficiency of the cell over time. In the solar cell, the dye transfers an electron from its electronically excited state to the TiO_2 film forming an oxidised species of the dye and therefore is also required to be in contact with the electrolyte in order for the lost electron to be replaced.

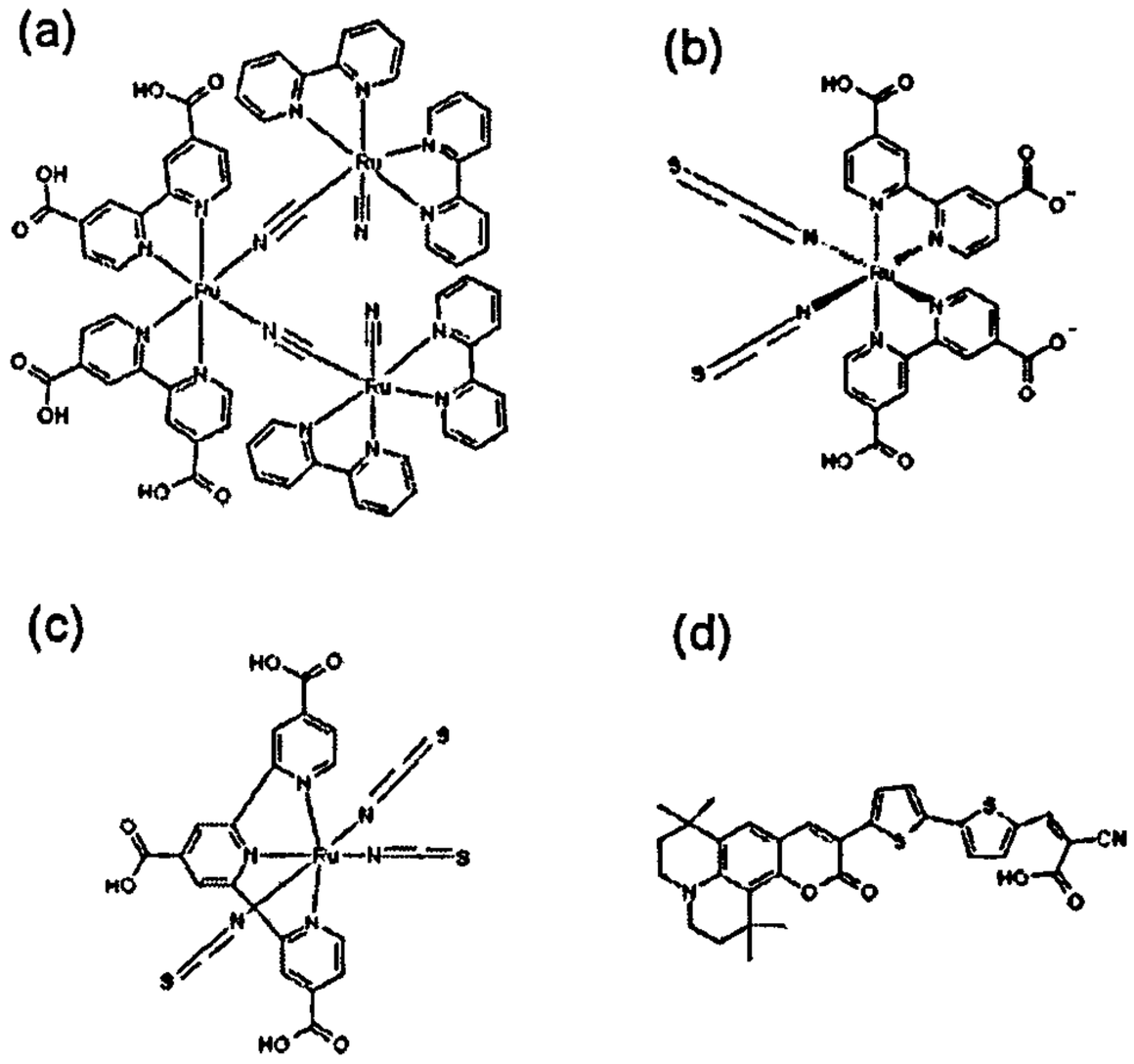

Figure 1.4: Chemical structures of (a) Ru(2,2'-bipyridyl-4,4'-dicarboxylic acid)$_2$(μ-(CN)Ru(CN)(2,2'-bipyridine)$_2$)$_2$, (b) the N3 dye, (c) black ruthenium dye and (d) Coumarin based dye NKX-2677.

1.1.3 The TiO_2 film

A TiO_2 film is employed in order to support the dye and transfer electrons from an electronically excited dye molecule to the conducting tin oxide electrode. In order to optimise the amount of light absorbed by the dye, a high surface area film of TiO_2 is used, as more dye molecules can be deposited on this film than on a flat surface, increasing the efficiency of light absorption as the surface area increases. A variety of TiO_2 substrates have been employed, however the method of choice involves the preparation of TiO_2 nanoparticles using a well established sol-gel method[8;9] that will be outlined in section 2.1, followed by spreading the nanoparticles over the SnO_2 electrode and calcin-

ing at 450 °C, in order to form the film. The calcination of the TiO_2 at 450 °C results in the formation of anatase TiO_2. The anatase form of TiO_2 is more attractive than the rutile form for use in solar cells, due to the higher activity of anatase TiO_2 compared to rutile TiO_2.

1.1.4 The electrolyte

The dye is regenerated by the donation of an electron from the electrolyte, which is in turn restored by an electron transfer from the counter electrode. The electrolyte generally consists of a redox couple, typically the iodide/triiodide couple, in an organic solvent. Equation 1.1 displays the oxidation of I^- to I_3^- which results in electron transfer to an oxidised dye molecule, thus restoring the original state of the dye.

$$3I^- \rightarrow I_3^- + 2e^- \text{(dye)} \tag{1.1}$$

I_3^- is then reduced at the counter electrode according to equation 1.2, returning the system to its original state.

$$I_3^- + 2e^- \text{(counter electrode)} \rightarrow 3I^- \tag{1.2}$$

As the electrolyte typically used in the Grätzel cell is a liquid, the cell is required to be well sealed, since any leak will result in the breakdown of the device. In order to eliminate cell failure from leaks, cells have been produced using solid state electrolytes, such as CuI, CuSCN and spirobiflourenes resulting in efficiencies of approximately 4 %[10;11]. Cells involving a solid state electrolyte are prepared by dropping a solution of the electrolyte onto the

dye coated TiO_2 film, allowing it to dry and repeating the previous two steps until sufficient electrolyte has been deposited.

1.2 Inorganic semiconductor nanoparticles

As the dyes currently studied photodegrade and the tuning of the absorption and electron transfer properties of the dye requires a new dye to be synthesised, involving a complex method of preparation for each dye to be tested, a suitable alternative to organometallic dyes is essential for progress in the optimisation of the Grätzel cell. Semiconductor particles of a size less than approximately 10 nm have properties that indicate that they are an alternative sensitiser to dyes in solar cells, as discussed below.

1.2.1 Electron transfer from semiconductor quantum dots

In order for a semiconductor nanoparticle sensitised solar cell to be viable, the particles need to be deposited on the TiO_2 film and exhibit the electron transfer process outlined in Fig.1.5. It should be noted that these processes are similar to the electron transfer processes involved in the Grätzel cell and the nanoparticle system is subsequently vulnerable to the loss mechanisms outlined for the Grätzel cell in section 1.1. Due to the small size of the particles, the composition of the surface and the presence of defects on the surface of the particles may produce surface states which may trap holes or electrons leading to further complications in the electron transfer processes.

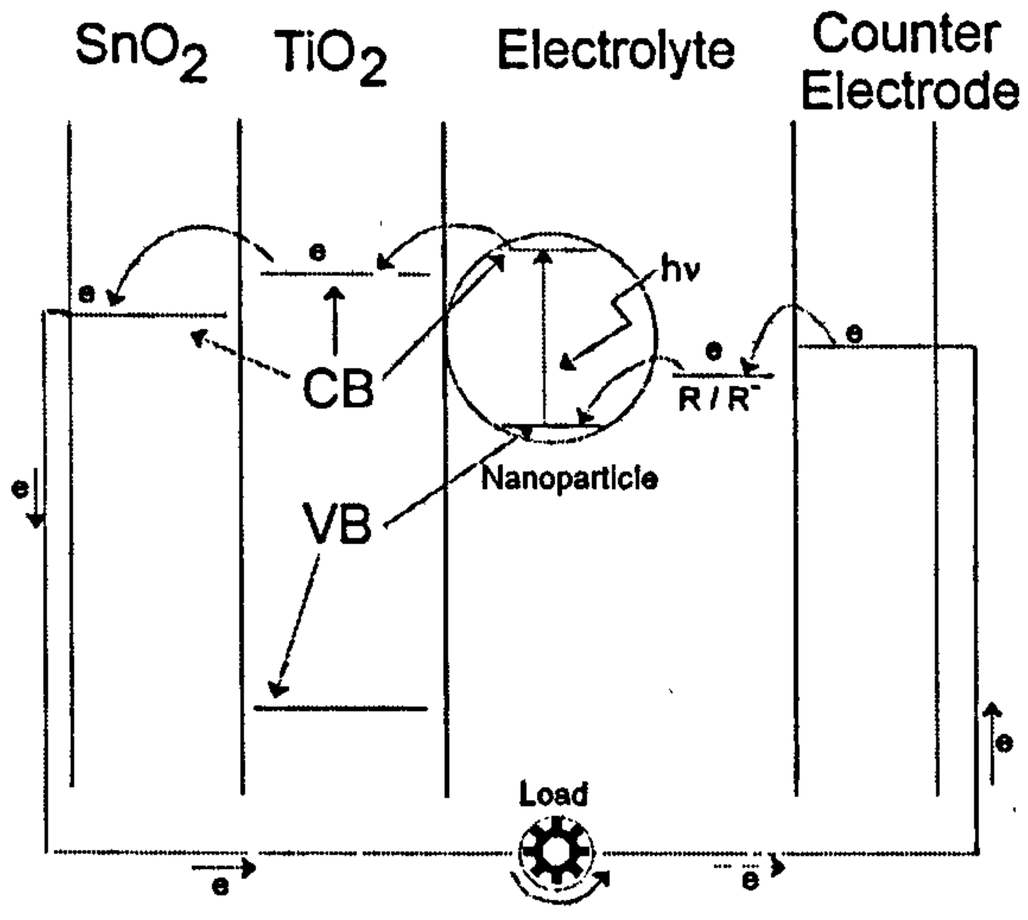

Figure 1.5: Schematic of the electron transfer processes involved in the semiconductor nanoparticle sensitised solar cell.

1.2.2 Why use inorganic semiconductors as a replacement for the organic dye

Inorganic semiconducting compounds of low solubility can generally be produced simply by the reaction of compounds containing the components of the semiconductor, for example the reaction of cadmium perchlorate with hydrogen sulfide to form cadmium sulfide. This method typically involves injecting H_2S gas into a solution of cadmium perchlorate and a stabiliser, for example hexanethiol, under an inert atmosphere at room temperature and stirring the solution for 1 hour. Using such methods, similar to the above example, it is clear that inorganic semiconductor nanoparticles are easier and quicker to prepare than organic dyes. The size of particles prepared by this method can be controlled via the concentration of the stabiliser. Fischer and

Henglein[12] proved this by showing that the size of CdS particles, prepared using hexanethiol as the stabiliser in the route detailed above, could be related to the concentration of hexanethiol according to the following equation:

$$\log d = 1.32 - 0.13 \log c \tag{1.3}$$

where d is the diameter of the particles in Angstroms and c is the hexanethiol concentration in mol dm^{-3}. Other stabilisers can be used to control the size of semiconductor nanoparticles, and equations relating the concentration of the stabiliser to the particle size can be formulated for each stabiliser. This was confirmed by Peter *et al.*[13], who prepared CdS particles by a similar method to Fischer and Henglein[12], using 3-mercaptopropionic acid (3-MPA) as the stabiliser instead of hexanethiol and found a similar expression for the particle size as a function of concentration as shown in the following equation:

$$\log R = -0.065 \log c + 0.236 \tag{1.4}$$

where R is the radius of the particles in nm and c is the concentration of 3-MPA in mol dm^{-3}. These changes in particle size are accompanied by a change in the band gap as measured from the optical absorption spectra by Fischer and Henglein[12] and Peter *et al.*[13]. Therefore the size of the semiconductor nanoparticles can be controlled and this size affects the wavelengths of light the particles can absorb. Inorganic semiconductors exhibit a broader absorption spectrum, ranging from the UV to the absorption edge of the material compared to the peaks observed in the spectra of organic dyes. This is illustrated in Fig.1.6, which displays the UV-vis spectra of coumarin based dye NKX-2677 and CdS. These compounds are also more photostable than

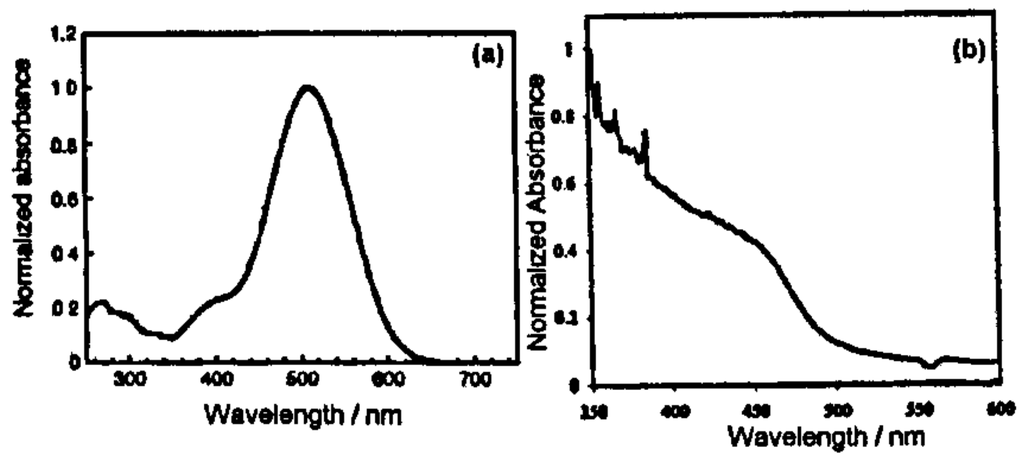

Figure 1.6: UV-Vis absorption spectra of a) coumarin based dye NKX-2677[6] and b) CdS[14].

the dyes used in the Grätzel cell. In order for an inorganic semiconductor to be suitable as replacement for the dye, it needs to be able to absorb light over the range of wavelengths observed in sunlight (300 to 885 nm), be easily deposited on the TiO_2 film and inject excited electrons, produced by the exposure of the system to light, into the TiO_2 film. As an inorganic semiconductor promotes an electron from its valence band (VB) to its conduction band (CB) when a photon with an energy equal to or greater than the band gap, E, is absorbed, as shown by Fig.1.7, a band gap of less than 1.4 eV is needed in order to absorb light from across the solar spectrum. Inorganic semiconductors experience a change in band gap when the size of the semiconductor particles is less than the Bohr radius of the exciton formed in the semiconductor when an electron and a hole approach each other in space. A material that experiences this effect is said to be quantum confined. The theory of why this happens and the relationship of the band gap to particle size has been discussed by Brus[15;16] and is summarised in section 1.2.3.

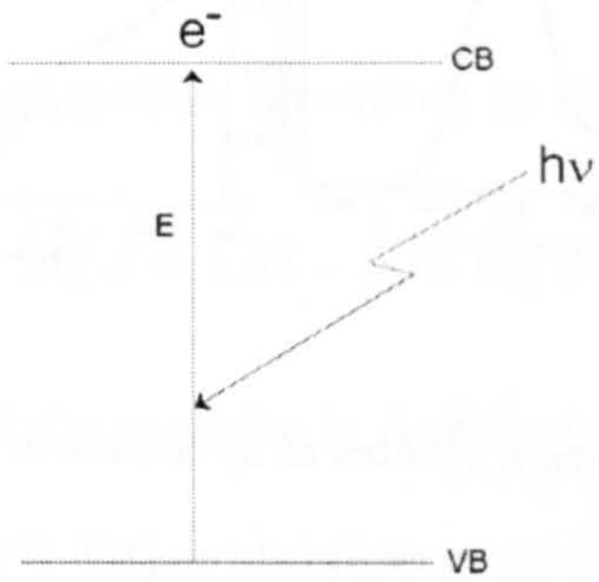

Figure 1.7: Absorption of a photon by a semiconductor.

1.2.3 Band Tuning

Semiconductor nanoparticles of less than approximately 10 nm show physical properties that differ from the bulk properties. The effect of particle size on the band gap was concluded by Brus *et al.*[15–17] to be due to the occurrence of an incomplete delocalisation of an electron. The theoretical evolution of the molecular orbitals (MO) as the size of a semiconductor compound is increased from a single molecule to a nanoparticle (typically a particle with a radius of less than 20 nm) and finally to a bulk crystalline compound is displayed in Fig.1.8. Brus[16] derived an expression that approximately relates the band gap of the quantum confined particles of a semiconductor to the size of the particles, given that the unit cell of the crystalline material is the same in a nanoparticle as in the bulk material. This assumption leads to the idea that the infinite crystal Bloch MOs, usually used to describe MOs in the

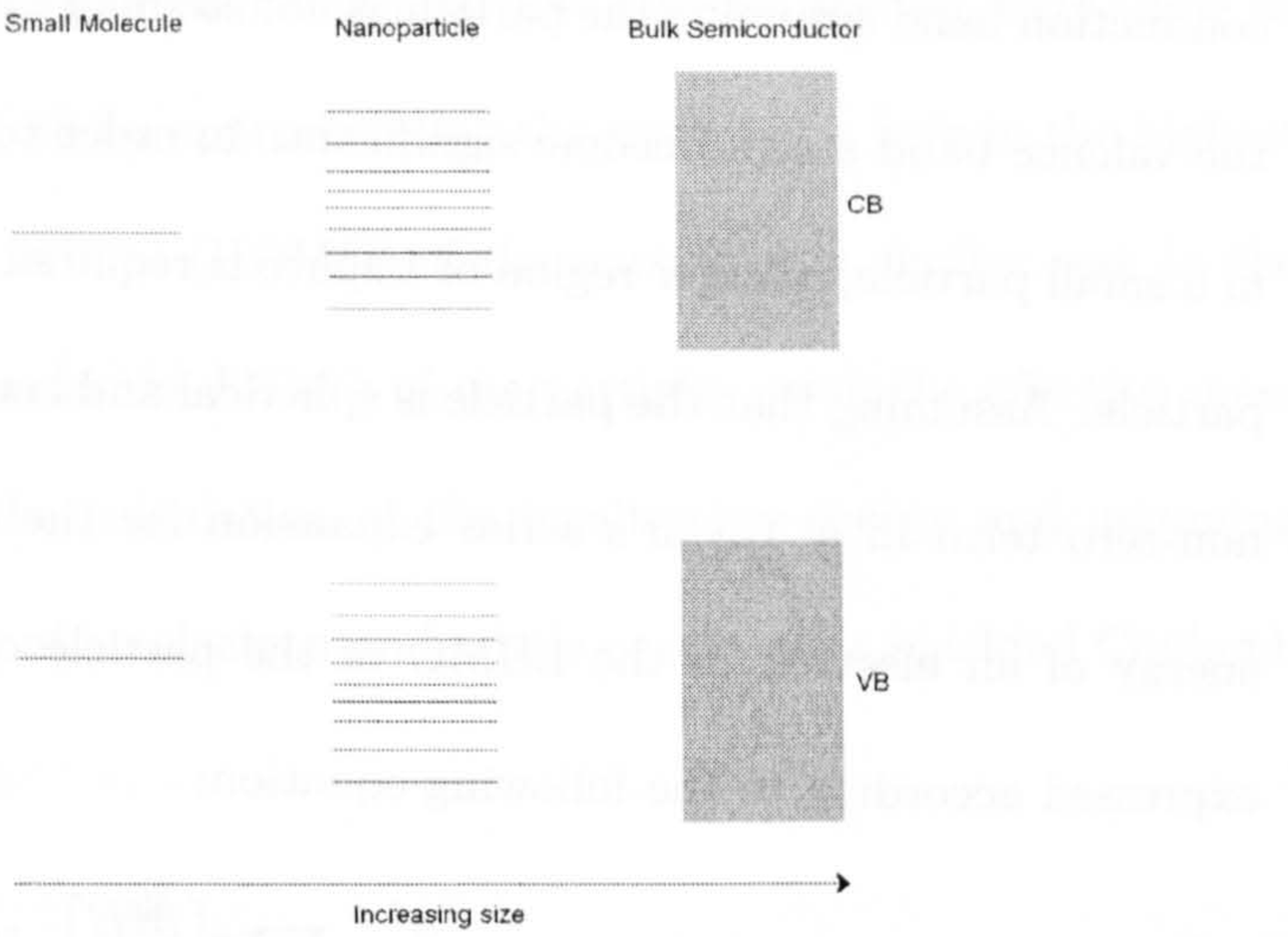

Figure 1.8: Schematic of molecular orbitals for a single molecule, a nanoparticle and the bulk semiconductor (CB=conduction band, VB=valence band).

bulk semiconductor crystals, are developed from the MOs of the nanoparticle as the size of particles increases. A Bloch MO can be represented as follows:

$$\Phi_{k,\mu}(r) = e^{ik\cdot r}\chi_{k,\mu}(r) \tag{1.5}$$

where $\chi_{k,\mu}$ includes the dimensions of the unit cell with a relatively weak dependence on k and $e^{ik\cdot r}$ represents an approximate plane wave with a wavelength $\lambda = 2\pi/k$ longer than a unit cell. This nature of Bloch MOs caused Brus[16;17] to approximate a nanoparticle MO, ψ_i(r), according to equation 1.6, which represents a MO localised in space as a Fourier transform wave packet of Bloch MOs, where μ is an index for summation over different bands,

$$\psi_i(\bar{r}) = \sum_{\mu}\int_k f_{i,\mu}\Phi_{k,\mu}(\bar{r})\,dk. \tag{1.6}$$

The lowest unoccupied molecular orbital (LUMO) that becomes the $k = 0$ state of the conduction band has contributions only from the k states of the

conduction band assuming the particle is not so small that contributions from the valence band states become significant. In order to localise the electron in a small particle, a larger region of k space is required compared to a larger particle. Assuming that the particle is spherical and keeping the lowest order non-zero term in a Taylor's series expansion for the energy, the expected energy of an electron in the LUMO of the particle can be approximately expressed according to the following equation:

$$E_i \approx E_c + \frac{\pi^2}{2R^2} \sum_{i=x,y,x} \left[\frac{\partial^2 E}{\partial k_i^2}\right] \tag{1.7}$$

where E_i is the expected energy of an electron, E_c is the energy of the conduction band and R is the radius of the particle. An effective mass tensor is defined by the second derivatives at every point on the conduction band, according to the following equation:

$$\bar{\bar{M}}_{ij} \equiv \frac{\hbar^2}{\left(\frac{\partial^2 E}{\partial k_i \partial k_j}\right)} \tag{1.8}$$

As this tensor is almost isotropic with an average diagonal element, m_e, when k approaches zero for the conduction band of most semiconductors, Brus[16] represented the energy of an extra electron in the conduction band as the sum of the energy of the conduction band, E_c, and effectively the particle in a box quantum energy of a pseudoelectron of effective mass, m_e, as shown in the following equation:

$$E_i \approx E_c + \frac{\pi^2 \hbar^2}{2m_e R^2} \tag{1.9}$$

This relationship is only valid as long as the unit cell of the material is the same in the nanoparticle as it is in the bulk semiconductor. Brus[15;16]

found the model Hamiltonian for the particle's lowest excited state to be as shown in equation 1.10 by approximating the energy of a hole in the highest occupied molecular orbital (HOMO) of the particle in a similar way to the energy of an electron in the LUMO of the particles using the effective mass of a hole, m_h, in the calculation of the localisation energy and assuming that the interaction of an electron and a hole occurs via a shielded Coulomb interaction.

$$\hat{H} = -\frac{\hbar^2}{2m_e}\nabla_e^2 - \frac{\hbar^2}{2m_h}\nabla_h^2 - \frac{e^2}{\epsilon|r_e - r_h|} + \text{polarisation terms} \qquad (1.10)$$

The first excited electronic state can therefore be approximated according to the following equation:

$$E^* = E_g + \frac{\hbar^2\pi^2}{2R^2}\left(\frac{1}{m_e} + \frac{1}{m_h}\right) - \frac{1.8e^2}{\epsilon R} \qquad (1.11)$$

where $\hbar = h/2\pi$, E^* is the band gap of the particles, E_g is the bulk band gap, R is the radius of the particles, m_e is the effective mass of the electron, m_h is the effective mass of the hole and $\epsilon = 4\pi\epsilon_r\epsilon_0$, where ϵ_r is the relative dielectric constant of the semiconductor and ϵ_0 is the dielectric constant of a vacuum. Rearranging the above equation yields an expression for the calculation of particle size from a measured band gap:

$$R = \frac{\left[\frac{1.8e^2}{4\pi\epsilon_r\epsilon_0} - \sqrt{\left(\frac{1.8e^2}{4\pi\epsilon_r\epsilon_0}\right)^2 - \frac{h^2(E_g - E^*)}{2}\left(\frac{1}{m_e} + \frac{1}{m_h}\right)}\right]}{2\left(E_g - E^*\right)}. \qquad (1.12)$$

Fig.1.9 displays a plot of the band gap of the particles E^* against the radius of the particle, R, using CdS as an example, which has values of m_e, m_h, ϵ_r and E_g are 0.19 m_o, 0.8 m_o, 5.7 and 2.42 eV respectively. This shows an increase

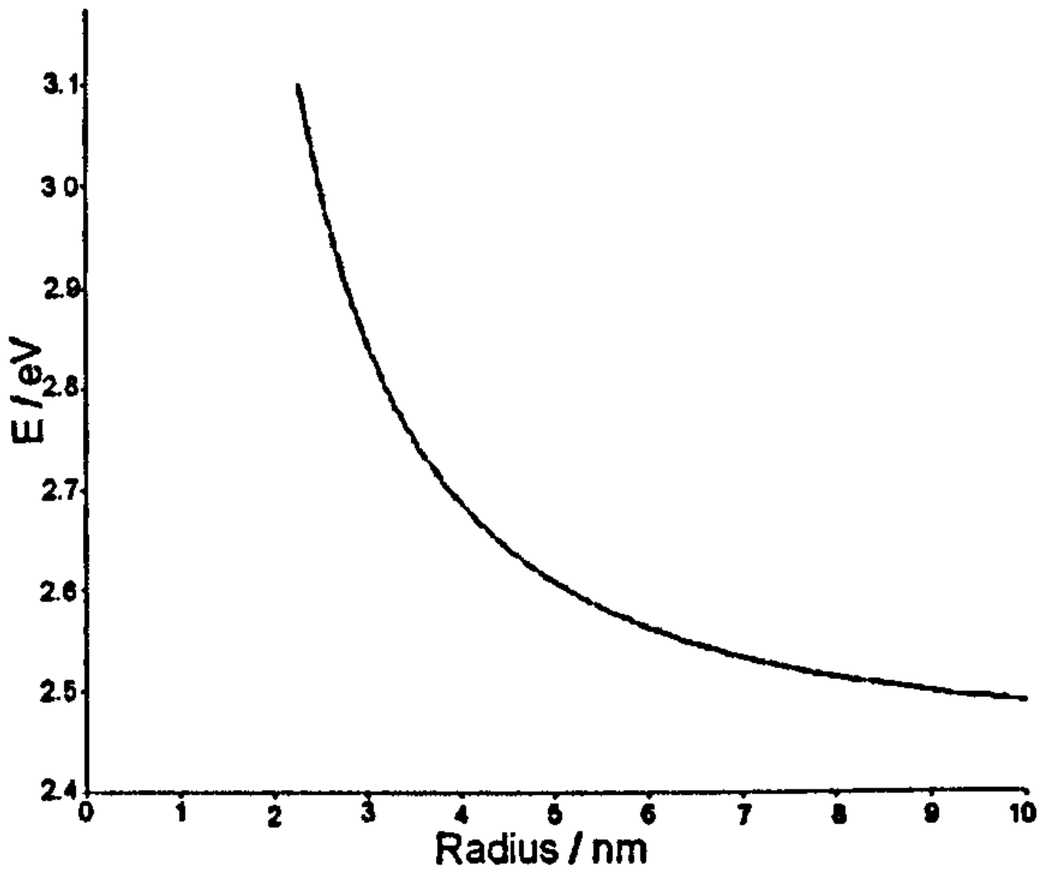

Figure 1.9: Calculated dependence of the band gap with radius of the particles for CdS particles.

in band gap with decreasing particle size and an asymptotic approach of E^* to the bulk band with increasing particle size. It is important to note that the estimation of particle size using this method is only valid if the particles are crystalline, spherical and have nearly identical unit cell structure and dimensions in both the particles and the bulk crystalline semiconductor material.

As the size of an inorganic semiconductor nanoparticle is decreased, the energy of the conduction band is increased and the energy of the valence band is decreased. This results in a larger band gap for smaller particles and the absorption of light at lower wavelengths than that observed for the bulk semiconductor. The transfer of electrons from the particle to TiO_2 will therefore become more favourable as the size of the particle is decreased, due to the associated increase in the conduction band energy. The properties described above lead to the conclusion that inorganic semiconductor particles,

with an appropriate band gap and a bulk conduction band position similar to that of TiO_2, are an interesting alternative to dyes for photosensitisation.

1.2.4 Proof of Concept

Cadmium sulfide was used by Peter *et al.*[13] in order to test the feasibility of using inorganic semiconductor nanoparticles as a replacement for organic dyes. This system was selected as quantum confinement effects in CdS and the preparation of CdS nanoparticles with control of the size of the particles have been widely studied. A number of different methods of preparing CdS particles have been reported.

Boxall and Albery[18] studied the photoelectrochemical properties of colloidal CdS using an optical rotating disc electrode. The particles were produced according to the method used by Duonghong *et al.*[19] as updated by Albery *et al.*[20], which involved the addition of H_2S gas to an aqueous solution of $Cd(NO_3)_2$ and sodium hexametaphosphate. The electrochemical system was formed by placing a transparent disc electrode, produced from a polished quartz rod with one end coated with Sb-doped SnO_2, into an aqueous solution of $KClO_4$, sodium hexametaphosphate and CdS particles. Light was focused on the uncoated end of the quartz rod of the electrode. The transfer of thermally generated electrons from the conduction band of the CdS particles to the electrode was observed in the dark. When exposed to light, an increase in current was observed at potentials greater than 0.6 V indicating that the particles deposit on the surface of the electrode at these potentials. The results obtained by Boxall and Albery[18] for the

steady state and transient photoelectrochemical behaviour of CdS particles indicate the presence of surface states in the CdS particles, corresponding to surface S^{2-} ions or sulfur vacancies. This was further confirmed by results obtained by Boxall[21] using a similar system with the addition of hole scavengers such as $Fe[(CN)_6]^{3-}$ and methyl viologen. An enhancement in the photocurrent was observed using $[Fe(CN)_6]^{3-}$ as the scavenger as opposed to methyl viologen due to the lower rate of electron transfer from the oxidised CdS particle to the reduced scavenger. Haram *et al.*[22] studied the electrochemical properties of CdS nanoparticles, prepared by the injection of H_2S in to an aqueous solution of $Cd(ClO_4)_2$ and 1-thioglycerol as discussed by Vossmeyer *et al.*[23] and size selected according to the method used by Murray *et al.*[24] to produce a range of monodisperse samples, using tetrahexylammonium perchlorate in N,N'-dimethylformamide as the electrolyte, Pt or Au as the working electrode, a Pt coil as the counter electrode and a silver wire as a quasi-reference electrode. The difference between the oxidation and reduction peaks in the cyclic voltammagrams exhibits a similar increase upon a decrease in particle size to the band gaps estimated from UV-Visible absorption spectra. Bakkers *et al.*[25] produced gold electrodes coated with CdS particles by first coating the electrodes with a self assembled monolayer of hexanedithiol by immersing a clean gold electrode in a solution of hexanedithiol and then immersing the electrode in a solution containing the CdS particles prepared according the method used by Fojtik *et al.*[26]. This synthetic technique involved the injection of H_2S gas into a basic aqueous solution of cadmium perchlorate and sodium hexametaphosphate under an

inert atmosphere in order to produce CdS particles with a coating of sodium hexametaphosphate. The particles were observed to cover the electrode surface by scanning tunnelling microscopy and had an average size of 5.0 nm (as measured by transmission electron microscopy). The electrochemical properties of the particles under chopped light were discussed. Photocurrent transients displaying a cathodic current when light was removed from the sample were observed between applied potentials of -0.9 and -0.6 V, indicating the occurrence of back electron transfer from the electrode to a CdS particle. Riley *et al.*[14;27–30] studied the photoelectrochemical properties of CdS particles deposited on tin oxide electrodes. The technique used by Fischer and Henglein[12] was adapted by Drouard *et al.*[14] in order to produce CdS particles deposited on tin oxide electrodes by placing tin oxide electrodes functionalised with 3-mercaptopropyltrimethoxysilane in a reaction vessel containing a solution of $Cd(ClO_4)_2$ and hexanethiol in tetrahydrofuran, followed by the addition of H_2S gas. Three different concentrations of hexanethiol were used to prepare CdS particles using this method. The sizes of the particles in solution were determined from the band gap found from the UV-Vis absorption spectra according to equation 1.12, resulting in particles with diameters of 2, 4 and 10 nm if hexanethiol concentrations of 0.4, 8.57×10^{-3} and 5.275×10^{-3} mol dm^{-3} respectively are used in the preparation of the particles. In order to confirm that the particles deposited on the tin oxide electrodes were the same size as the particles formed in solution, the photocurrent spectroscopy technique was employed as described in section 2.7.2. The photocurrent spectra displayed results consistent with the

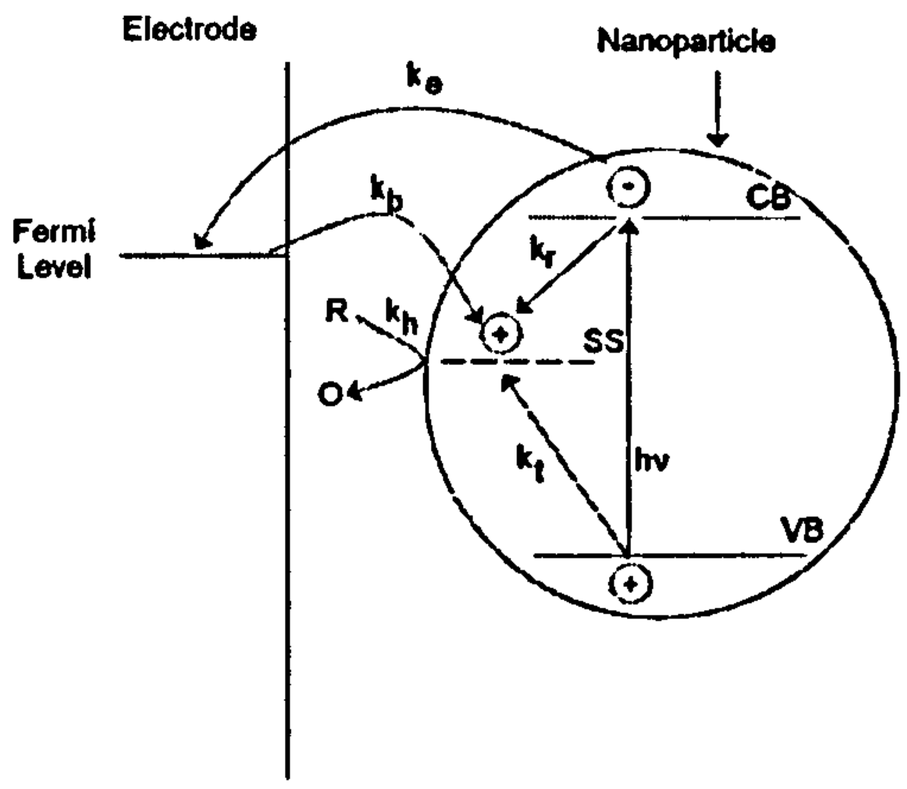

Figure 1.10: A schematic of the charge transfer processes occurring in CdS coated electrode in electrolyte system. SS = a surface state, R = reduced form of the electrolyte hole scavenger, O = oxidised form of the electrolyte hole scavenger, k_t, k_r, k_e, k_h and k_b = the rate constants of trapping a hole in the surface state, recombination, electron transfer, hole transfer and back electron transfer respectively[29].

UV-Vis absorption spectra indicating that the particles are the same size on the surface of the electrodes and in the as-prepared solution. This system was studied by intensity modulated photocurrent spectroscopy, potential modulated absorbance spectroscopy and photocurrent spectroscopy by Riley *et al.*[27–30]. Photocurrent transients display the presence of a surface state that traps holes at -0.4 V, as no back electron transfer occurred at higher potentials, while back electron transfer was observed at more negative potentials, suggesting that the charge transfer processes in a CdS coated tin oxide electrode occur as shown in Fig.1.10. The rate constants of the electron

Potential / V	k_r / (rad s^{-1})	k_h / (rad s^{-1})	k_b / (rad s^{-1})	$\alpha e I_{ac} k_e$ / (rad s^{-1})
0.0	35000	18	0	8.05×10^{-3}
-0.4	35000	18	1	4.20×10^{-3}
-0.6	35000	18	3	1.26×10^{-3}
-0.7	35000	18	6	7.35×10^{-4}

Table 1.2: Rate constants of charge transfer processes at a number of potentials [29].

transfer processes were determined over a range of potentials and are shown in Table 1.2. It was concluded that k_r and k_h are independent of applied potential, while k_b decreases as the potential is increased until the energy level of the hole trapping surface state is above the Fermi Level of the electrode preventing further back electron transfer and k_e increases as the potential is increased. Potential modulated absorption spectroscopy was used by Hickey *et al.*[28] in order to study the effect of excess charge carriers on a tin oxide electrode coated with CdS nanoparticles. A potential dependent bleaching was observed near the band edge from the potential modulated absorbance spectroscopy. It was also concluded by Hickey *et al.*[28] that the bleaching process occurs via a band filling model and that surface states are not involved as modulations in the absorbance of the particles were not observed unless the Fermi level of the tin oxide electrode was above the conduction band of the nanoparticles. This occurred if the applied potential was less than -1.0 V during the potential cycle. Riley and Tull[30] also concluded that the electron

transfer between the particles and the substrate occurs via diffusion as the charge on the particles is shielded from the tin oxide electrode by the diffuse double layer of the electrolyte.

Peter *et al.*[13] employed a method similar to that used by Fischer and Henglein[12] and Drouard *et al.*[14] in order to prepare a TiO_2 film coated with CdS nanoparticles on a tin oxide electrode as this method produces the CdS coated electrodes simply and the electron transfer properties of the particles on tin oxide have been thoroughly studied. This method placed a TiO_2 coated electrode, prepared as discussed in section 1.1.3 for a Grätzel cell, in a reactant solution containing cadmium perchlorate and 3-mercaptopropionic acid (3-MPA) in THF and under an inert atmosphere and then injected H_2S into the system. 3-MPA was used in place of hexanethiol as the carboxylic acid group on 3-MPA enables the particles to bind to the TiO_2 surface. Similar control of particle size to that found if hexane thiol is used as a stabiliser was displayed by 3-MPA. Band gaps of 2.53 and 2.88 eV were observed in the UV-Vis spectra of the particles in solution if 7.5×10^{-5} mol dm^{-3} or 0.38 mol dm^{-3} of 3-MPA, respectively, is used in the preparation. This displays quantum confinement and the size of the particles have been calculated to be 3.1 and 1.9 nm for concentrations of 3-MPA of 7.5×10^{-5} mol dm^{-3} or 0.38 mol dm^{-3} of 3-MPA, respectively, using equation 1.12 and these band gaps. An equation relating the size of the particles to the concentration of stabiliser was formulated and is shown in section 1.2.2. Photocurrent spectra of CdS particles on TiO_2 electrodes were recorded and a higher efficiency was observed for CdS coated TiO_2 electrode compared to flat tin oxide electrodes

coated with CdS, indicating that the particles were deposited inside the pores of the TiO_2 film. This result demonstrated that an inorganic semiconductor can sensitise a TiO_2 film in much the same way the dyes used in the Grätzel cell do. It is clear from the above results that a number of factors are involved in the efficiency of the photocurrent observed from electrodes coated with semiconductor nanoparticles. These factors include the coverage of the particles on the electrode, the relative energy of the conduction bands of the semiconductor particle and TiO_2 or tin oxide, the rates of all the electron transfer processes shown in Fig.1.10 and the length of organic chain in the stabiliser, which if too long could prevent the transfer of excited electrons from the semiconductor to TiO_2. The results in this thesis will be discussed according to these factors.

1.2.5 Possible Materials

Having shown that sensitisation of a TiO_2 electrode with an inorganic semiconductor is possible, it is now necessary to find a material that absorbs light across the solar spectrum when quantum confined, can be deposited on TiO_2 and then exhibits efficient photocurrent under solar illumination. Table. 1.3 displays materials that may be suitable for use as a sensitiser in a quantum dot sensitised solar cell. These materials have either a bulk band gap of less than 1.4 eV or are known to be highly efficient light absorbers.

Semiconductor	Band Gap / eV
CdSe	1.71
CdTe	1.52
Sb_2S_3	1.2
HgS	0.54
PbS	0.41
PbSe	0.27
Bi_2S_3	1.3
Bi_2Se_3	0.21
FeS_2	1.2
$FeSe_2$	0.6
Cr_2S_3	0.9
Cu_2S	1.21
Cu_2Se	1.23

Table 1.3: Suitable materials for the sensitisation of TiO_2.

1.2.6 Materials to be studied

This thesis will study the preparation of Bi_2S_3, CdSe, RuS_2, Cu_2S and PbS nanoparticles in solution and the deposition of these particles on tin oxide electrodes or electrodes coated with a TiO_2 film. Fig.1.11 displays the band edge positions of SnO_2, TiO_2, CdSe, RuS_2, Cu_2S, PbS and CdS. This shows that particles consisting from CdSe, RuS_2, Cu_2S or PbS should inject electrons into the conduction bands of TiO_2 or SnO_2, provided the particles

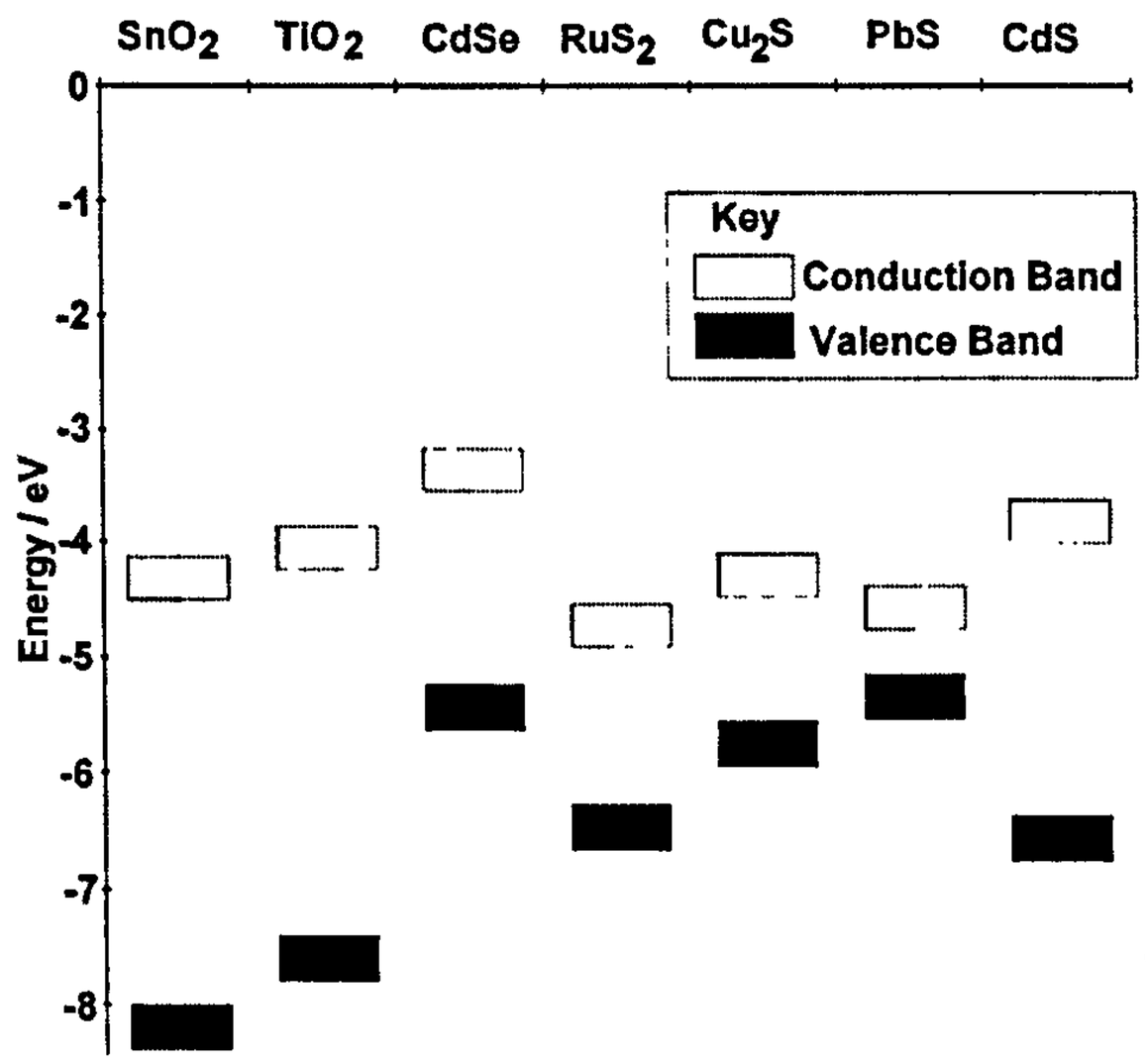

Figure 1.11: Positions of band edges for materials used in this study[31;32].

exhibit size quantisation effects. The properties of these particles in solution will be studied by UV-Visible Absorption spectroscopy, transmission electron microscopy (TEM) and electrophoresis. Cyclic voltammetry under chopped light and photocurrent spectroscopy are used to characterise the properties of the inorganic semiconductor particles on a tin oxide or TiO_2 coated tin oxide surface and to determine their suitability for use as a sensitiser in the Grätzel cell.

References

[1] O'Regan, B.; Grätzel, M. *Nature* **1991**, *353*, 737.

[2] Grätzel, M. *J. Photochem. Photobio. C-Photochem. Rev.* **2003**, *4*(2), 145–153.

[3] Nazeeruddin, M. K.; Pechy, P.; Renouard, T.; Zakeeruddin, S. M.; Humphry-Baker, R.; Comte, P.; Liska, P.; Cevey, L.; Costa, E.; Shklover, V.; Spiccia, L.; Deacon, G. B.; Bignozzi, C. A.; Grätzel, M. *J. Am. Chem. Soc.* **2001**, *123*(8), 1613–1624.

[4] Grunwald, R.; Tributsch, H. *J. Phys. Chem. B* **1997**, *101*(14), 2564–2575.

[5] Benko, G.; Kallioinen, J.; Korppi-Tommola, J. E. I.; Yartsev, A. P.; Sundstrom, V. *J. Am. Chem. Soc.* **2002**, *124*(3), 489–493.

[6] Hara, K.; Kurashige, M.; Dan-oh, Y.; Kasada, C.; Shinpo, A.; Suga, S.; Sayama, K.; Arakawa, H. *New Journal of Chemistry* **2003**, *27*(5), 783–785.

[7] Hara, K.; Sayama, K.; Ohga, Y.; Shinpo, A.; Suga, S.; Arakawa, H. *Chem. Commun.* **2001**, (6), 569–570.

[8] Nazeeruddin, M. K.; Kay, A.; Rodicio, I.; Humphry-Baker, R.; Muller, E.; Liska, P.; Vlachopoulos, V.; Grätzel, M. *J. Am. Chem. Soc.* **1993**, *115*, 6382.

[9] Peter, L. M.; Wijayantha, K. G. U. *Electrochim. Acta* **2000**, *45*(28), 4543–4551.

[10] Meng, Q. B.; Takahashi, K.; Zhang, X. T.; Sutanto, I.; Rao, T. N.; Sato, O.; Fujishima, A.; Watanabe, H.; Nakamori, T.; Uragami, M. *Langmuir* **2003**, *19*(9), 3572–3574.

[11] Kruger, J.; Plass, R.; Grätzel, M.; Matthieu, H. J. *Appl. Phys. Lett.* **2002**, *81*(2), 367–369.

[12] Fischer, C. H.; Henglein, A. *J. Phys. Chem.* **1989**, *93*, 5578.

[13] Peter, L. M.; Riley, D. J.; Tull, E. T.; Wijayantha, K. G. U. *Chem. Commun.* **2002**, *10*, 1030–1031.

[14] Drouard, S.; Hickey, S. G.; Riley, D. J. *Chem. Commun.* **1999**, (1), 67–68.

[15] Brus, L. E. *J. Chem. Phys.* **1984**, *80*(9), 4403–4409.

[16] Brus, L. *J. Phys. Chem.* **1986**, *90*, 2555.

[17] Rossetti, R.; Hull, R.; Gibson, J. M.; Brus, L. E. *J. Chem. Phys.* **1985**, *83*, 1406.

[18] Boxall, C.; Albery, W. J. *Phys. Chem. Chem. Phys.* **2000**, *2*, 3641.

[19] Duonghong, D.; Ramsden, J.; Grätzel, M. *J. Am. Chem. Soc.* **1982**, *104*, 2977.

[20] Albery, W.; Bartlett, P.; Porter, J. *J. Electrochem. Soc.* **1984**, *131*, 2896.

[21] Boxall, C. *J. Photochem. Photobio. A:Chemistry* **2002**, *148*, 375.

[22] Haram, S. K.; Quinn, B. M.; Bard, A. J. *J. Am. Chem. Soc.* **2001**, *123*(36), 8860–8861.

[23] Vossmeyer, T.; Katsikas, L.; Giersig, M.; Popovic, I. G.; Diesner, K.; Chemseddine, A.; Eychmuller, A.; Weller, H. *J. Phys. Chem.* **1994**, *98*, 7665.

[24] Murray, C. B.; Norris, D. J.; Bawendi, M. G. *J. Am. Chem. Soc.* **1993**, *115*, 8706.

[25] Bakkers, E. P. A. M.; Reitsma, E.; Kelly, J. J.; Vanmaekelbergh, D. *J. Phys. Chem. B* **1999**, *103*, 2781.

[26] Fojtik, A.; Weller, H.; Koch, U.; Henglein, A. *Ber. Bunsenges. Phys. Chem.* **1984**, *88*, 969.

[27] Hickey, S. G.; Riley, D. J. *J. Phys. Chem. B* **1999**, *103*(22), 4599–4602.

[28] Hickey, S. G.; Riley, D. J.; Tull, E. J. *J. Phys. Chem. B* **2000**, *104*(32), 7623–7626.

[29] Hickey, S. G.; Riley, D. J. *Electrochim. Acta* **2000**, *45*(20), 3277–3282.

[30] Riley, D. J.; Tull, E. J. *J. Electroanal. Chem.* **2001**, *504*(1), 45–51.

[31] Xu, Y.; Schoonen, M. *American Mineralogist* **2000**, *85*, 545.

[32] Wang, L.; Zunger, A. *Phys. Rev. B* **1996**, *53*, 9579.

Chapter 2

Experimental

The techniques described in this chapter are common to several chapters in this thesis.

2.1 Preparation of TiO_2 Film

A solution containing 3.7 ml of titanium (IV) isopropoxide and 1 ml isopropanol was stirred for 5 minutes in a measuring cylinder. A 100 ml conical flask containing 8 ml glacial acetic acid and 25 ml deionised water was placed in an ice bath and stirred vigorously while the titanium (IV) isopropoxide and isopropanol mixture was added dropwise over a period of 30 minutes. The contents of the flask were then heated to 80 °C for 8 hours. The resulting sol-gel was then placed in an autoclave and heated to 230 °C for 12 hours. After cooling, the solution of TiO_2 particles was placed in a 50 ml round bottomed flask and sonicated for 5 minutes. The solution was concentrated to a third of its original volume by rotary evaporation and 0.4 g carbowax

was stirred into the solution overnight to form the final viscous TiO_2 colloid solution. The TiO_2 colloid was spread on a precleaned SnO_2 glass electrode in a layer and then annealed at 450 °C for 30 minutes in order to form the TiO_2 film.

2.2 UV-Vis Spectroscopy

A Perkin Elmer Lambda Bio 10 UV-Visible spectrometer was used to measure the UV-Vis absorption spectra. A schematic of this machine is shown in Fig.2.1. The spectrometer passes light from either a deuterium or halo-

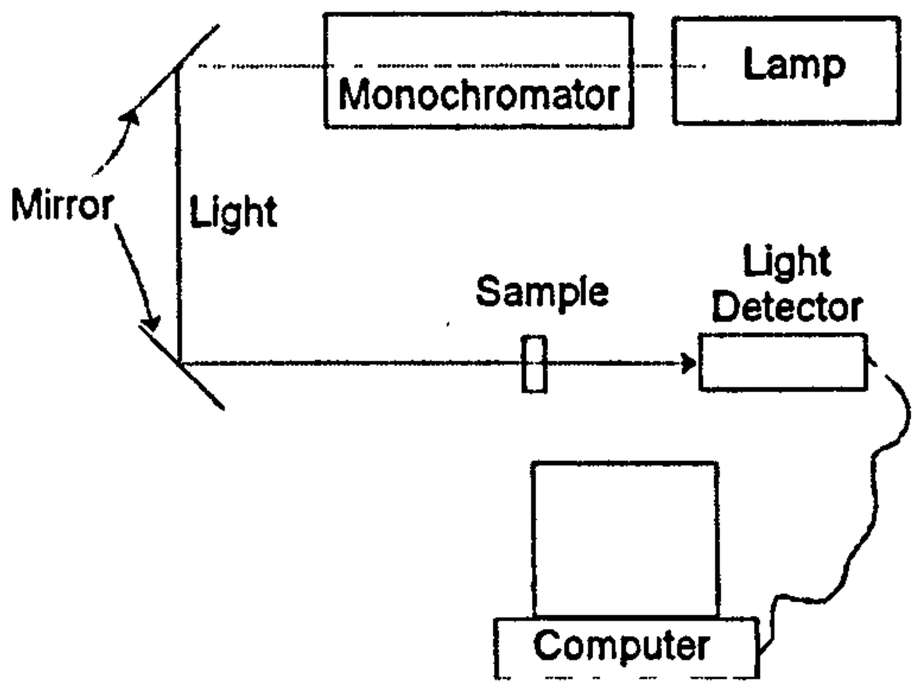

Figure 2.1: Schematic of the UV-Vis spectrometer.

gen lamp through a monochromator in order to select the wavelength and then passes the light through the sample. These two lamps were used in order to produce wavelength over a range between 190 and 1100 nm. The light that passes through the sample is then detected by a photodiode. The

spectrometer then sends the intensity of light as represented by the voltage measured by the photodiode to a computer. This is carried out over a range of wavelengths for both the sample itself and a reference, the solvent in which the sample is suspended. The results from the reference are then subtracted from the sample by the computer and an absorption spectrum reported. Close to the absorption edge, the absorption coefficient, α, of a semiconducting material can be expressed by the following equation[1]:

$$\alpha \approx (h\nu - E_g)^{\gamma} \tag{2.1}$$

where $h\nu$ is the photon energy, E_g is the band gap of the material and for direct allowed, direct forbidden or indirect allowed transitions, γ takes values of 0.5, 1.5 or 2 respectively. Rearranging 2.1 results in the equation:

$$\alpha^{\frac{1}{\gamma}} \approx hc\left(\frac{1}{\lambda}\right) - E_g \tag{2.2}$$

Therefore if the measured optical response to the appropriate power of $\frac{1}{\gamma}$ is plotted against $\frac{1}{\lambda}$, the band gap can be evaluated from the intercept of the straight line portion of the graph with the y-axis. The above approach is inappropriate for a polydisperse solution of particles, such as those produced in this research, as differing band gaps and absorption coefficients occur for different sized particles. In these cases the band gap can be estimated by converting the wavelength at which the absorption onset occurs to energy using the following equation.

$$E_g = \frac{hc}{\lambda e} \tag{2.3}$$

where h is Planck's constant, c is the speed of light. The size of the particles can be estimated from the band gap using equation 1.12.

2.3 Electron Microscopy Methods

The transmission electron microscope (TEM), displayed schematically in Fig.2.2[2], operates in a similar fashion to an optical microscope but uses high energy electrons to greatly increase the magnification. Electrons must pass through the sample, hence it is required to be thin and usually consists of the compound to be imaged supported on a copper grid. An electron beam

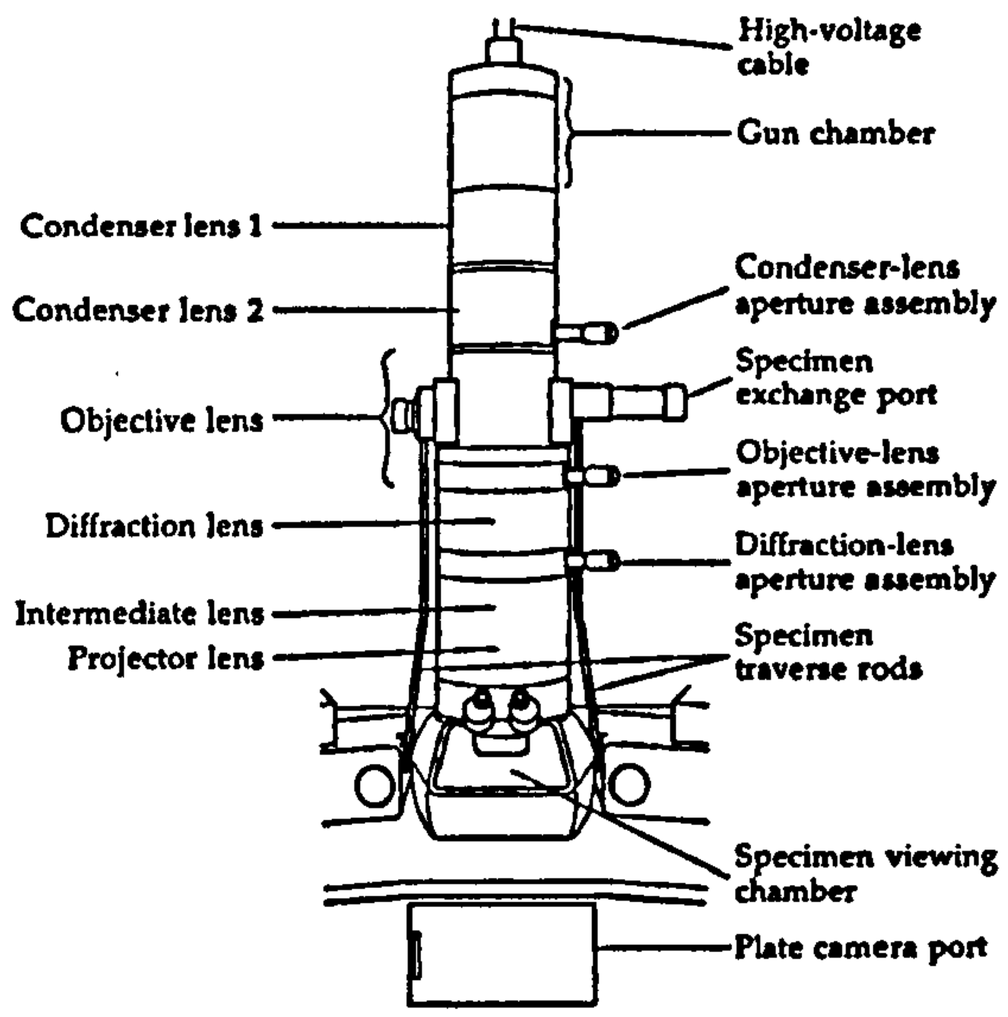

Figure 2.2: Schematic of a TEM. The controls and vacuum system lines are not shown[2].

is produced in the gun chamber, using accelerating voltages between 20 kV and 1 MV depending on the resolution required (the higher the accelerating voltage, the greater the theoretical resolution of the microscope), the beam is then passed through condenser lenses in order to condense the electrons into a narrow beam, which is then focused on the sample by the objective lens. The image is then brought into focus in the viewing chamber or onto a

film by the projector lens.

In order to image the particles produced in this research, a drop of solution containing the particles was allowed to dry on a copper grid coated with carbon. The particles were imaged using either a JEOL JEM 2010 TEM operating at 200 kV giving a maximum magnification of 1.2 million, recording the images on KODAK Electron Image Film SO-163, or a JEOL JEM 1200 EX MK2 TEM operating at 120 kV, with a maximum resolution of one million and using a MegaView III digital camera to record the images. Size analysis was carried out using the Soft Imaging Systems GmbH analySIS 3.0 image analysis software. An Oxford Instruments ISIS 310 X-Ray analysis system with a silicon detector was used to perform elemental analysis of the nanoparticles.

Fig.2.3[2] shows a basic schematic of a scanning electron microscope (SEM).

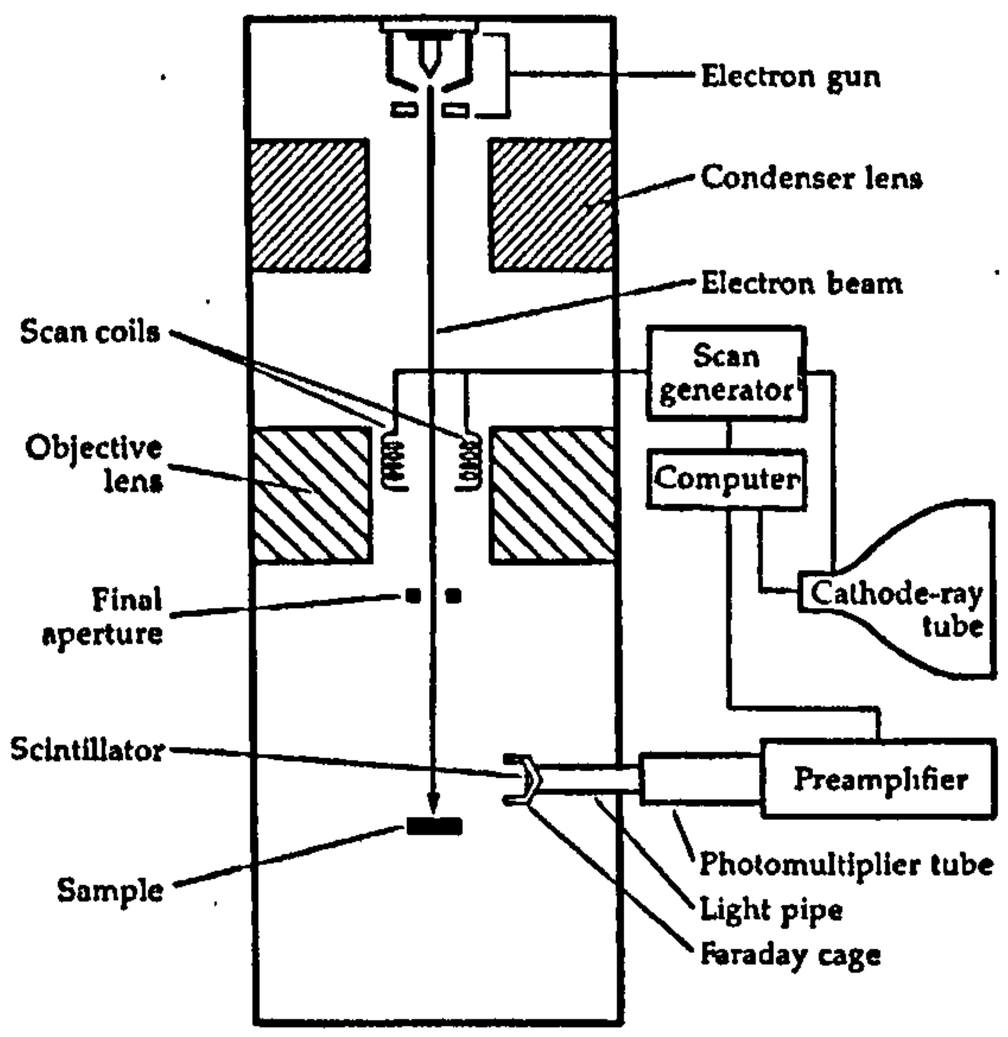

Figure 2.3: Schematic of a SEM[2].

A condensed electron beam is focused as a small spot on the sample by the objective lens. A varying voltage is applied to the scan coils by the scan generator in order to deflect the electron beam across the surface of the sample in a controlled manner and a set of deflection coils around the neck of a cathode ray tube (CRT) is exposed to the same varying voltage to deflect a spot of light across the surface of a digital light detector in the same pattern as the deflection of the electron beam on the sample. Secondary electrons are produced from the sample by the complex series of interactions of the electron beam with the sample. These electrons are collected and converted into light by the scintillator, then transferred to a photomultiplier by the light pipe. The photomultiplier converts the photon back to an electron and amplifies the signal. The voltage produced by the photomultiplier is amplified by the pre amplifier and applied to the grid of the CRT, modulating the intensity of the spot of light produced by the CRT according to the number of secondary electrons detected, such that a bright spot or a darker spot is seen if the electron beam is on a projection or a depression on the surface of the sample respectively. This then results in an image consisting of thousands of spots, with a variety of intensities corresponding to the topography of the sample, that can be captured by the digital light detector and sent to a computer. The samples studied consisted of tin oxide or TiO_2 covered tin oxide electrodes coated with the nanoparticles. The surface of the electrodes were connected to earth in order to stop the electron beam causing surface charging.

A JEOL JSM 6330 F SEM operating at 10 kV was used to image the

nanoparticle modified electrode surfaces produced in this research. An Oxford Instruments ISIS 310 X-Ray analysis system with a silicon detector was used to carry out elemental analysis of the nanoparticles and the electrode surface.

A schematic of the equipment used in the TEM and SEM to carry out the elemental analysis is displayed in Fig. 2.4. When the electron beam in

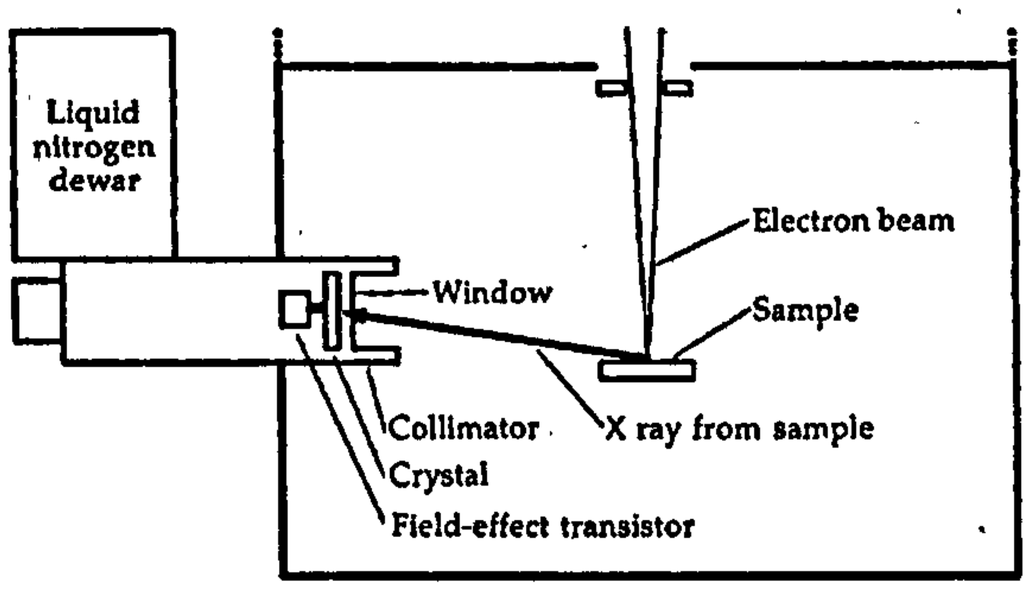

Figure 2.4: Schematic of the machine used for elemental analysis in the SEM and TEM machines[2].

the microscope hits the sample, electrons may be ejected from orbitals in the atoms in the sample. Subsequent relaxation results in the emission of an X-ray from the sample with an energy unique to the atom from which it was emitted. The X-ray is detected by the crystal in the detector and is converted into a voltage pulse that is amplified by the field effect transistor. This results in an energy dispersive X-ray analysis (EDAX) spectrum that shows a series of peaks at different energies, which can be used to identify the elements that are present in the sample. This system will also display the composition of the particle support. Therefore, in this work, the elemental analysis will display peaks representing copper in the case of the TEM and tin

or tin and titanium in the case of the SEM for samples of particles deposited on tin oxide or TiO_2 coated tin oxide electrodes. If the particles to be studied were thought to contain copper, a nickel supporting grid was used, so that copper could be unambiguously identified.

2.4 Electrophoresis

A Brookhaven Instruments Corporation Zeta PALS Zeta Potential Analyser was used to measure the zeta potentials of the nanoparticles in solution. The zeta potential found is the potential at the shear plane of the particles. The ZetaPALS method of finding the zeta potential involves the measurement of the mobility of the particles using electrophoretic light scattering. A schematic of the apparatus is displayed in Fig.2.5. The technique involves modulation of the electric field and phase modulation of the reference beam

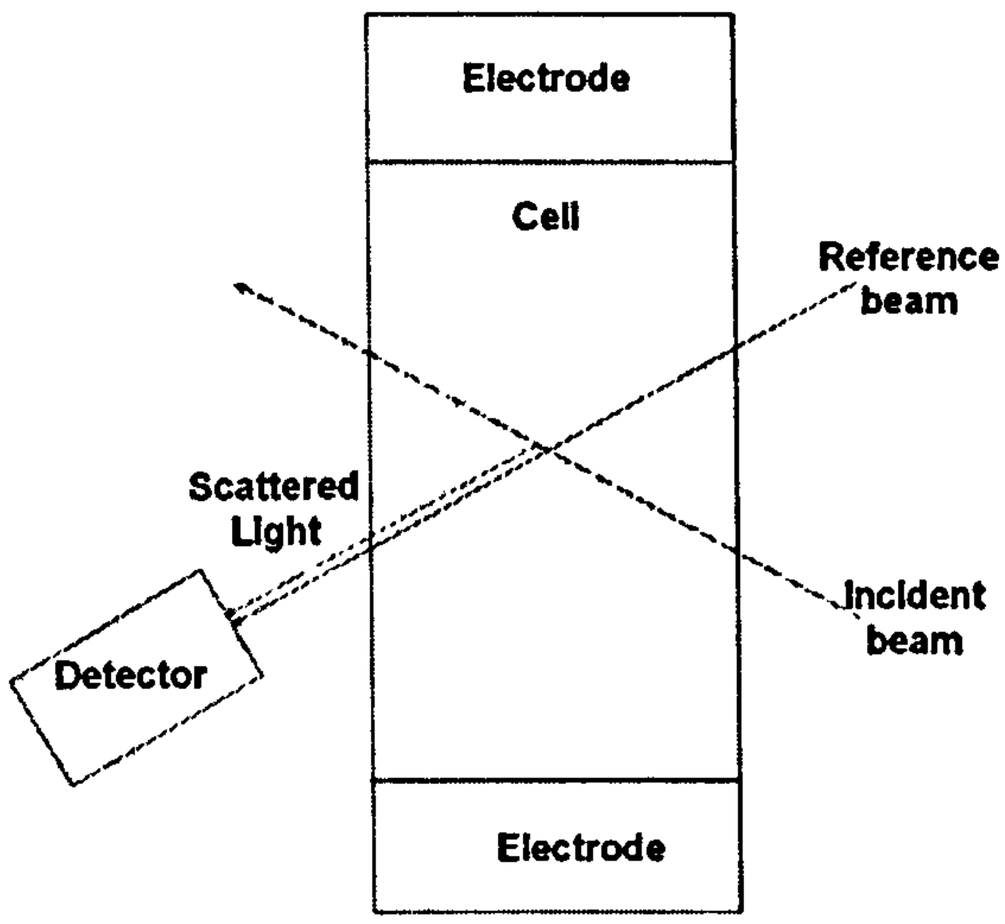

Figure 2.5: Schematic of the electrophoresis apparatus.[2].

at the frequency of the scattered beam found under no electric field. A shift in phase is observed between the scattered and reference beams. This phase shift is constant when no electric field is applied and is time dependent when a field is applied. The Zeta PALS instrument records the difference between the phase shift at time t and the constant phase shift in the absence of an electric field, the relative phase shift, as a function of time while the solution is under a sinusoidal electric field of frequency in the range of 5 to 60 Hz. The mobility of the particles can then be determined from the amplitude of the modulated relative phase shift. The particle suspension is required to be stable and transparent for the measurements to be obtained. Results were obtained by measuring the mobility of the particles in a set of ten readings, removing the highest and lowest values from the set and taking the average of the rest. The zeta potential (ζ) can be calculated from the mobility (μ_E) by one of two models. The choice of model depends on a comparison of the particle size with the Debye length, which is defined as the distance from the surface of the particle at which the Volta potential difference between a point at a known distance from the particle and the bulk electrolyte is 37 % of its magnitude at the surface of the particles. Smoluchowski's equation, equation 2.4, is employed if the Debye length is smaller than the particle size.

$$\mu_E = \frac{\epsilon\zeta}{\eta} \tag{2.4}$$

where ϵ is the dielectric constant of the solvent and η is the viscosity. If, however, the particles are smaller than the Debye length, as in the work

reported in this thesis, the Hückel model is used:

$$\mu_E = \frac{2\epsilon\zeta}{3\eta} \tag{2.5}$$

This method can be used to determine the surface charge on the particles.

The Debye length, λ_D, can be calculated using the following equation:

$$\lambda_D = \left(\frac{\epsilon_0 \epsilon_r k_B T}{2 N_A e^2 I}\right)^{(\frac{1}{2})} \tag{2.6}$$

where ϵ_0 is the permittivity of a vacuum, ϵ_r is the dielectric constant of the solvent, k_B is the Boltzmann constant, N_A is Avogadro's number and I is the ionic strength. This equation only applies for 1:1 electrolytes. The maximum ionic strength of the solutions of the bismuth sulfide particles prepared in Chapter 3 were calculated using equation 2.7, assuming that the pH of the solution is at least 7, giving a maximum concentration of H^+ ions of 10^{-7} mol dm^{-3}.

$$I = \frac{1}{2}\sum_i c_i z_i^2 \tag{2.7}$$

where c_i is the concentration of ion i in moles m^{-3}, z_i is the charge on ion i and the sum is carried out over all the ions in solution. Therefore an estimated minimum Debye length for a Bi_2S_3 solution in ethanol, as prepared in chapter 3, can be calculated using the ionic strength, the dielectric constant of ethanol (25.3) and a temperature of 293 K. This debye length was found to be 8 nm. As the particle sizes for Bi_2S_3 are less than the Debye length, the Hückel model is used to determine the zeta potential.

2.5 Powder X-Ray Diffraction

A Bruker AXS diffractometer D8 was used to determine the powder X-ray diffraction pattern of nanoparticle samples. The nanoparticle powders were mounted on a rotating stage, in the geometry shown in Fig.2.6[3], with a Cu Kα X-ray source operating at 40 kV. 2θ, where θ is the angle between the X-ray source or the detector and the horizontal plane, was scanned between 20 ° and 90 °.

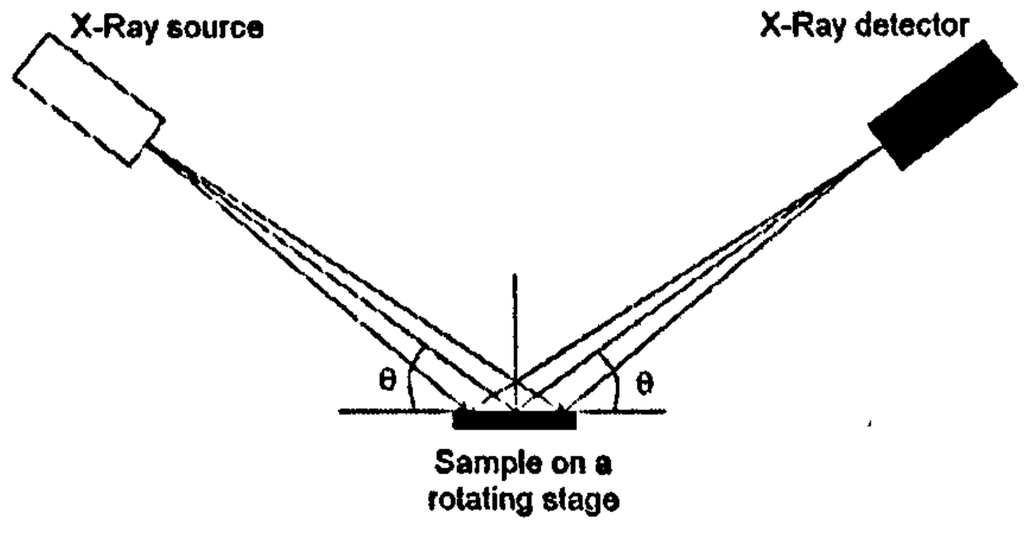

Figure 2.6: Schematic of the powder X-ray diffractometer[3].

Crystal planes parallel to the sample and the X-ray source, and therefore the detector, that meet the Bragg condition (equation 2.8,

$$2d\ sin\ \theta = \lambda \tag{2.8}$$

where λ is wavelength of the X-rays and d is the lattice spacing), result in constructive diffraction and hence peaks in the intensity versus angle spectrum[4]. Using powder X-ray diffraction, it is possible to approximate the

size of the particles using the Debye-Scherrer relationship[5], as shown in the equation below:

$$\text{particle diameter} = \frac{1.3\lambda}{\Delta(2\theta)\cos\theta} \tag{2.9}$$

where λ is the wavelength of the X-rays, $\Delta(2\theta)$ is the peak full width at half maximum in radians and θ is the position of the peak. However, caution was taken when using this formula on very broad peaks as these could be due to small particles or large particles with defects.

2.6 X-ray Photoelectron Spectroscopy

A schematic of an X-ray photoelectron spectrometer (XPS) is shown in Fig.2.7[6]. This technique, as applied in this thesis, involves bombarding the

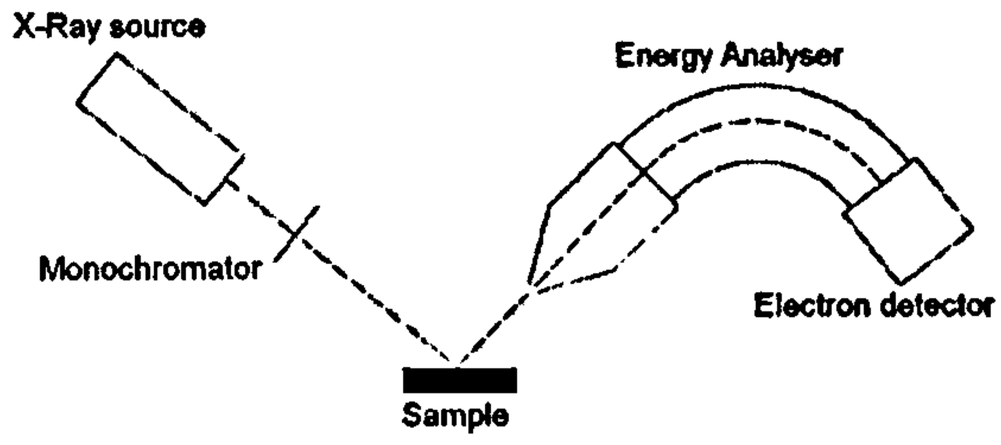

Figure 2.7: Schematic of an X-ray photoelectron spectrometer[6].

nanoparticulate sample, produced by drying a solution of the nanoparticles on a glass slide, with X-rays with a defined energy, hν. This results in the ejection of electrons from core orbitals of atoms on the surface of the nanoparticles. These electrons are known as photoelectrons and have a kinetic energy equal to the difference between the energy of the X-rays used and the ionisation potentials for the orbitals from which the electrons were

removed. These kinetic energies can be measured by finding the electric field necessary to deflect the photoelectrons through an electroanalyser of known curvature so the electrons hit an electrodetector, as illustrated in Fig.2.7[6;7]. A spectrum is built up by counting the electrons occurring at specific energies. The ionisation potentials for electrons coming from the orbitals from which photoelectrons originated can be calculated and are closely related to the binding energy of that orbital. There are two other processes called the X-ray fluorescence process and the Auger process that can occur simultaneously with this photoionisation process and these are summarised in Fig.2.8[7]. The X-ray fluorescence process involves the relaxation of a valence electron

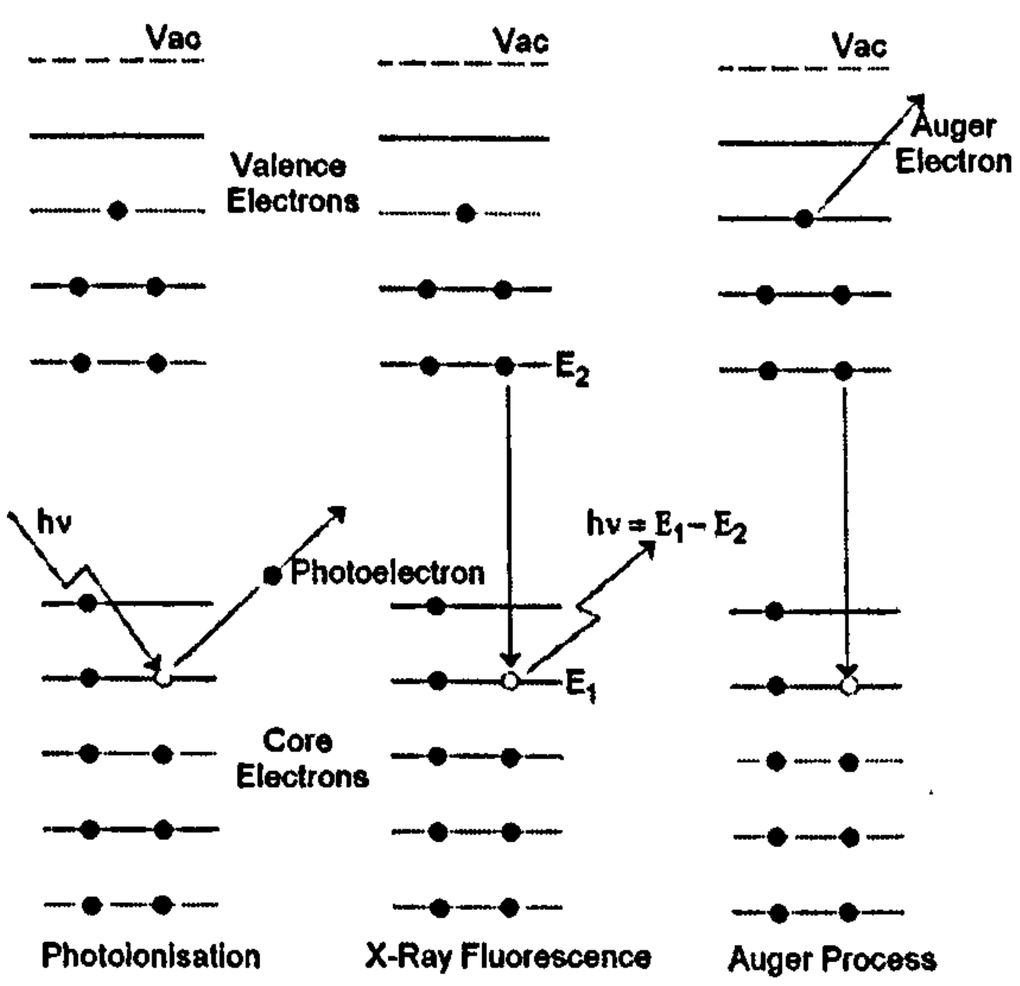

Figure 2.8: Photoionisation, X-ray fluorescence and Auger processes[7].

into the gap in the core orbitals left by the photoelectron, resulting in the emission of an X-ray with energy equal to the difference in energy between the two energy levels. In the Auger process, the energy produced by the relaxation of an electron in a valence orbital to a core orbital is transferred

to a second electron in a valence orbital with a low ionisation potential (I_p), resulting in this electron being ejected from the atom with a kinetic energy of $E_1 - E_2 - I_p$, where E_1 is energy of the valence orbital of the electron involved in the relaxation step and E_2 is the energy of the core orbital to which the electron is relaxing. The ejected electron is called an Auger electron and the energy of this electron is also measured with photoelectrons produced by photoionisation. However, the kinetic energy of the Auger electron is independent of the energy of the X-ray responsible for the photoionisation of the atom. Therefore, if two XPS experiments are carried out using X-rays of different energies then peaks due to Auger electrons can be differentiated from the photoelectrons. A Fisons Instruments Escascope X-ray Photoelectron Spectrometer using a Mg K_α X-ray source was employed in order to measure the X-ray photoelectron spectra of the samples studied in this work. The spectra were measured a second time using an Al K_α X-ray source in order to determine the position of the peak corresponding to Auger electrons. The assignment of the peaks was carried out by comparing the energies of the observed peaks with the energies found in reference tables containing the energies of photoelectrons from the elements expected to be present in the sample. The samples were etched by exposing the samples to a beam of argon ions for 10 minutes. The measurements were then repeated to determine the composition of the material inside the particles.

2.7 Photoelectrochemical Techniques

The photoelectrochemical methods employ a standard three electrode electrochemical cell as shown in Fig.2.9. A tin oxide glass electrode coated with

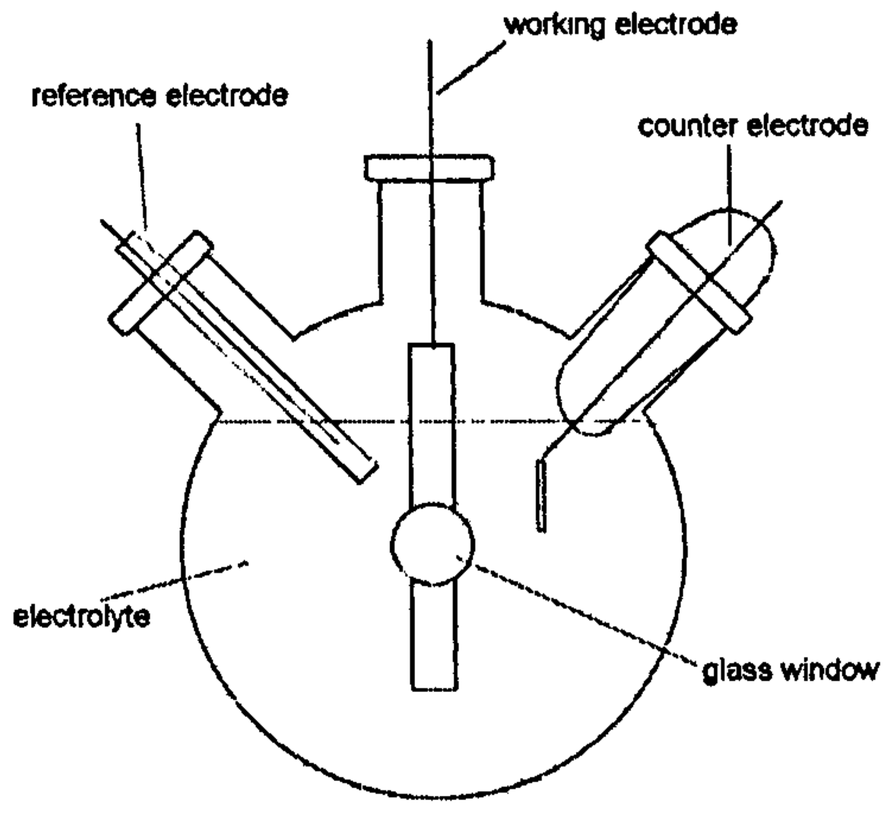

Figure 2.9: The electrochemical cell.

the particles to be studied was used as the working electrode. The counter electrode was a platinum wire mesh. An Ag|AgCl|3 mol dm^{-3} KCl electrode was used as the reference electrode. The electrolyte used was 1 mol dm^{-3} Na_2SO_3 aqueous solution buffered to pH 12 by NaOH and $NaHPO_4$.

2.7.1 Photocurrent-Potential Curves

Producing photocurrent transients involves exposing the working electrode to a square wave illumination pattern while measuring its cyclic voltammogram. The set up used is illustrated in Fig.2.10. White light from a 75 W USH10 Xenon short arc lamp bulb in a LPS-220B Photon Technology International

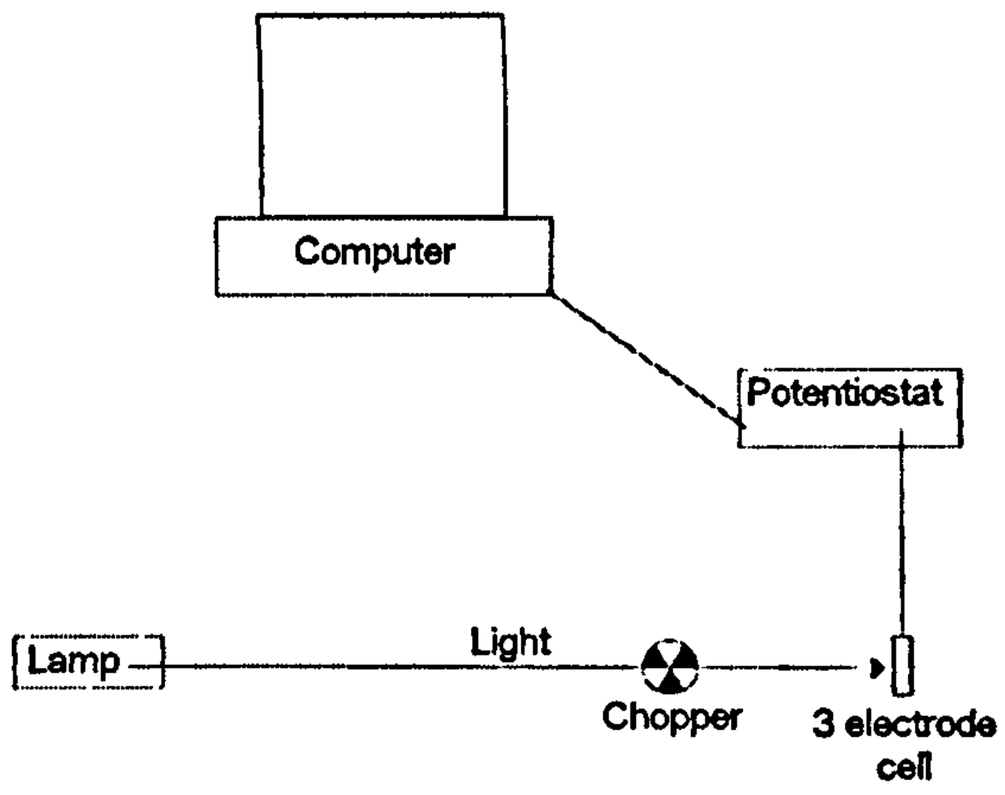

Figure 2.10: Schematic of the apparatus used to measure the photocurrent-potential curves.

lamp power supply, chopped at 0.1 Hz by an OC4000 Photon Technology International digital optical chopper, was employed to illuminate an electrode area of 1 cm^2. An Eco Chemie Autolab potentiostat was used to control the potential and measure the current. If electron transfer from the nanoparticle to the electrode occurs, an immediate rise to a steady photocurrent when the light is switched on and a rapid decay to zero photocurrent on switch off is expected.

2.7.2 Photocurrent Spectroscopy

Fig.2.11 shows the equipment used in photocurrent spectroscopy. The light from the Xe arc lamp used in the photocurrent transient experiments was passed through a Photon Technology International monochromator of 3 nm resolution. An area of 0.4 cm^2 of the working electrode was exposed to

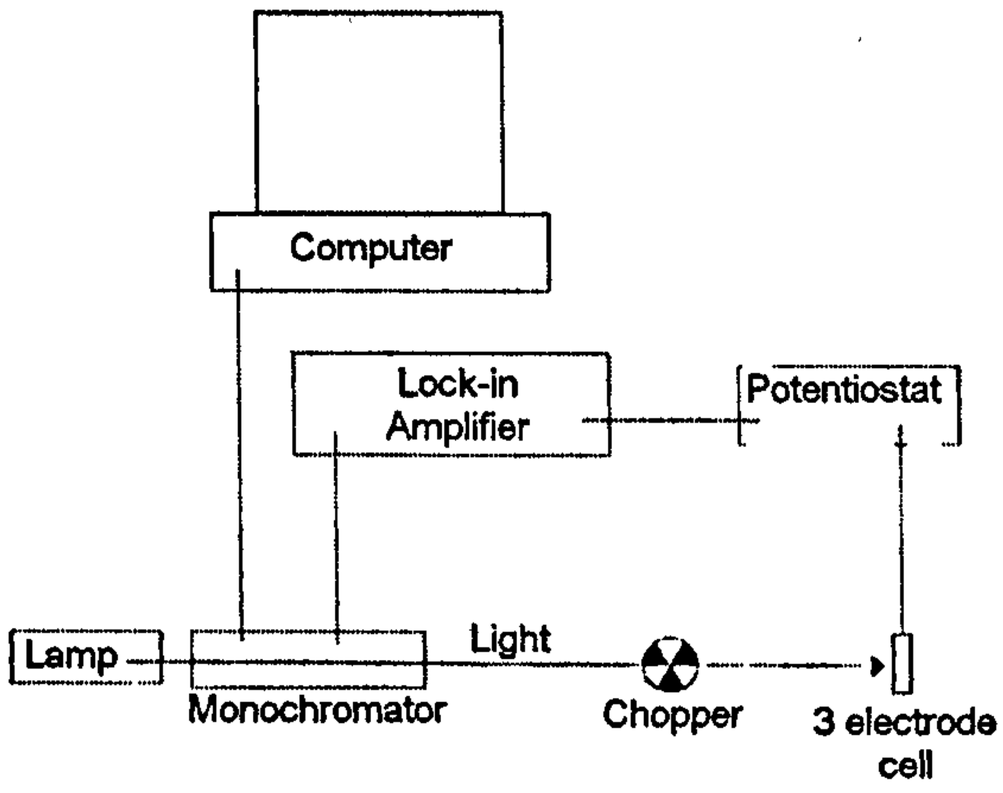

Figure 2.11: Schematic of the apparatus used to measure the photocurrent spectra.

the monochromatic light, chopped at 17 Hz by an OC4000 Photon Technology International optical chopper and an in-house built potentiostat was employed to measure the total cell current. This current measurement was transferred to a SR830DSP Stanford Research Systems Lock-in Amplifier. This instrument isolates the response corresponding to the frequency of the chopped light, obtaining a steady state photocurrent reading. The photocurrent data and corresponding wavelength are then sent to a computer via the monochromator and processed using in-house written software. Readings were measured at 2 nm intervals over a range of wavelengths. The recorded photocurrent, i, can be expressed by the following equation:

$$i = \phi_e I_{Ph} \tag{2.10}$$

where I_{Ph} is the intensity of the incident light and ϕ_e is the percentage of incident photons resulting in the release of an electron into the external

circuit, the Incident Photon to Current conversion Efficiency (IPCE).

A photocurrent spectrum of a photodiode of known light to electron conversion efficiency, which was put in place of the electrochemical cell in Fig.2.11, was measured in order to correct the data for changes in lamp signal, illumination area and alignment. The voltage output of the photodiode was directly connected to the lock-in amplifier and the photodiode current, i_{PD}, over the same wavelength range as the sample was recorded. There is a similar expression, shown below, for the photodiode current to the equation for the recorded photocurrent.

$$i_{PD} = \phi_{PD} I_{Ph} \tag{2.11}$$

where ϕ_{PD} is the known efficiency of the photodiode.

IPCE can be calculated using the following equation as the photodiode efficiency is known and the incident intensity is the same for both experiments.

$$\phi_e = \frac{i\phi_{PD}}{i_{PD}} \tag{2.12}$$

The above calculation is used to calculate the values of the IPCE for each wavelength measured and a plot of IPCE against wavelength is produced. The band gap is then determined to be the point at which a photocurrent signal is first observed. The wavelength at which this occurs is converted to energy according to equation 2.3. The effective-mass model of quantum confinement can be used to estimate the size of the particles from their band gap and equation 1.12 as discussed in section 1.2.3.

References

[1] Sze, S. M. *Semiconductor devices, physics and technology;* 1985.

[2] Fleger, S. L.; Heckman, J. W.; Klompare, K. L. *Scanning and Transmission Electron Microscopy:An Introduction;* W. H. Freeman, 1993.

[3] Aslanov, L. A.; Fetisov, G. V.; Howard, J. A. K. *Crystallographic Instrumentation;* Oxford University Press: Oxford, 1998.

[4] Woolfson, M. M. *An Introduction To X-ray Crystallography;* Cambridge University Press: Cambridge, second edition ed., 1997.

[5] Hodes, G. *Electrochemistry of Nanomaterials;* Wiley-VCH: Weinheim, 2001.

[6] Hufner, S. *Photoelectron Spectroscopy:Principles and Applications;* Springer: Berlin, third edition ed., 2003.

[7] Ghosh, P. K. *Introduction To Photoelectron Spectroscopy*, Vol. 67 of *Chemical Analysis;* John Wiley and Sons: New York, 1983.

Chapter 3

Bismuth Sulfide

The work contained in this chapter has been published in J. Mater. Chem.[1].

3.1 Introduction

The direct band gap of bulk Bi_2S_3 is reported to be in the region of 1.3 - 1.7 eV[2–5]. As discussed in section 1.1.2, a solar cell sensitiser should have a band gap of approximately 1.4 eV. Thus bismuth sulfide is a candidate as a sensitiser.

A number of methods have been reported for the preparation of Bi_2S_3 nanoparticles.

3.1.1 Methods of Preparation

Ultrasonic Methods

Wang *et al.*[6] prepared bismuth sulfide nanorods by exposing a mixture of $Bi(NO_3)_3$, triethanol amine and $Na_2S_2O_3$ in water to high intensity ultra-

sound irradiation for 2 hours. The rods were observed to have diameters between 20 and 30 nm and lengths in the range of 200 to 250 nm, as measured by TEM. The rods are thought to be formed according to the following mechanism:

$$\begin{aligned} H_2O &\xrightarrow{\text{ultrasound}} H^\bullet + OH^\bullet \\ 2H^\bullet + S_2O_3^{2-} &\rightarrow S^{2-} + 2H^+ + SO_3^{2-} \\ 2Bi^{3+} + 3S^{2-} &\rightarrow Bi_2S_3 \end{aligned} \tag{3.1}$$

The nanorods formed were highly crystalline as determined by powder X-ray diffraction. However, this method required water to be present during the synthesis, which made deposition of the rods on to a nanocrystalline substrate difficult. Bismuth sulfide thin films have been prepared by Wang *et al.*[7] using an asynchronous-pulse ultrasonic spray pyrolysis method. This technique sprayed a heated substrate alternately with thiourea and $Bi(NO_3)_3$ in an inert atmosphere. The spray is produced using commercial ultrasound humidifiers. This methods produces microstructured bismuth sulfide films consisting of nano-crystalline grains with grain sizes in the range of 44.1 to 67.5 nm, as calculated from the X-ray diffraction peaks using the Debye-Scherrer equation.

Microwave Heating Methods

A method of preparing bismuth sulfide particles using microwave radiation was reported by Liao *et al.*[8;9] The experiment involved heating a solution of $Bi(NO_3)_3$ and thiourea or thioacetamide in formaldehyde with microwave

irradiation. This resulted in nanorods with an average diameter of 10 nm and length of about 300 nm when thiourea was used or nanorods with an average diameter of 50 nm and lengths between 1 and 2 μm when thioacetamide was used. These sizes were obtained using TEM and the rods were determined to be crystalline from the powder X-ray diffraction patterns. Liao *et al.*[9] suggest that the reaction proceeds as follows:

$$\begin{aligned}
CH_3CSNH_2 + H_2O &\rightarrow CH_3(NH_2)C(OH) - SH \\
CH_3(NH_2)C(OH) - SH + H_2O) &\rightarrow CH_3(NH_2)C(OH)_2 + H_2S \\
CH_3(NH_2)C(OH)_2 &\rightarrow CH_3(NH_2)C = O + H_2O \\
3H_2S + 2Bi(NO_3)_3 &\rightarrow Bi_2S_3 + 6HNO_3
\end{aligned} \tag{3.2}$$

It is extremely complicated to produce a reflux system that can be irradiated with microwaves safely.

Hydrothermal and Solvothermal Methods

Bismuth sulfide has also been prepared by Zhang *et al.*[10], Yu[11] and Shao *et al.*[12] using hydrothermal techniques. In order to produce the bismuth sulfide, a solution of Na_2S and BiI_3 or $Bi(NO_3)_3$ in water is placed in an autoclave and heated for 12 hours. The bismuth sulfide particles could be produced by this method as $Bi(NO_3)_3$ is strongly hydrolysed by water to form $BiONO_3$, which has a higher solubility product than Bi_2S_3 thus enabling the formation of bismuth sulfide particles under hydrothermal conditions[10]. Zhang *et al.* prepared nanorods with dimensions of 10-50 nm by 1-5 μm, as measured by TEM. Yu *et al.* determined that the size of nanorods prepared

using this technique increased from 80 nm x 40 nm when the particles were prepared at 100 °C to 150 nm x 40 nm if a preparation temperature of 150 °C was used. These sizes were obtained using TEM. Crystalline nanorods were observed as long a temperature above 100 °C was used in the preparation. Shao *et al.* showed that the crystallinity of the nanorods could be improved if the reaction mixture was stirred during the hydrothermal process. This process yields poor quality polycrystalline particles unless the solution is stirred during the reaction and is too time and energy intensive to be used as a commercial preparation.

Yu *et al.*[13;14] have also synthesised bismuth sulfide using a solvothermal technique. This alternate method involved the heating of a solution of $BiCl_3$ and thiourea in an autoclave at 140 °C for 12 hours. This method produces bismuth sulfide in the form of nanorods, which were determined to be crystalline by powder X-ray diffraction. A number of different solvents can be used and the choice of solvent affects the particle size as shown in Table 3.1. These sizes were measured by TEM. Yu *et al.* determined that

Solvent	Average nanorod dimensions / nm
Ethanol	30 x 500
Pyridine	20-30 x 1000-3000
Ethylene glycol	130-200 x 3500
Water	300 x 2250

Table 3.1: Average size of the nanorods produced in different solvents by Yu *et al.*[13;14].

bismuth sulfide is only formed in polar solvent and that the preparation of the particles occurs via the formation of Bi-thiourea complex and subsequent thermal decomposition of thiourea as outlined in the following equation:

$$Bi^{3+} + NH_2CSNH_2 \overset{\text{solvent}}{\rightarrow} Bi - NH_2CSNH_2 \text{complexes} \overset{\text{decomposition}}{\rightarrow} Bi_2S_3 \tag{3.3}$$

There are a number of similar methods of preparing bismuth sulfide, including the thermal decomposition of bismuth ethylxanthate[15], thiosulfatobismuth [16], Bi-thiourea complex[17] and bismuth dithiocarbamate[18].

Chemical Bath Deposition Methods

Chemical bath deposition is a widely studied method[19–24]. In this technique, a substrate is immersed in a temperature controlled bath typically containing an aqueous solution of $Bi(NO_3)_3$ and thioacetamide at around pH 2. Deposition is normally carried out on SnO_2, glass or glass pretreated with an organosilane substrates. Nair *et al.*[19;24] have shown that films deposited on SnO_2 conducting glass electrodes produced using this method display photosensitization, as a small increase in the current measured in a three electrode system when the electrode coated with bismuth sulfide is illuminated with light, compared to the measured current in the dark. Films of bismuth sulfide on glass slides were prepared by Mane *et al.*[20] using the chemical bath technique and it was determined that the grain size increased from 6.85 nm to 33.86 nm, as calculated from the X-ray diffraction peaks using the Debye-Scherrer equation, as the deposition time was increased from 5 hours to 25 hours. The band gap of bismuth sulfide in the films were found, from the

absorption spectra, to be 2.06 and 1.6 eV for the films deposited for 5 and 25 hours respectively. Mane *et al.*[20] proposed the following mechanism for the formation of Bi_2S_3 in an acidic medium, such as the chemical bath:

$$CH_3CSNH_2 + H^+ \rightarrow CH_3C \equiv NH^+ + H_2S$$
$$2Bi^{3+} + 3H_2S \rightarrow Bi_2S_3 + 6H^+ \quad (3.4)$$

Mane and Lokhande[21] reviewed the preparation of bismuth sulfide films on glass or tin oxide glass electrodes produced by a number of researchers using different chemical baths, summarised in Table 3.2. The band gaps were obtained from UV-Vis absorption spectra.

Huang *et al.*[22] synthesised Bi_2S_3 thin films on glass slides pretreated with an organosilane using immersion in a chemical bath containing $Bi(NO_3)_3$, triethanolamine and thioacetamide for 2 to 7 hours. Rincón *et al.*[23] used the same bath as Nair *et al.*[24] in order to produce bismuth sulfide thin films on glass or tin oxide glass electrode substrates. A photocurrent response was observed, but control of the band edge was difficult to obtain using this preparation.

Ref.	Bath Composition	pH	DT / °C	Deposition time	Band gap / eV
[25]	EDTA + NaOH + thioacetamide	8-9	27	2.5-3 hours	1.68
[26]	TEA + NH_4OH + thiourea	8	100	40 minutes	1.47
[27]	TEA + NH_4OH + thiourea	9.29	-	30 minutes	-
[28]	TEA + thioacetamide	-	27	-	1.7
[29]	EDTA + $Na_2S_2O_3$	2	27	9 hours	1.67
[30;31]	EDTA + thioacetamide	2	27	8 hours	1.84
[32]	$Na_2S_2O_3$ in CH_3COOH or CH_2O	1.4	27	4 hours	1.9
[33]	EDTA + $Na_2S_2O_3$	2	60	1-6 hours	2.22 - 1.67
[34]	TEA + thioacetamide	-	27	7 hours	-
[35;36]	TEA + thioacetamide	8.5	24	6 hours	-
[20]	EDTA + $Na_2S_2O_3$	2-3	27	10 minutes	1.7
[37;38]	EDTA + thioacetamide	2	6	5-25 hours	2.04 - 1.60

Table 3.2: Summary of chemical bath preparations. N.B. $Bi(NO_3)_3$ was used as the bismuth source in all the baths, the solvent used was water unless otherwise stated and the dashes represent unknown values. DT = deposition temperature, EDTA=ethylenediamine tetra-acetic acid, TEA=triethanolamine.

Thermal Evaporation Methods

Films of bismuth sulfide on substrates have been prepared by Rincón *et al.*[23] by thermal evaporation. This involved heating a quantity of bismuth sulfide to 800-900 °C above a substrate heated to a known temperature in vacuum conditions. Rincón *et al.*[23] observed limited photosensitization of a SnO_2 glass substrate using this technique.

Reactive Evaporation Methods

Pradeep *et al.*[39] prepared bismuth sulfide by reactive evaporation. This involved evaporating Bi and S in a high vacuum chamber and subsequent deposition of bismuth sulfide on glass or quartz substrates heated to 473 K. The films produced by this method are polycrystalline and have a band gap of 1.38 eV as determined from transmission spectra.

Successive Ion Layer Adsorption and Reaction (SILAR) Methods

The methods discussed above are time consuming, use complex equipment, involve high temperature reactions, are carried out under vacuum or employ complex multi-stage processes. The adaption of these techniques for deposition on high surface area substrates is difficult. The successive ion layer adsorption and reaction (SILAR) method can be used to sensitize SnO_2 and nanocrystalline TiO_2[40] electrodes simply. This involves dipping the substrate in a solution of BiO^+ followed by immersion in a Na_2S solution. However, controlling the absorption spectrum of the deposit using this technique is difficult.

Arrested Precipitation Methods

Colloidal routes to nanoparticles allow control of the size of the particles[2] and the deposition of the as-prepared particles on to nanocrystalline substrates. Hence, they represent a flexible and attractive method of achieving photosensitization. Suarez *et al.*[2] prepared bismuth sulfide nanoparticles by adding H_2S or Na_2S to a solution of BiI_3 and Nafion in acetonitrile. This resulted in particles with an average diameter of less than 5 nm, as measured by TEM, and an absorption onset in the UV-Vis absorption spectra at 500 nm indicating the occurrence of size quantisation for these particles. These particles were deposited on a tin oxide electrode by successively immersing the substrate in solutions of Na_2S and Bi_2S_3 particles. These electrodes were observed to generate photocurrent under visible light with a low incident photon to current conversion efficiency.

A simple route to bismuth sulfide nanoparticles has been reported by Peter *et al.*[41] This method is based on the arrested precipitation technique of preparing CdS used by Riley *et al.*[42] The particles are prepared by adding H_2S to an ethanolic solution of BiI_3 and 3-mercaptopropionic acid. The as-prepared particles self assemble and sensitize TiO_2. The particles were observed to have an average particle size of 4.1 nm with a broad size distribution as determined using TEM. Photoelectrochemical experiments were carried out by Peter *et al.*[41], using 1 M Na_2S, 1 M Na_2SO_3 and their mixtures at different volume ratios as the electrolyte. It was discovered that the injection from the polydisperse Bi_2S_3 particles can be tuned by altering

the sulfide concentration[41].

This chapter will discuss the influence of the concentration of stabiliser on the size of the Bi_2S_3 particles formed and the photoelectrochemical properties of quantum confined bismuth sulfide modified tin oxide electrodes[1]. A change in the particle size resulting from a change in the stabiliser concentration of more than two orders of magnitude is shown. However only a limited alteration in the absorption spectrum is observed. The results are discussed in terms of the effective mass model of quantum confinement. The optical properties and the size of bismuth sulfide particles prepared from the addition of H_2S to a solution of triphenylbismuth in THF after different stirring times are also studied.

3.2 Preparation of Nanoparticles

3.2.1 Preparation by Arrested Precipitation (Method 1)

Clean tin oxide glass electrodes were hydrolysed in a 5 mol dm^{-3} potassium hydroxide solution and then were washed and dried. The electrodes were then placed in a 250 ml conical flask, conducting side up. 50 ml of anhydrous ethanol solution, containing 40×10^{-6} mol dm^{-3} BiI_3 and a measured amount of stabiliser, was added to the conical flask. Oxygen was then removed by bubbling nitrogen through the vigourously stirred solution for 30 minutes. After injecting 0.5 cm^3 of H_2S, 4.2×10^{-4} mol dm^{-3}, into the solution, forming

Bi_2S_3, the reaction mixture was stirred for 40 minutes. The electrodes were then removed from the solution, washed with ethanol, dried and stored. The stabiliser, 3-mercaptopropionic acid (3-MPA), was used in the following two concentrations; (A) 5 x 10^{-4} mol dm^{-3} and (B) 0.1 mol dm^{-3}. Particles prepared used using stabiliser concentrations A and B will be referred to as Bi_2S_3 A and Bi_2S_3 B respectively.

3.2.2 Synthesis from Triphenylbismuth (Method 2)

10 ml of a 0.02 mol dm^{-3} triphenylbismuth solution in THF was placed in a test tube, degassed with N_2 and stirred for either 1 hour or 12 hours, followed by injection of 2.5 ml of H_2S, 0.01 mol dm^{-3}, and subsequent stirring of the solution for 1 hour. Samples resulting from this synthesis using initial stirring times of 1 hour and 12 hours will be referred to as Bi_2S_3 C and Bi_2S_3 D respectively. These samples were analysed using TEM and UV-Vis absorption spectroscopy only.

3.3 Transmission Electron Microscopy

Typical TEM images of Bi_2S_3 A and Bi_2S_3 B are shown in Fig.3.1 (a) and (b) respectively. Fig.3.1 (a) shows clear evidence of crystallinity as shown by the lattice fringes in the circled particles. Lattice fringes corresponding to the $\bar{1}00$, $\bar{1}10$, $\bar{2}10$, $23\bar{1}$ and $33\bar{1}$ faces of Bi_2S_3 were observed. The average particle diameters of Bi_2S_3 A and Bi_2S_3 B are 4.1 $\pm$ 1.0 nm and 3.0 $\pm$ 0.6 nm respectively. These diameters are calculated by statistical analysis of the size dis-

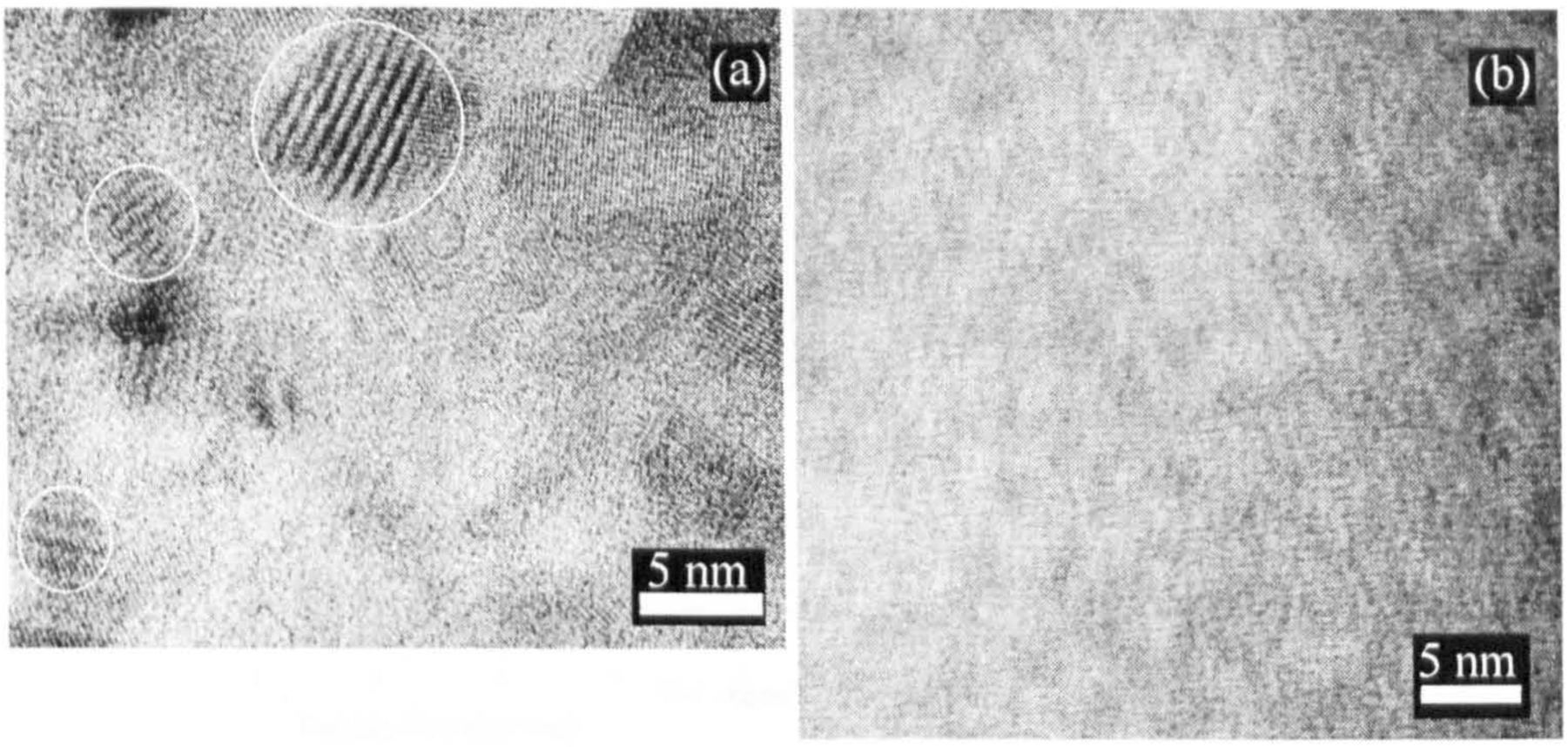

Figure 3.1: TEM images of samples a) Bi_2S_3 A and b) Bi_2S_3 B.

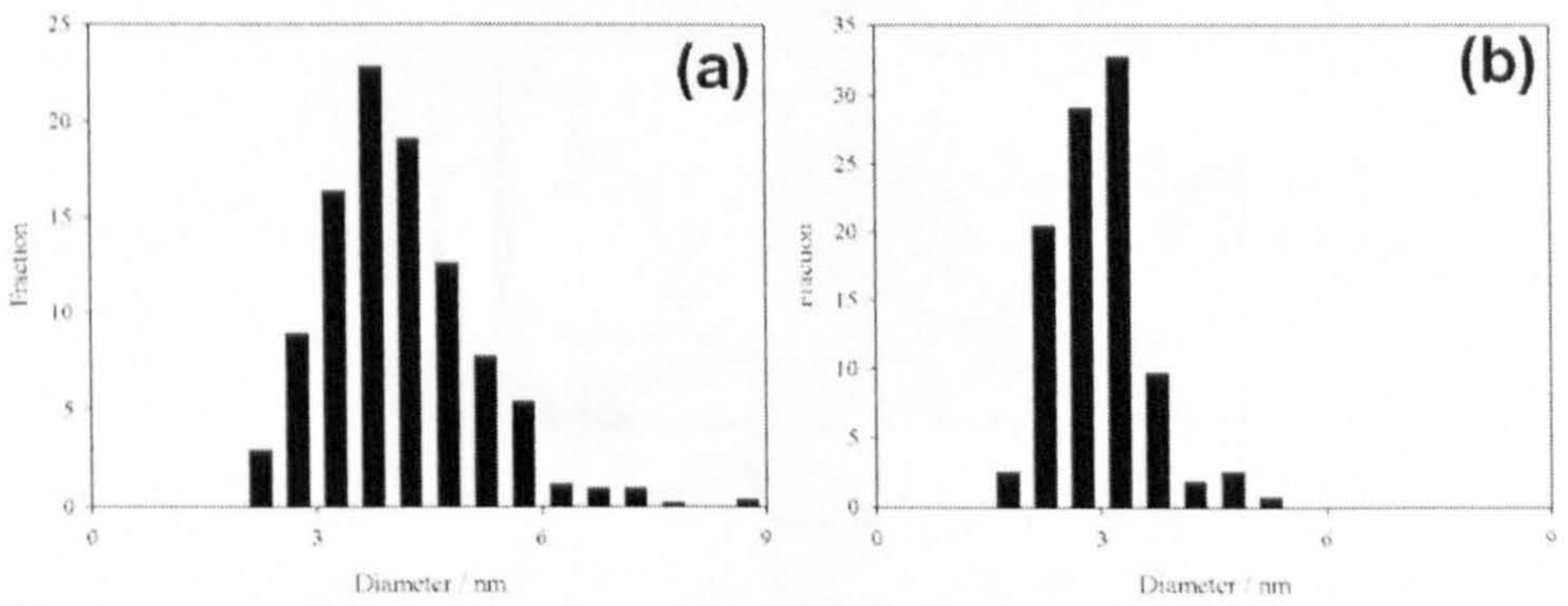

Figure 3.2: Size distribution of samples a) Bi_2S_3 A and b) Bi_2S_3 B.

tributions displayed in Fig.3.2. The respective number of particles measured for the statistical analysis from the Bi_2S_3 A and Bi_2S_3 B samples are 512 and 256. The presence of bismuth in the particles is clearly shown by the Energy Dispersive X-Ray analysis spectrum, depicted in Fig.3.3. The existence of sulfur is not proved by the data as the bismuth peak at 2.57 eV overlaps the emission from sulfur. The X-ray data shows the absence of other elements as the major copper peak arises from the TEM grids. The crystallographic in-

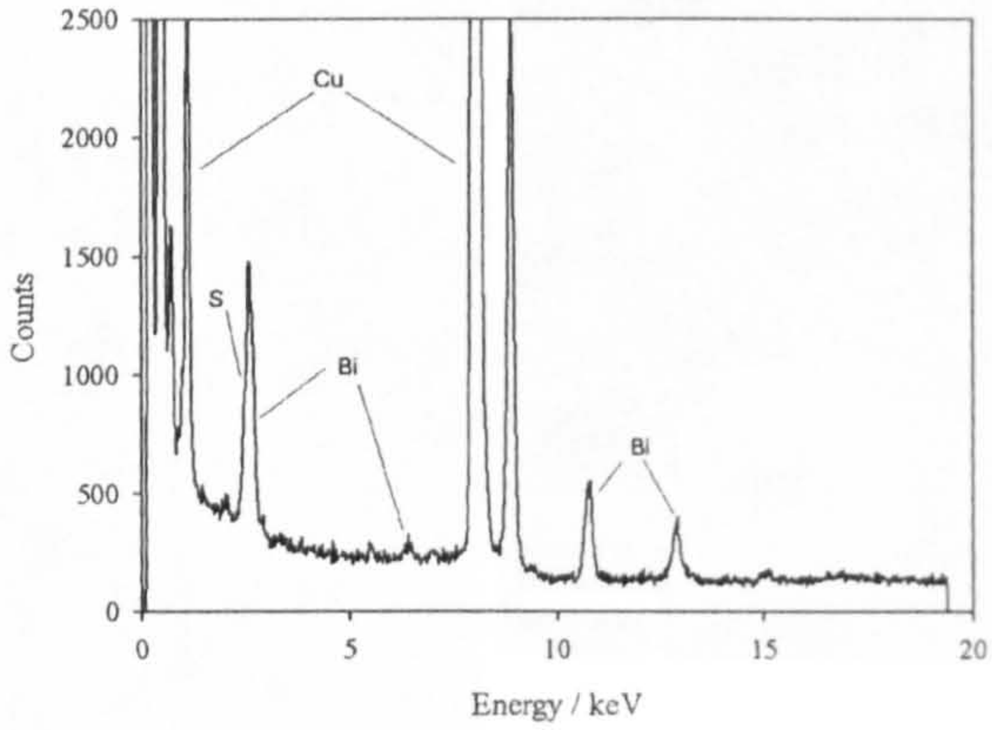

Figure 3.3: Energy dispersive X-ray Spectrum of sample Bi_2S_3 A.

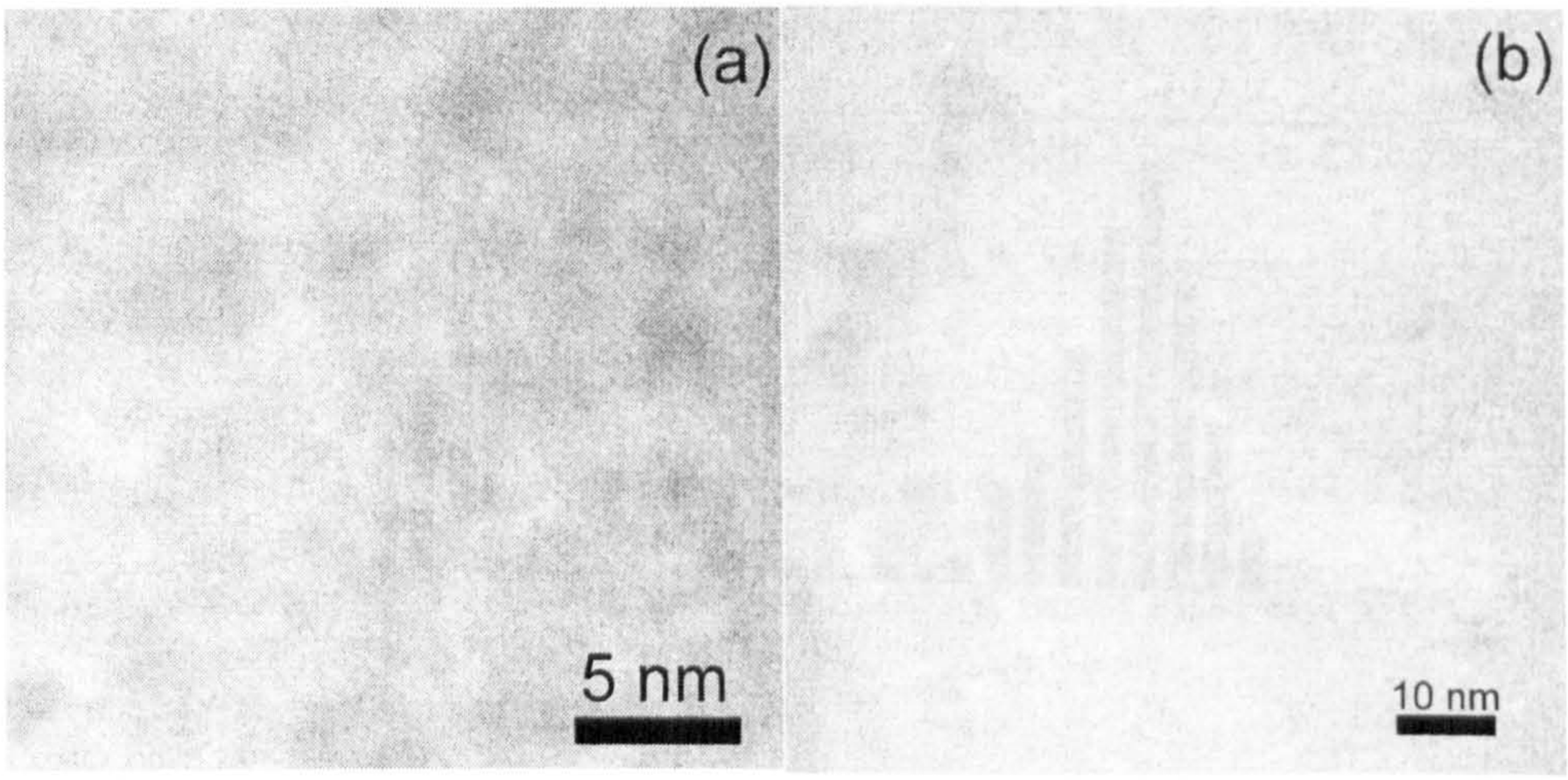

Figure 3.4: TEM images of samples a) Bi_2S_3 C and b) Bi_2S_3 D.

formation, above, along with the X-ray data, confirm the particles are Bi_2S_3.

Fig.3.4 shows typical TEM images of Bi_2S_3 C and Bi_2S_3 D. The size distributions of Bi_2S_3 C and Bi_2S_3 D, depicted in Fig.3.5, were statistically analysed in order to determine the average particle size and the standard deviation or error in this average size. The average particle diameters for Bi_2S_3 C and Bi_2S_3 D were found to be 2.1 $\pm$ 0.5 and 4.4 $\pm$ 1.2 nm as measured from 153 and 45 particles respectively.

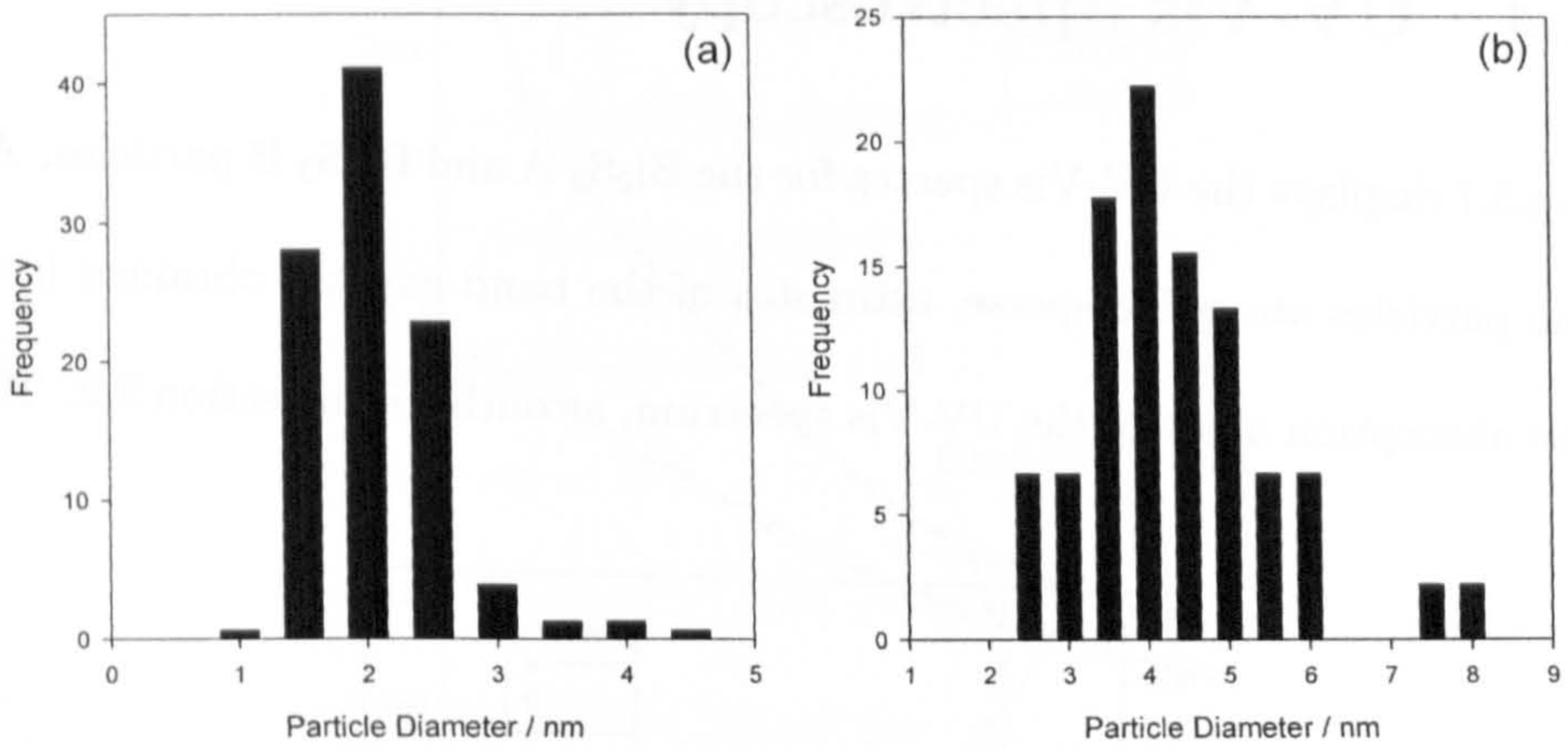

Figure 3.5: Size distribution of samples a) Bi_2S_3 C and b) Bi_2S_3 D.

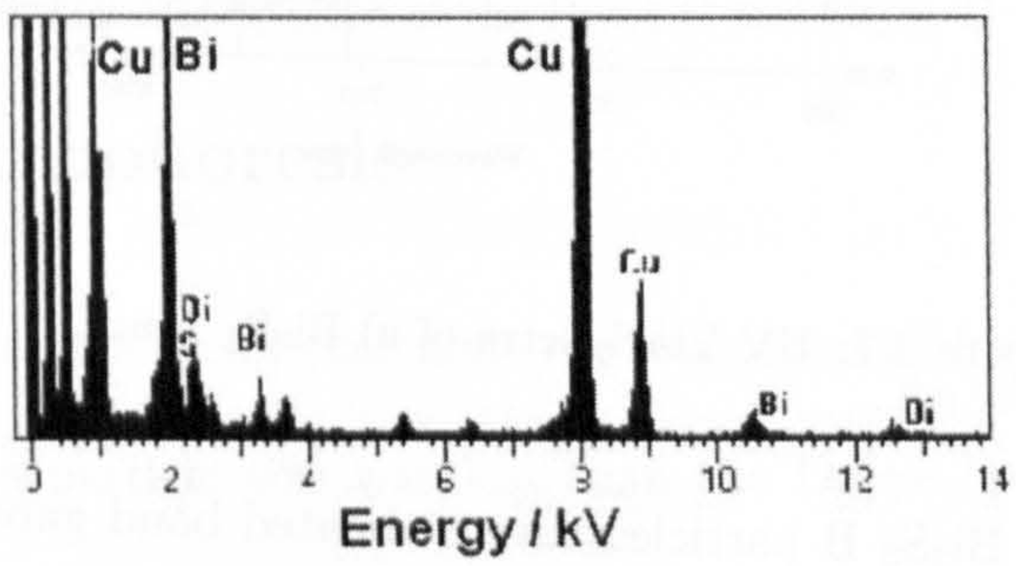

Figure 3.6: Energy dispersive X-ray Spectrum of sample Bi_2S_3 D.

Fig.3.6 displays the Energy Dispersive X-Ray analysis spectrum of Bi_2S_3 D and clearly shows the presence of bismuth in the sample. The presence of sulfur is not confirmed in this spectrum as the sulfur peak is obscured by the bismuth peak at 2.57 eV.

3.4 UV-Vis Spectroscopy

Fig.3.7 displays the UV-Vis spectra for the Bi_2S_3 A and Bi_2S_3 B particles. As the particles are polydisperse, estimates of the band gap are obtained from the absorption onset in the UV-Vis spectrum, as outlined in section 2.2. The

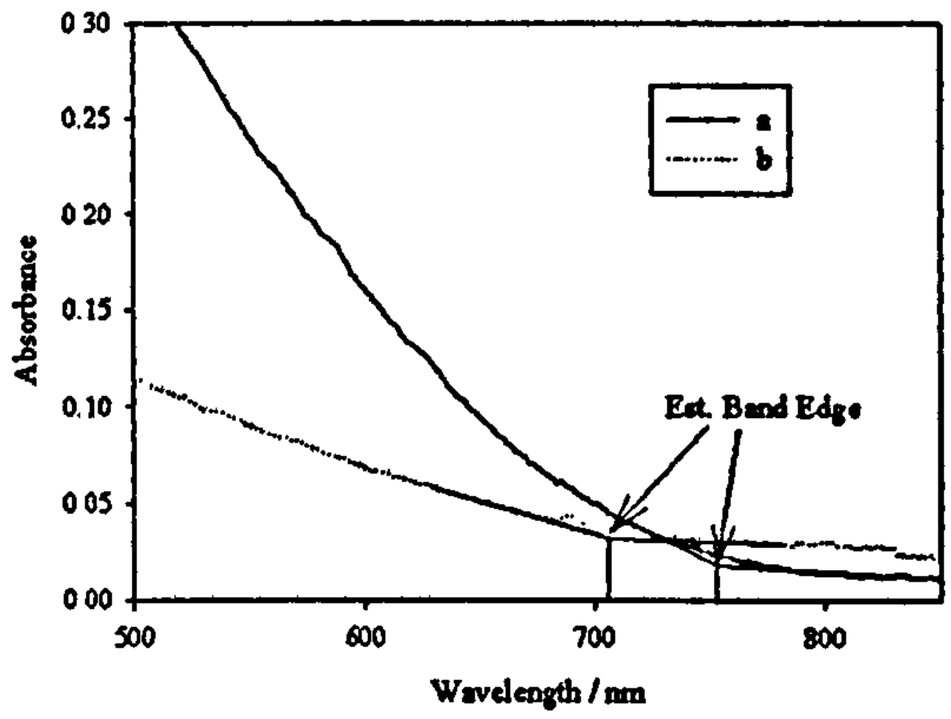

Figure 3.7: UV-Vis Spectra of a) Bi_2S_3 A and b) Bi_2S_3 B.

Bi_2S_3 A and Bi_2S_3 B particles have estimated band gaps of 1.6 and 1.7 eV respectively. The UV-Vis spectra for the Bi_2S_3 C and Bi_2S_3 D particles are illustrated in Fig.3.8. The band gaps for Bi_2S_3 C and Bi_2S_3 D were estimated to be 1.51 and 1.52 eV respectively according to the method used for polydisperse particles in solution as discussed in section 2.2.

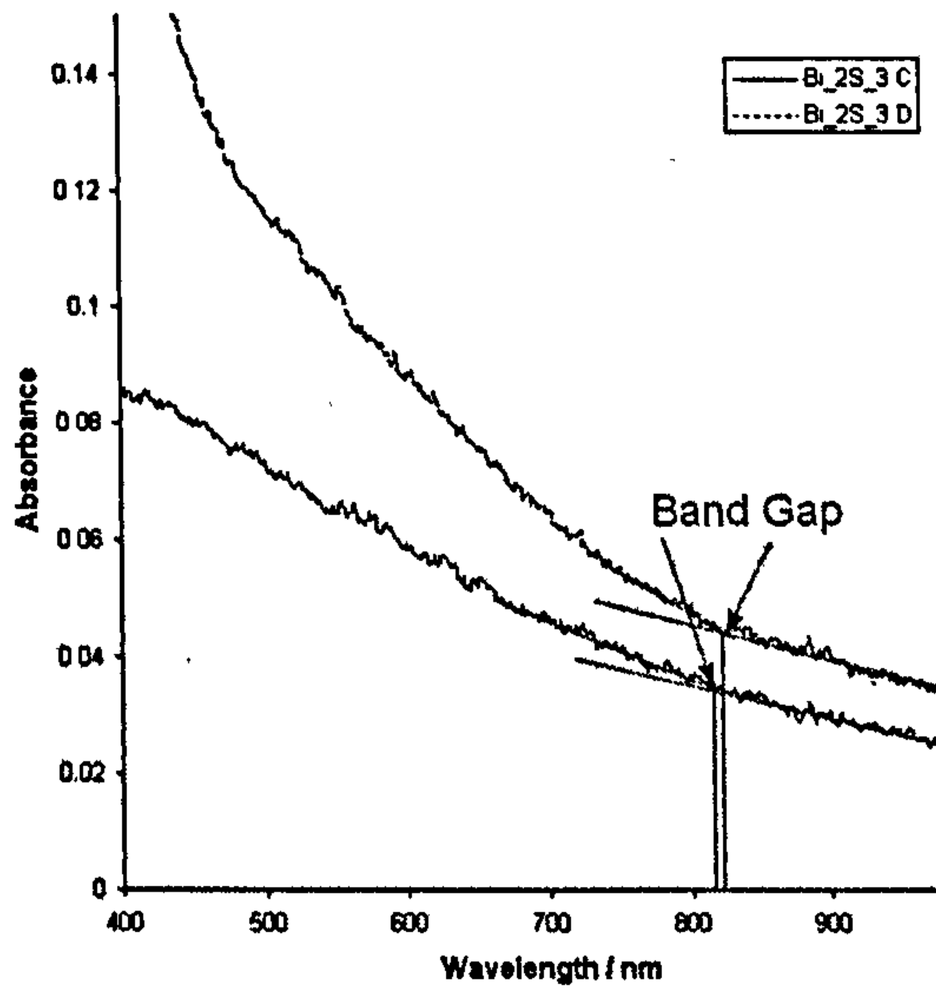

Figure 3.8: UV-Vis Spectra of the Bi_2S_3 C and Bi_2S_3 D samples.

3.5 Electrophoresis

The Hückel model was used to calculate the zeta potential from the measured mobilities as the particle size was less than the Debye length. The zeta potentials of the particles, found by electrophoresis, were -65.9 ± 2.6 mV and -25.7 ± 6.0 mV for the Bi_2S_3 A and Bi_2S_3 B particles respectively. By assuming the reaction of BiI_3 with H_2S goes to completion, the number of particles synthesised for each of the samples can be estimated and the total surface area can be calculated. This leads to the estimation of zeta potential per unit area to be -4300 mV m^{-2} and -1218 mV m^{-2} for the Bi_2S_3 A and Bi_2S_3 B particles respectively. From these estimates, it can be concluded that the surface of Bi_2S_3 A particles are more negatively charged than the surface of Bi_2S_3 B particles. This implies that the larger Bi_2S_3 A particles are coated with more 3-MPA molecules than the Bi_2S_3 B particles. However,

the opposite of this is expected, as the higher concentration of 3-MPA used in the preparation of Bi_2S_3 B particles terminates particle growth earlier than a low concentration of 3-MPA, by attaching more 3-MPA molecules to growth sites. As the I^- ions from the BiI_3 precursor, the higher negative charge observed for the Bi_2S_3 A particles could be due to high adsorption of the I^- ions on the particle compared to the Bi_2S_3 B particles, which have less sites available for I^- ion adsorption due to the higher concentration of 3-MPA molecules of the surface.

3.6 Photocurrent-Potential Curves

Fig.3.9 shows a current *vs.* potential curve for an electrode that was coated with Bi_2S_3 A and illuminated with chopped irradiation. It can be seen that there are two different phototransient responses. An immediate rise to a steady anodic photocurrent when the light was switched on and a rapid

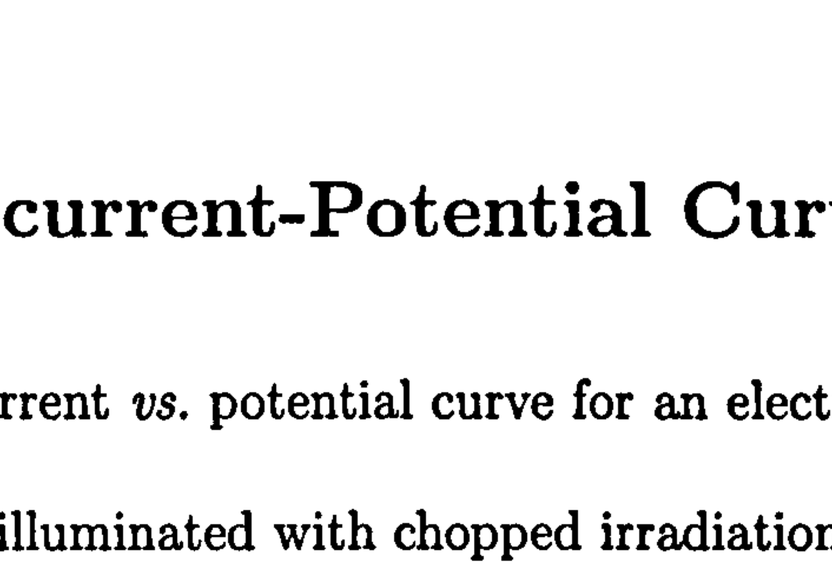

Figure 3.9: Photocurrent voltage curve of an electrode modified with Bi_2S_3 A nanoparticles. The potential was scanned from positive to negative potentials at a rate of 1 mV s^{-1} with the incident light chopped at 0.1 Hz.

decay to zero photocurrent on switch off is displayed in the current transient at potentials greater than -0.15 V. In contrast, at potentials less than -0.15 V, a slow decay transpires after the abrupt rise in anodic photocurrent that happens when the light is switched on and at switch off a cathodic current flows that relaxes to zero.

3.7 Photocurrent Spectroscopy

The IPCE spectra, recorded at 0 V vs Ag|AgCl|3 mol dm^{-3} KCl, for Bi_2S_3 A and Bi_2S_3 B particles are shown in Fig.3.10. The band gaps are 1.63 ± 0.03 and 1.71 ± 0.03 eV for Bi_2S_3 A and Bi_2S_3 B nanoparticles respectively. At a wavelength of 600 nm, less than 0.1 % of the incident photons were converted to electrons.

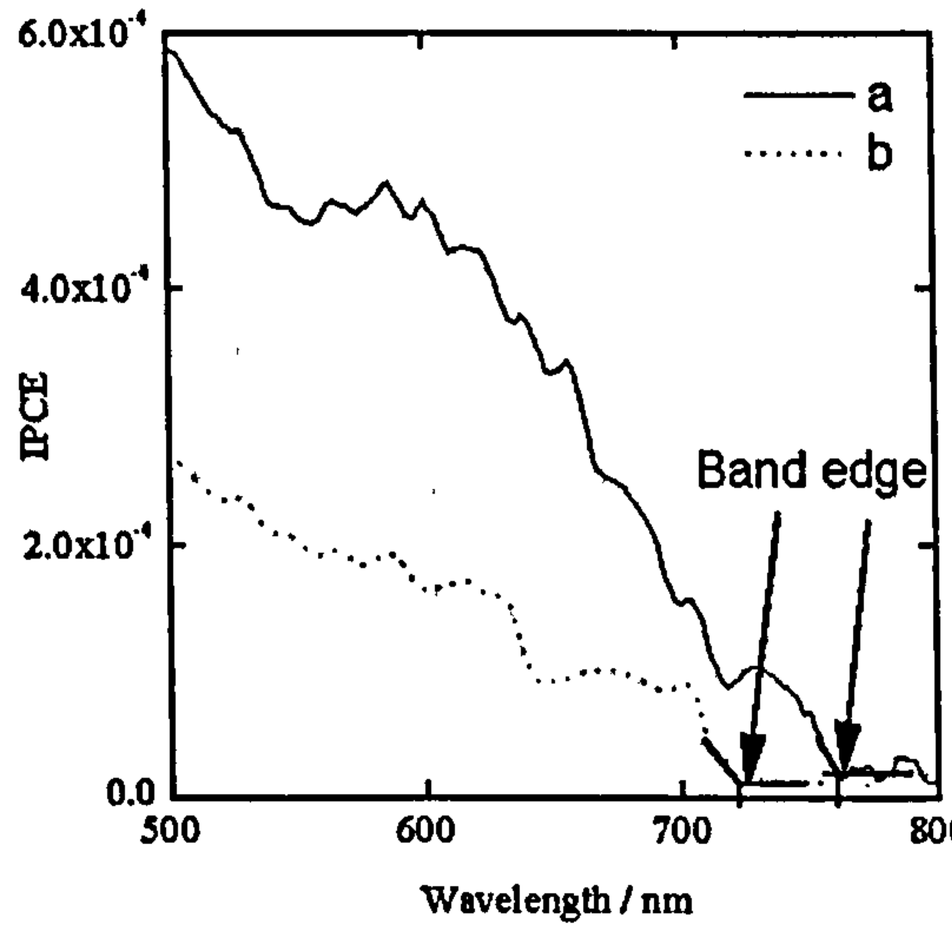

Figure 3.10: Photocurrent spectra of a) Bi_2S_3 A and b) Bi_2S_3 B.

3.8 Discussion

A significant change in the mean particle diameter of approximately 25% has been achieved by reducing the stabiliser concentration 200 times, demonstrating that the size of Bi_2S_3 particles prepared by arrested precipitation may be controlled by changing the stabiliser concentration. However, only a small shift in the bandgap, 1.63 ± 0.03 eV to 1.71 ± 0.03 eV, results from a marked change in mean particle diameter, 4.1 ± 1.0 nm to 3.0 ± 0.6 nm. The effective mass model of quantum confinement[43;44] may be used to estimate the dependence of semiconductor bandgap, E*, on the particle size according to equation 1.11. The electronic properties of Bi_2S_3 have not been well studied. The density of states relative electron effective mass of Bi_2S_3 has been calculated as 0.68[3]. Measurements indicate that the effective mass is anisotropic and is approximately 2.2 along the *a*-axis and 0.6 along the *c*-axis, therefore an effective mass of an electron of 0.68 probably represents a lower limit. The high frequency relative dielectric constant is 10.9[45]. As the p-doped material is impossible to make[46], the effective mass of a hole in bismuth sulfide is uncertain. The band gap of Bi_2S_3 as a function of particle size, using m_h in the range 0.8 - 2.4, and a bulk band gap of 1.57 eV is displayed in Fig.3.11. The range of m_h used was defined by the values that would fit the data for the Bi_2S_3A sample, within experimental error. From calculations using equation 1.11, a change in band gap of 0.1 eV on a increase of particle size from 2.9 nm to 4.1 nm requires a hole effective mass of 2.4. The band gap of CdS nanoparticles (E_g = 2.4 eV, m_e = 0.19, m_h = 0.8 and ϵ = 5.6)

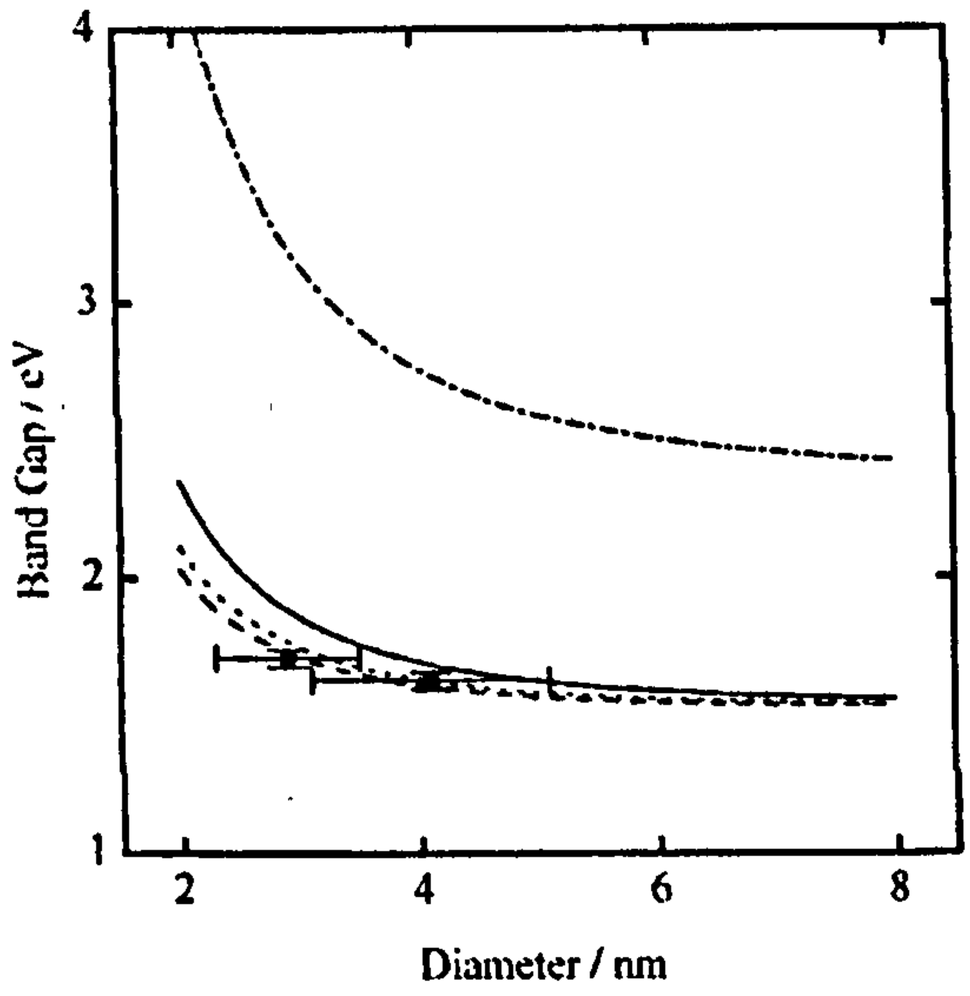

Figure 3.11: CdS and Bi_2S_3 semiconductor band gap dependence on particle size, calculated using the effective mass model of quantum confinement. $\epsilon = 10.9$, $m_e = 0.68$ and $m_h = 0.8$ (—), 1.6 ($\cdots$) or 2.4(– – –) for Bi_2S_3. $\epsilon = 5.6$, $m_e = 0.19$ and $m_h = 0.8$ for CdS($\cdot - \cdot$).

as a function of particle size is also shown in Fig.3.11 as a comparison. The change of band gap with particle size for Bi_2S_3 is much slower than that for CdS, as bismuth sulfide has a low electron mobility.

The photocurrent transients of electrodes coated with CdS particles exhibit similar potential dependent behaviour to that shown by an electrode coated with Bi_2S_3 A in Fig.3.9[47–49]. These results indicates that at approximately -0.15 V *vs.* Ag|AgCl|3.0 mol dm^{-3} KCl, there is a hole accepting state on Bi_2S_3. An electron is promoted from the valence band to the conduction band of the semiconductor upon illumination with supra-band gap irradiation. The photoexcited electron is transferred to the tin oxide substrate and the valence band hole is trapped in, or oxidises, the surface state. The surface

trap lies higher in energy than the Fermi level of the tin oxide, at potentials greater than -0.15 V. Therefore, the majority of holes are captured by the electrolyte and an anodic current flows. At potentials less than -0.15 V, the trap state is at lower energy than the Fermi level of the substrate. Hence, two electron transfer processes exist in competition. These processes are the hole capture by the electrolyte and the electron transfer from the substrate to the oxidised trap state, termed back electron transfer. Initially, there are no holes trapped in the surface states in Bi_2S_3, so the first excited electron produced in each particle is unlikely to undergo back electron transfer. After this, holes are trapped in the surface state and back electron transfer occurs, decreasing the photocurrent until the population of holes trapped in the surface is constant. This results in a sharp photoanodic peak occurring in the photocurrent transient when the light is switched on, followed by a decay in the photocurrent to a lower constant value, as found in the observed transients. After the light is turned off, the back electron transfer process is continued giving rise to the cathodic current observed. The electron transfer processes observed at potentials less than -0.15 V are shown schematically in Fig.3.12.

Comparison of the particle sizes and the band gaps found from the TEM images and absorption spectra of the Bi_2S_3 C and Bi_2S_3 D indicates that the band gap is extremely difficult to tune by changing the size of the nanoparticles. The absorption properties of Bi_2S_3 nanoparticles can not be tuned to match the solar spectrum due to the limited change in band gap with particle size. Hence these particles are not ideal for sensitisation of TiO_2 in solar cells.

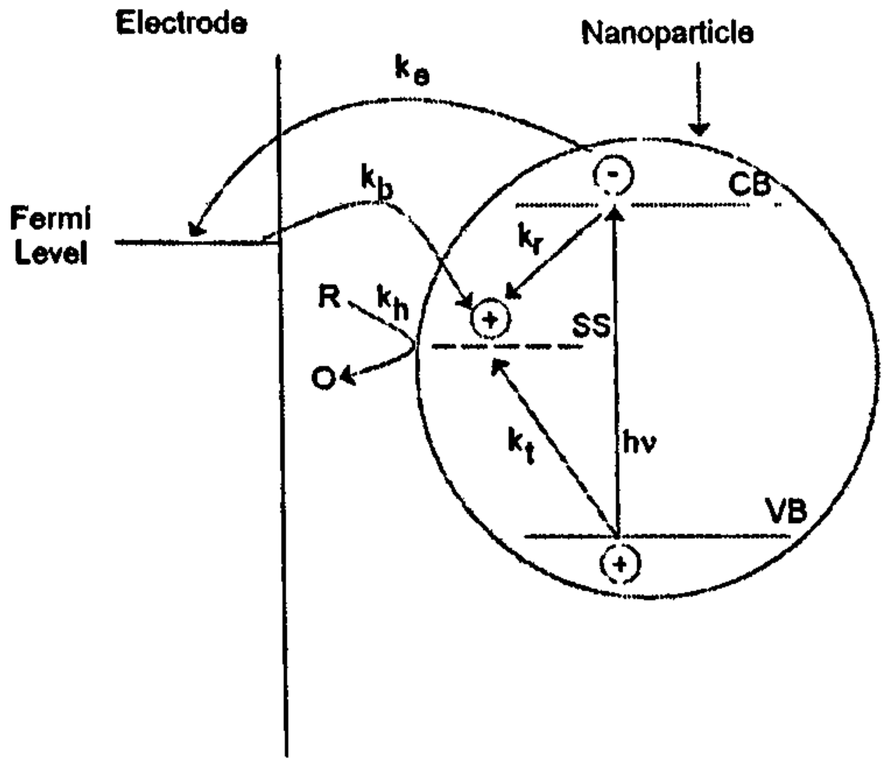

Figure 3.12: A schematic of the charge transfer processes occurring in Bi_2S_3 coated electrode in electrolyte system. SS = a surface state, R = reduced form of the electrolyte hole scavenger, O = oxidised form of the electrolyte hole scavenger, k_t, k_r, k_e, k_h and k_b = the rate constants of trapping a hole in the surface state, recombination, electron transfer, hole transfer and back electron transfer respectively.

3.9 Summary

Bismuth sulfide nanoparticles have been prepared by an arrested precipitation technique. These particles exhibit photocurrent properties and a hole trapping surface state was observed at -0.15 V. However the band gap was determined to undergo a limited change upon changing the particle size, therefore the use of these particles as a sensitiser of TiO_2 in solar cells is not ideal.

References

[1] Riley, D. J.; Waggett, J. P.; Wijayantha, K. G. U. *J. Mater. Chem.* **2004**, *14*(4), 704–708.

[2] Suarez, R.; Nair, P. K.; Kamat, P. V. *Langmuir* **1998**, *14*(12), 3236–3241.

[3] Cantarero, A.; Martinezpastor, J.; Segura, A.; Chevy, A. *Phys. Rev. B* **1987**, *35*(18), 9586–9590.

[4] Grigas, J.; Talik, E.; Lazauskas, V. *Phys. Status Solidi B* **2002**, *232*(2), 220–230.

[5] Larson, R.; Greanya, V. A.; Tonjes, W. C.; Liu, R.; Mahanti, S. D.; Olson, C. G. *Phys. Rev. B* **2002**, *65*(8), art. no. –085108.

[6] Wang, H.; Zhu, J. J.; Zhu, J. M.; Chen, H. Y. *J. Phys. Chem. B* **2002**, *106*(15), 3848–3854.

[7] Wang, S. Y.; Du, Y. W. *J. Cryst. Growth* **2002**, *236*(4), 627–634.

[8] Liao, X. H.; Wang, H.; Zhu, J. J.; Chen, H. Y. *Mater. Res. Bull.* **2001**, *36*(13-14), 2339–2346.

[9] Liao, X. H.; Zhu, J. J.; Chen, H. Y. *Mater. Sci. Eng. , B* **2001**, *85*(1), 85–89.

[10] Zhang, W. X.; Yang, Z. H.; Huang, X. M.; Zhang, S. Y.; Yu, W. C.; Qian, Y. T.; Jia, Y. B.; Zhou, G. I.; Chen, L. *Solid State Commun.* **2001**, *119*(3), 143–146.

[11] Yu, S. H.; Yang, J.; Wu, Y. S.; Han, Z. H.; Xie, Y.; Qian, Y. T. *Mater. Res. Bull.* **1998**, *33*(11), 1661–1666.

[12] Shao, M. W.; Mo, M. S.; Cui, Y.; Chen, G.; Qian, Y. T. *J. Cryst. Growth* **2001**, *233*(4), 799–802.

[13] Yu, S. H.; Qian, Y. T.; Shu, L.; Xie, Y.; Yang, L.; Wang, C. S. *Mater. Lett.* **1998**, *35*(1-2), 116–119.

[14] Yu, S. H.; Shu, L.; Yang, J. A.; Han, Z. H.; Qian, Y. T.; Zhang, Y. H. *J. Mater. Res.* **1999**, *14*(11), 4157–4162.

[15] Larionov, S. V. ; Patrina, L. A. . U. E. M. *Ser. Khim. Nauk* **1979**, *3*, 94.

[16] Cyganski, A.; Kobylecka, J. *Thermochimica Acta* **1981**, *45*(1), 65–77.

[17] Popov, V. N. ; Kolodezev, A. B. S. V. P. *Appar. Kach. Prom. Lyuminoforov* **1977**, page 98.

[18] Nomura, R.; Kanaya, K.; Matsuda, H. *Bull. Chem. Soc. Japan* **1989**, *62*(3), 939–941.

[19] Nair, P. K.; Nair, M. T. S.; Garcia, V. M.; Arenas, O. L.; Pena, Y.; Castillo, A.; Ayala, I. T.; Gomezdaza, O.; Sanchez, A.; Campos, J.; Hu, H.; Suarez, R.; Rincon, M. E. *Sol. Energy Mater. Sol. Cells* **1998**, *52*(3-4), 313–344.

[20] Mane, R. S.; Sankapal, B. R.; Lokhande, C. D. *Mater. Res. Bull.* **2000**, *35*(4), 587–601.

[21] Mane, R. S.; Lokhande, C. D. *Mater. Chem. Phys.* **2000**, *65*(1), 1–31.

[22] Huang, L.; Nair, P. K.; Nair, M. T. S.; Zingaro, R. A.; Meyers, E. A. *Thin Solid Films* **1995**, *268*(1-2), 49–56.

[23] Rincon, M. E.; Sanchez, M.; George, P. J.; Sanchez, A.; Nair, P. K. *J. Solid State Chem.* **1998**, *136*(2), 167–174.

[24] Nair, M. T. S.; Nair, P. K. *Semicond. Sci. Technol.* **1990**, *5*(12), 1225–1230.

[25] Desai, J. D.; Lokhande, C. D. *Ind. J. Pure Appl. Phys.* **1994**, *32*, 964.

[26] Pramanik, P.; Bhattacharya, R. N. *J. Electrochem. Soc.* **1980**, *127*, 2087.

[27] Battacharya, R. N.; Pramanik, P. *J. Electrochem. Soc.* **1982**, *129*, 332.

[28] Biswa, S.; Mondal, A.; Mukharjee, D.; Pramanik, P. *J. Electrochem. Soc.* **1986**, *133*, 48.

[29] Desai, J. D.; Lokhande, C. D. *Ind. J. Pure Appl. Phys.* **1993**, *31*, 152.

[30] Desai, J. D.; Lokhande, C. D. *Mater. Chem. Phys.* **1995**, *42*, 98.

[31] Desai, J. D.; Lokhande, C. D. *SAEST* **1994**, *29*, 111.

[32] Desai, J. D.; Lokhande, C. D. *Mater. Chem. Phys.* **1993**, *34*, 313.

[33] Lokhande, C. D.; Ubale, A. U.; Patil, P. S. *Thin Solid Films* **1997**, *302*, 1.

[34] Nair, P. K.; Campos, J.; Sanchez, A.; Banos, L.; Nair, M. T. S. *Semicond. Sci. Technol.* **1991**, *6*(5), 393–396.

[35] Deshmukh, L. P.; Zipre, K. V.; Palve, A. B.; Rane, B. P.; Hankare, P. P.; Manikshete, A. H. *Solar Energy Mater. Solar Cells* **1992**, *28*, 249.

[36] Nair, P. K.; Nair, M. T. S.; Gomezdaza, O.; Zingaro, R. A. *J. Electrochem. Soc.* **1993**, *140*, 1085.

[37] Mane, R. S.; Sankapal, B. R.; Lokhande, C. D. *Mater. Chem. Phys.* **1999**, *60*, 196.

[38] Acharya, B. S.; Naik, B. B.; Rath, D. P. *Ind. J. Phys. Part A* **1986**, *60*, 71.

[39] Lukose, J.; Pradeep, B. *Solid State Commun.* **1991**, *78*(6), 535–538.

[40] Vogel, R.; Hoyer, P.; Weller, H. *J. Phys. Chem.* **1994**, *98*, 3183.

[41] Peter, L. M.; Wijayantha, K. G. U.; Riley, D. J.; Waggett, J. P. *J. Phys. Chem. B* **2003**, *107*, 8378–8381.

[42] Peter, L. M.; Riley, D. J.; Tull, E. T.; Wijayantha, K. G. U. *Chem. Commun.* **2002**, *10*, 1030–1031.

[43] Pesika, N. S.; Hu, Z. S.; Stebe, K. J.; Searson, P. C. *J. Phys. Chem. B* **2002**, *106*(28), 6985–6990.

[44] Brus. *J. Chem. Phys.* **1984**, *80*(9), 4406–4409.

[45] Cantarero, A.; Martinez, J. P.; Segura, A.; Chevy, A. *Phys. Status Solidi A* **1987**, *101*(2), 603–609.

[46] Bacewicz, R.; Ciszek, T. F. *J. Cryst. Growth* **1991**, *109*(1-4), 133–136.

[47] Hickey, S. G.; Riley, D. J.; Tull, E. J. *J. Phys. Chem. B* **2000**, *104*(32), 7623–7626.

[48] Hickey, S. G.; Riley, D. J. *Electrochim. Acta* **2000**, *45*(20), 3277–3282.

[49] Bakkers, E. P. A. M.; Reitsma, E.; Kelly, J. J.; Vanmaekelbergh, D. *J. Phys. Chem. B* **1999**, *103*, 2781.

Chapter 4

Preparation of Cadmium Sulfide, Ruthenium Sulfide and Copper Sulfide Nanoparticles in Oleylamine

4.1 Introduction

In 2003 Joo *et al.*[1] reported a general method for synthesising metal sulfide nanoparticles. This method involved preparing metal-oleylamine complexes by heating the metal chloride in oleylamine and then adding a solution of sulfur in oleylamine, followed by further heating. Monodisperse crystalline nanometer sized particles of CdS, PbS, ZnS and MnS have been produced by Joo *et al.* using this method. In the case of cadmium sulfide, this resulted in nanorods, with an average thickness of 5.4 nm and an average length of

20 nm when a cadmium to sulfur ratio of 1:6 was used, or spherical particles, with an average diameter of 5.1 nm when a cadmium to sulfur ratio of 2:1 was used. The sizes of the particles were measured using TEM. Absorption spectroscopy indicated that the spherical CdS particles had a band gap of 2.63 eV. The above method was used to prepare 13 nm diameter PbS particles, 11 nm diameter ZnS particles and 5.1 nm diameter CdS particles and excitonic peaks at 310 nm and 472 nm were observed for the ZnS and CdS particles respectively. The sizes were found from TEM images. No photoelectrochemical properties of particles prepared from this method and deposited on an electrode have been reported. This synthesis will hereafter be referred to as the oleylamine method.

4.1.1 Compounds to be prepared using the oleylamine method

The oleylamine method appeared to be a simple way of preparing nanoparticles of any metal sulfide. Here cadmium sulfide, ruthenium sulfide and copper (I) sulfide nanoparticles were prepared using this method and the properties of these particles studied. As the oleylamine method was used to prepare cadmium sulfide by Joo *et al.*[1] and the properties of CdS nanoparticles have been widely investigated, cadmium sulfide particles were prepared using the oleylamine method as a preliminary test of the method. Previous work on CdS deposited on an electrode has been discussed in section 1.2.4. Ruthenium sulfide and copper (I) sulfide nanoparticles prepared using the

oleylamine method were studied as these particles have not been previously prepared using the oleylamine method and have appropriate physical properties for use as sensitisers in solar cells, as discussed below. The preference for copper (I) sulfide nanoparticles over copper (II) sulfide nanoparticles is also discussed. Ruthenium sulfide may be a suitable sensitiser for use in a solar cell as it has been reported that the bulk band gap is 1.3 eV[2]. Ruthenium sulfide is also known to be very photostable. Copper (I) sulfide and copper (II) sulfide nanoparticles have been prepared by a variety of methods. As copper (I) sulfide has a band gap of 1.21 eV[3] and copper (II) sulfide has a band gap of 2 eV[4], Cu_2S particles are the preferred particles to synthesise for the sensitisation of TiO_2 in solar cells.

4.1.2 Ruthenium Sulfide

A variety of methods have been employed to produce RuS_2 nanoparticles and thin films in order to study the photocatalytic and photocurrent properties of the particles.

4.1.3 Ruthenium Sulfide Syntheses

Electrodeposition Methods

Gurunathan *et al.*[5] prepared RuS_2 thin films by electrodeposition on Ti and conducting glass substrates. This method involved cathodic deposition on the substrates in a bath containing $RuCl_3$, $Na_2S_2O_3$ and Na_2SO_4 and resulted in a poly-crystalline thin film with a band gap of 1.48 eV. The average size

of the grains in the film was determined to be 3 μm using SEM. Due to the large size of the grains, the observed band gap was expected to be the bulk band gap, however, an unexplained difference between the measured band gap and the bulk band gap of 1.3 eV was found.

Solution Methods

Hara *et al.*[6] and Jobic *et al.*[7] synthesised RuS_2 particles on SiO_2 by depositing $RuCl_3$ on SiO_2 followed by exposure to H_2S gas at 400 °C. Hara *et al.*[6] reported on the photocatalytic properties of RuS_2 on SiO_2 with respect to water decomposition. Adsorption of hydrogen on ruthenium sulfide prepared by this method was discussed by Jobic *et al.*[7].

Passeretti *et al.*[8] employed the reaction between H_2S gas and $(NH_4)_2RuCl_6$ in order to prepare ruthenium sulfide. This resulted in a poorly crystallised material. Crystallisation of the material was observed after annealing at a temperature of 350 °C or higher, which resulted in crystals with an estimated size of 2.6 nm, as calculated from the X-ray diffraction peaks using the Debye-Scherrer equation.

RuS_2 nanoparticles have been synthesised by bubbling hydrogen sulfide through $RuCl_3$ solutions in water and sulfolane by Ashokkumar *et al.*[2]. The particles had an estimated average size of 10 nm, as calculated from the X-ray diffraction peaks using the Debye Scherrer equation. These particles were deposited on TiO_2 electrodes and the absorption, photoluminescence and photocurrent spectra of these electrodes were studied. The photocurrent spectra displayed a low sensitisation efficiency, while broad features were

observed in the absorption and photoluminescence spectra indicating a broad size distribution.

Reverse Micelle Methods

Hirai *et al.*[9] prepared ruthenium sulfide nanoparticles, smaller than 3 nm in size, in a reverse micelle system. This synthesis involved the injection of H_2S gas into a reverse micellar system consisting of bis(2-ethylhexyl)sulfosuccinate (aerosol OT, AOT), water containing $RuCl_3$ and iso-octane. The resulting particles were then immobilised on polystyrene particles modified with a thiol. This resulted in particles with a diameter of less than 3 nm as measured by TEM. The photocatalytic properties of the ruthenium sulfide particles have been reported by Hirai *et al.*[9].

4.1.4 Copper Sulfide

A number of methods have used in order to prepare copper (I) sulfide nanoparticles.

4.1.5 Synthetic Methods for producing Copper (I) Sulfide

Solvothermal Methods

Lu *et al.*[10;11] employed an organic ligand assisted solvothermal method in order to synthesise Cu_2S nanoparticles. This technique involved the dissolution of triethylenediamine, trimethylethylenediamine or di-n-butylamine in

a thiourea solution and addition of CuCl followed by heating the resultant mixture to 110 °C in a Teflon lined bomb. Nanorods, nanotubes and nanoparticles consisting of polycrystalline Cu_2S were produced by this method depending on the organic ligand used, as detailed in Table 4.1, the sizes were determined via TEM. The particles were shown to consist of copper (I) sulfide

Stabiliser	Morphology	Dimensions
triethylenediamine	nanorods	120 x 2000 nm
trimethylethylenediamine	nanotubes	ϕ 40 - 200 nm, | 400 - 4000 nm
di-n-butylamine	nanovesicles	between 50 and 180 nm

Table 4.1: Morphologies of copper (I) sulfide particles prepared by Lu *et al.*[10;11].

from the selected area electron diffraction pattern. The UV-visible spectra of Cu_2S produced by this method have been reported and showed a peak at 555 nm.

Preparations in Microemulsions

Copper sulfide nanoparticles have been synthesised in water-in-oil microemulsions by Haram *et al.*[12]. A copper ammonia complex and thiourea were emulsified in a non-ionic surfactant solution (such as polyoxyethylene teoctylphenyl ether, polyoxyethylenes and sodium dodecyl sulfate) in cyclohexane or toluene. These emulsions were then stabilised by the addition of 2-methylpropan-1-ol and the copper sulfide particles were produced by mixing the thiourea and copper ammonia complex containing microemulsions. This resulted in copper

sulfide particles with a band gap of 2.6 eV, as determined from the absorption spectra[12]. The authors inferred, from comparison with other absorption spectra, that copper (I) sulfide particles were produced. The particles are thought to form on the inside wall of a polyoxyethylene teoctylphenyl ether inverse micelle, as shown in Fig. 4.1.

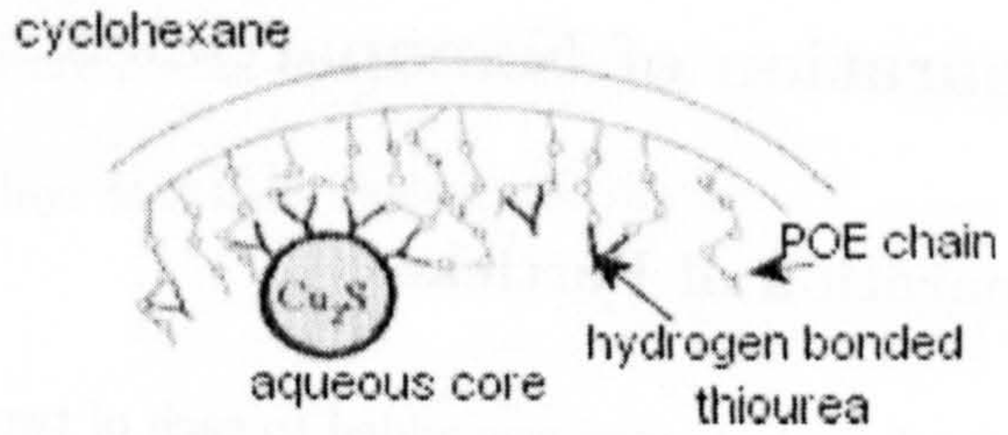

Figure 4.1: Schematic of the formation of Cu_2S particles on the inner wall of polyoxyethylene teoctylphenyl ether inverse micelles. POE = polyoxyethylene.

Solution Methods

Kore *et al.*[13] reported the disproportionation of Cu_2S nanoparticles in aqueous solutions. Copper (I) sulfide was prepared from mixing copper acetate with sodium sulfide in aqueous solution. Absorption spectra of the resulting particles were measured by Kore *et al.*[13] over a period of time. In the spectra an increase over time in the peak height for a feature that corresponded to CuS was observed. It was suggested that the Cu_2S particles were gradually decomposing to CuS. Kore *et al.*[13] analysed these results to find the rate constant of this decomposition to be 3.72 x 10 $^{-5}$ s^{-1}, assuming the following reaction:

$$Cu_2S \xrightarrow{k} CuS + Cu^0 \tag{4.1}$$

This chapter will discuss the preparation and characterisation of cadmium sulfide, ruthenium sulfide and copper sulfide nanoparticles. The as-prepared particles were deposited on tin oxide electrodes and the photocurrent response of the particles prepared using the oleylamine methods investigated.

4.2 Preparation of Nanoparticles

4.2.1 Preparation of Particles

In a dry box, 2.5 ml of oleylamine was added to each of two vials containing a known amount of i) sulfur and ii) $CdNO_3.4H_2O$, $RuCl_3$ or CuI respectively. The vials were then heated to 90°C for 30 mins and then mixed. The resulting mixture was then heated to 160°C for 1 hour. After being allowed to cool to room temperature, 50 ml ethanol was added and the solution was filtered through a 350 μm nylon filter. The resulting solid was resuspended in hexane.

The quantities of the chemicals used in the preparation of cadmium sulfide, ruthenium sulfide and copper sulfide nanoparticles are outlined in Table 4.2

Heavy Metal Source	wt of heavy metal source / g	wt of S used / g
$CdNO_3.4H_2O$	0.1575	0.0082
$RuCl_3$	0.0522	0.008
CuI	0.195	0.0325

Table 4.2: Quantities of chemicals used in the preparation of CdS, RuS and CuS nanoparticles.

4.2.2 Deposition on Conducting Tin Oxide Glass

Clean tin oxide coated glass slides were hydrolysed in 5 mol dm^{-3} potassium hydroxide solution for *ca.* 2 hours, washed and dried. The slides were then immersed, face up, in a 10 % 3-mercaptopropyltrimethyl silane solution overnight in order to obtain an -SH functionalised surface, washed and dried. Then the slides were placed in a solution containing the nanoparticles to be deposited for 4 days and then washed and dried.

4.3 Characterisation

4.3.1 UV-Vis Spectroscopy

Fig.4.2 displays the UV-Visible spectra of the cadmium sulfide, ruthenium sulfide and copper sulfide particles. Non-zero baselines were observed due

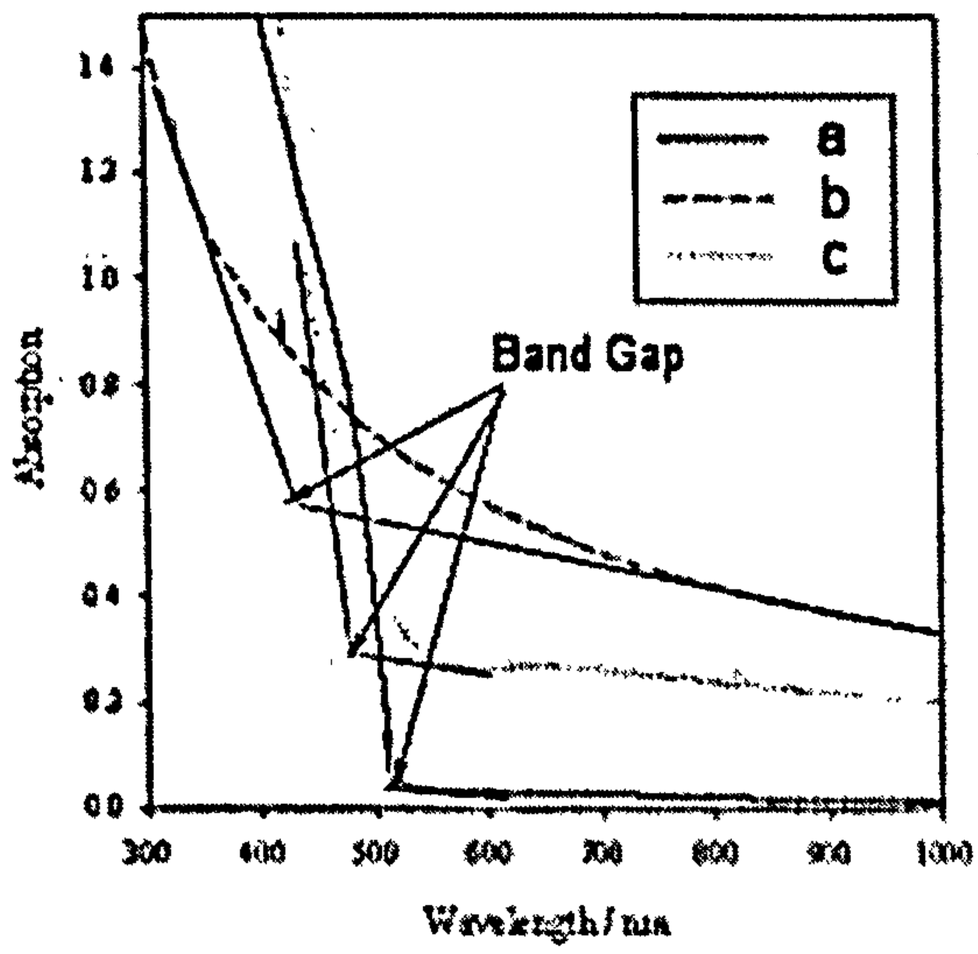

Figure 4.2: UV-Vis spectra of a) CdS, b) RuS and c) CuS nanoparticles.

to the scattering of light by the particles in solution. The band gaps of the materials have been estimated from the wavelength of the absorption edge using equation 2.3 as outlined in section 2.2 and are shown in Table. 4.3.

Material	Absorption edge / nm	Estimated Band Gap /eV	Band gap from literature / eV
Cadmium Sulfide	515	2.41	2.42
Ruthenium Sulfide	800	1.4	1.3
Copper Sulfide	485	2.56	1.2

Table 4.3: Estimated band gaps of materials prepared using the oleylamine method.

4.3.2 Transmission Electron Microscopy

Typical TEM images of cadmium sulfide, ruthenium sulfide and copper sulfide nanoparticles are shown in Fig.4.3. Table.4.4 displays the average particle size of the materials produced as calculated by statistical analysis of the size distributions illustrated in Fig.4.4. The number of particles used in the calculation are also included in the table and the errors were calculated as the standard deviation of the sample.

The Energy Dispersive X-Ray analysis spectra of cadmium sulfide, ruthenium sulfide and copper sulfide are displayed in Fig.4.5.

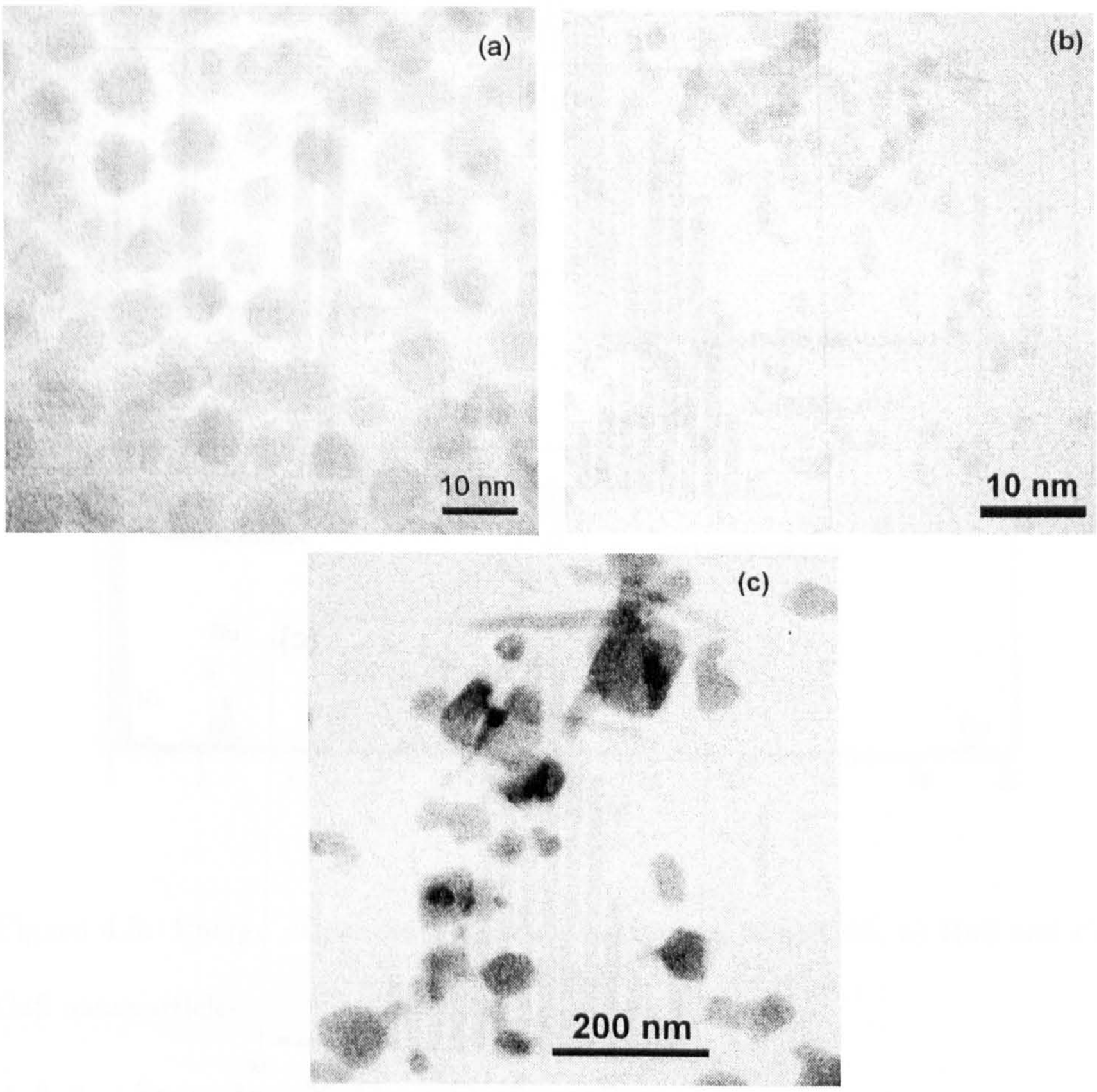

Figure 4.3: TEM images of a) CdS, b) RuS and c) CuS nanoparticles.

Material	Particle diameter / nm	sample size
Cadmium Sulfide	7.4 ± 0.9	388
Ruthenium Sulfide	1.4 ± 0.5	361
Copper Sulfide	39.4 ± 16.8	481

Table 4.4: Average particle diameter of cadmium sulfide, ruthenium sulfide and copper sulfide particles with the respective number of measurements used in the statistical analysis.

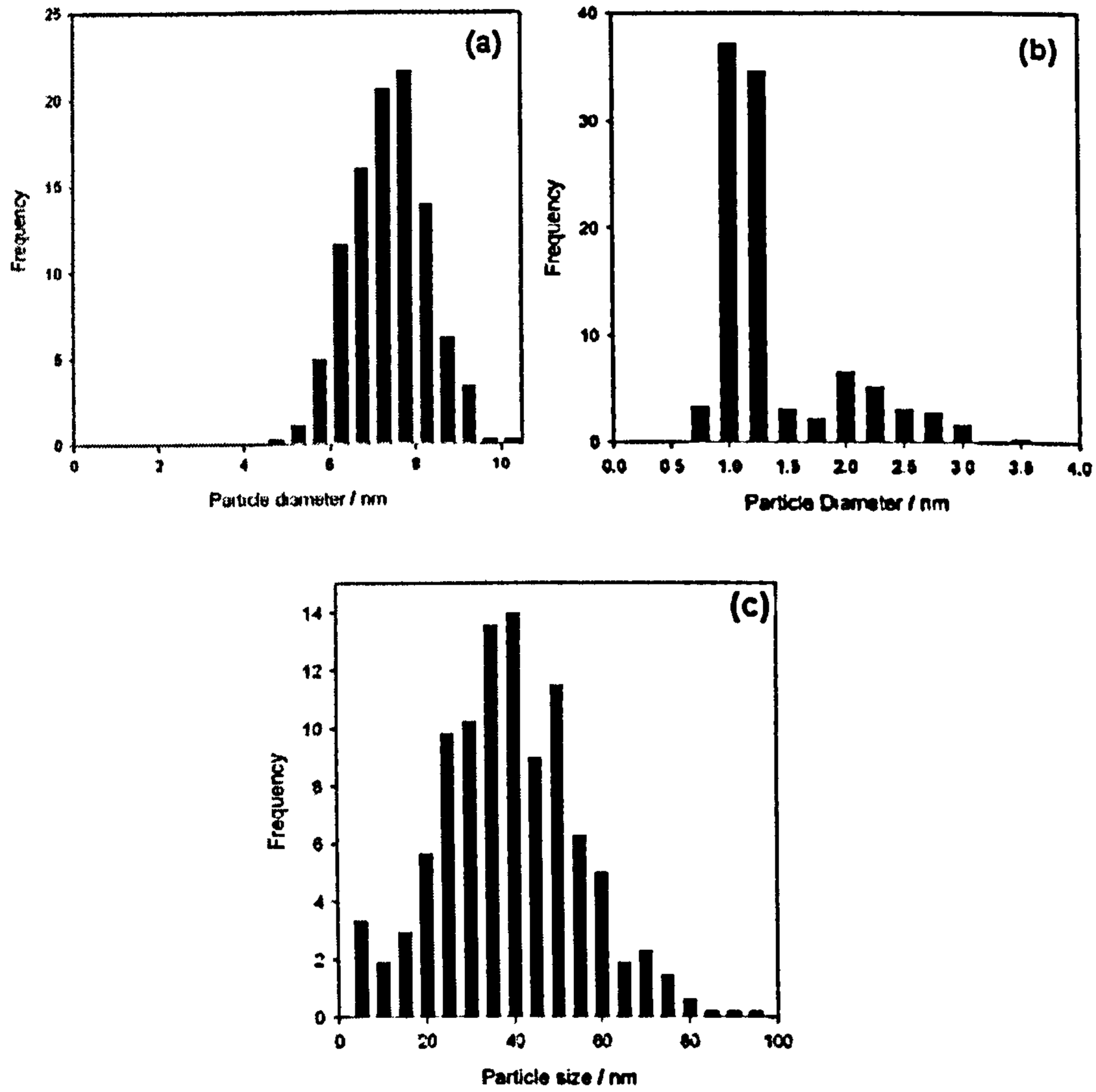

Figure 4.4: Size distributions of a) CdS, b) RuS and c) CuS nanoparticles.

These confirm the presence of the components of the compounds. The copper peaks in the cadmium sulfide spectrum are present as the supporting grid is composed of copper. Nickel peaks were observed in the ruthenium sulfide spectrum, as a nickel grid was used. A nickel grid was used to support the copper sulfide particles, therefore the copper peaks in Fig.4.5c are due to the copper in the particles, while the nickel peaks originate from the supporting grid.

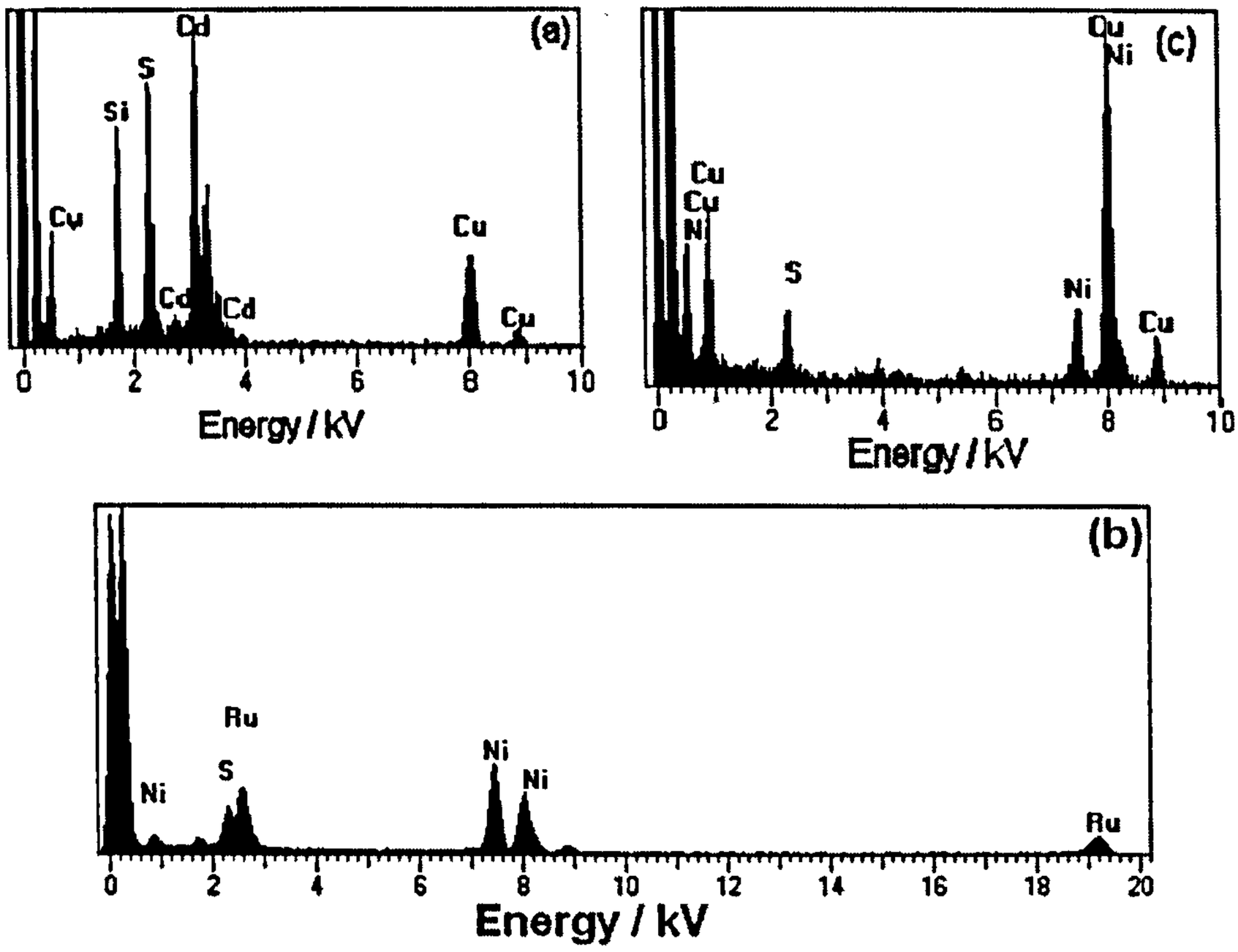

Figure 4.5: Energy dispersive x-ray analysis spectra of a) CdS, b) RuS and c) CuS nanoparticles.

4.3.3 Powder X-Ray Diffraction

Fig. 4.6 shows the powder X-ray diffraction pattern obtained from cadmium sulfide, ruthenium sulfide and copper sulfide particles and the known X-ray diffraction pattern of hexagonal CdS particles is also shown. This demonstrates that the cadmium sulfide particles are crystalline, while the ruthenium sulfide and copper sulfide particles are amorphous. The CdS particles have a hexagonal lattice structure as shown by the match between peaks in the measured powder X-ray diffraction pattern for the CdS particles and the known X-ray diffraction pattern of CdS with a hexagonal structure.

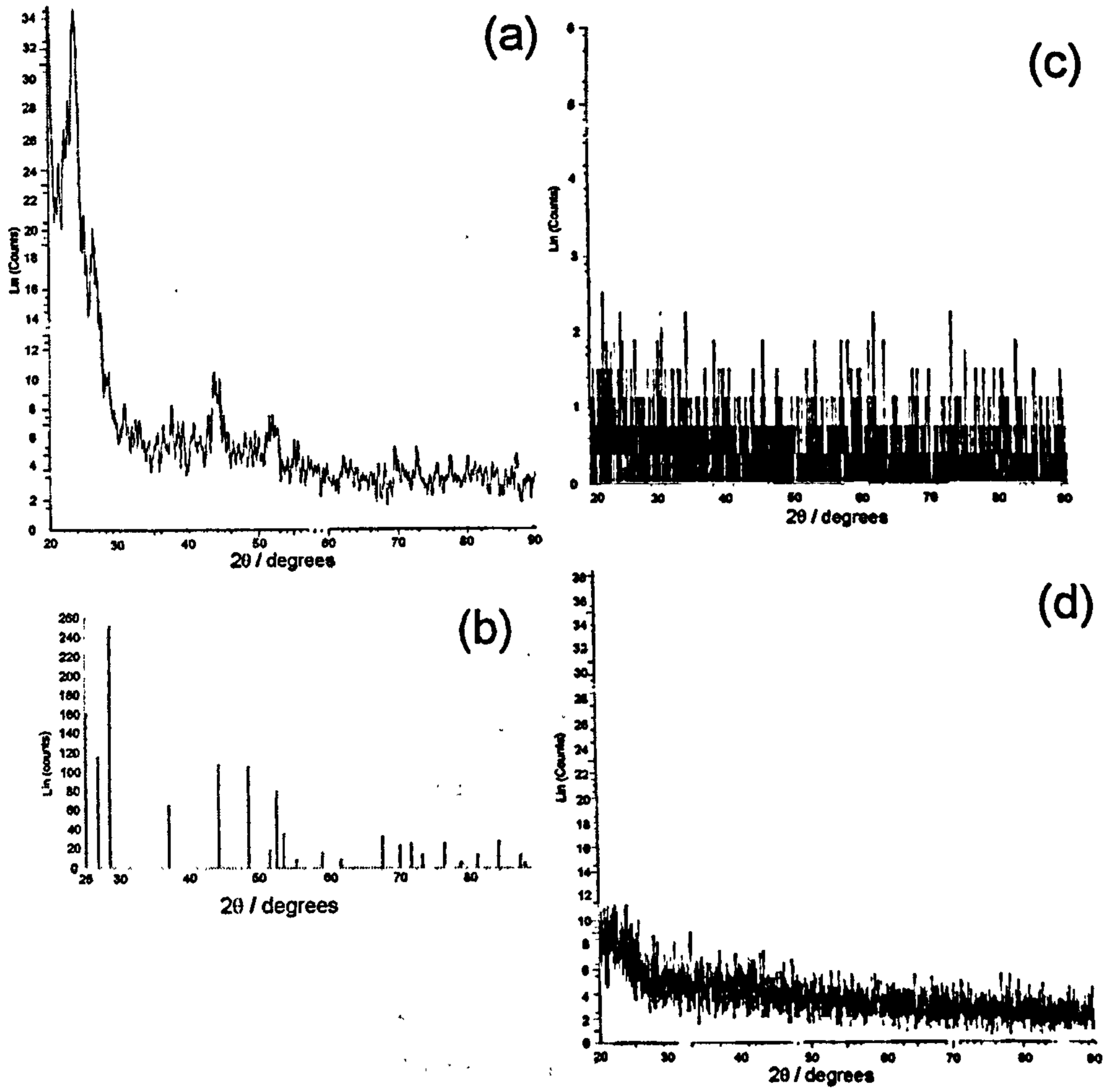

Figure 4.6: Powder X-ray diffraction patterns of a) CdS, b) theoretical pattern for hexagonal CdS crystals found in the EVA analysis software, c) RuS and d) CuS nanoparticles.

4.3.4 XPS

In order to prepare Cu_2S using the oleylamine method, the reaction of elemental sulfur and a copper (I) salt in oleylamine during heating is employed. Disproportionation of Cu (I) in the resultant particles may occur in solution producing CuS with Cu(0) instead of Cu_2S according to the following

equation:

$$Cu_2S \xrightarrow{k} CuS + Cu^0 \tag{4.2}$$

X-ray photoelectron Spectroscopy (XPS) has therefore been employed in order to determine the oxidation state of the copper.

XPS measurements of etched and non-etched copper sulfide particles deposited on a glass slide using Al and Mg sources of x-rays are shown in Figs.4.7 and 4.8. The peaks were identified from reference tables in Prac-

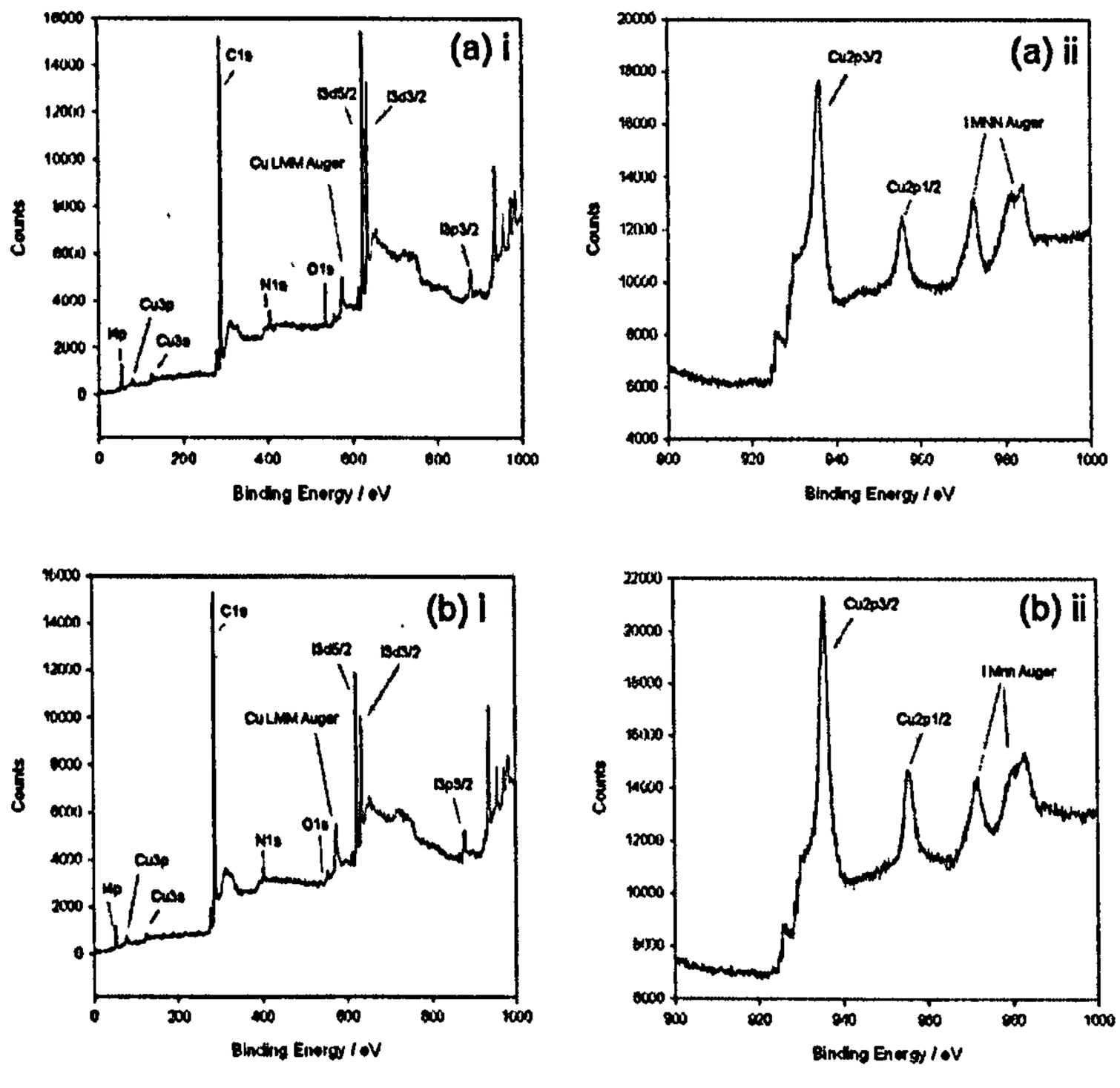

Figure 4.7: X-Ray photoelectron spectra a) before etch (i) complete scan and ii) scan over binding energy of 900 keV to 1000 keV) and b) after etch (i) complete scan and ii) scan over binding energy of 900 keV to 1000 keV) of CuS nanoparticles using Al X-ray source.

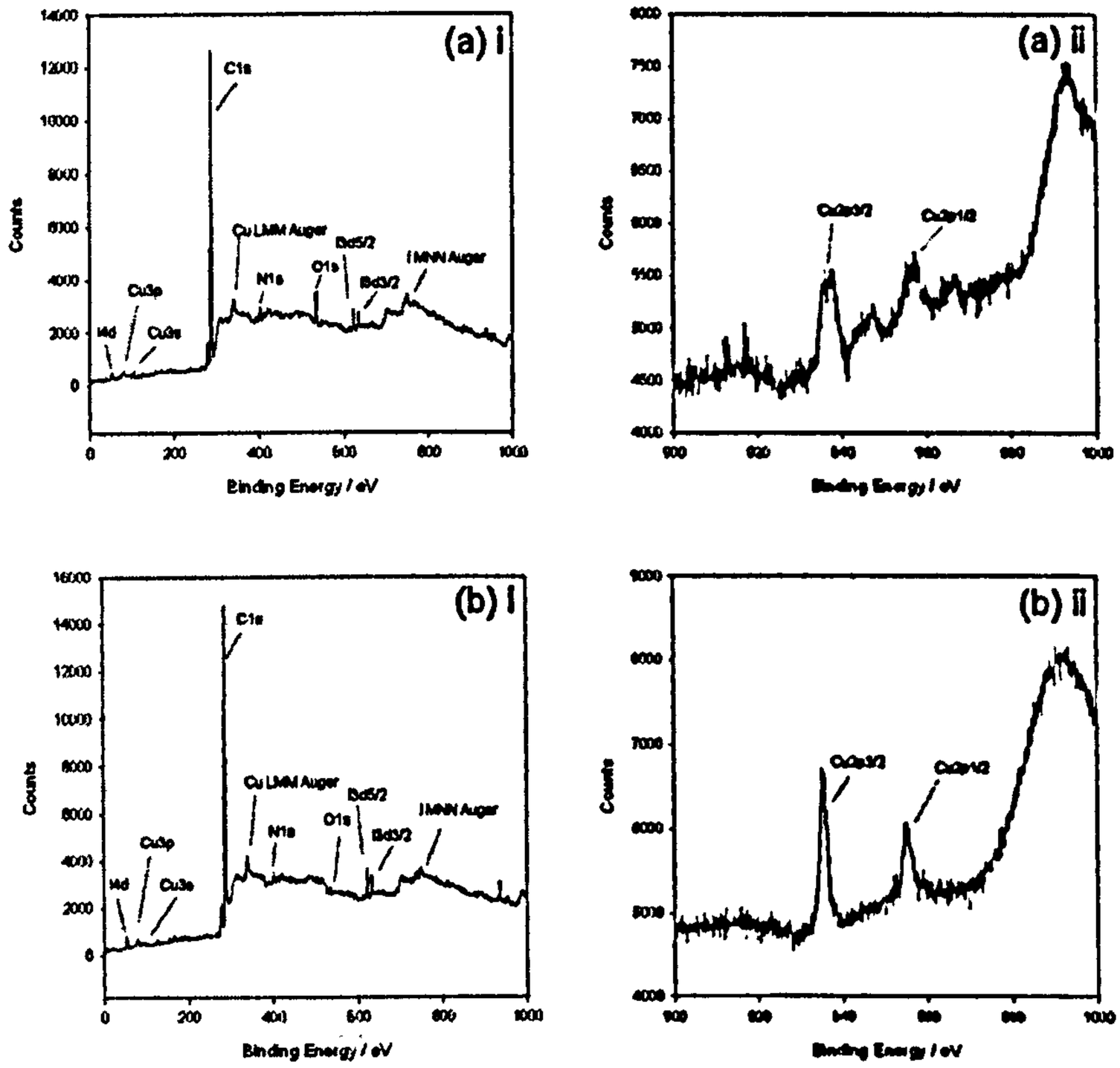

Figure 4.8: X-Ray photoelectron spectra a) before etch (i) complete scan and ii) scan over binding energy of 900 keV to 1000 keV) and b) after etch (i) complete scan and ii) scan over binding energy of 900 keV to 1000 keV) of CuS nanoparticles using Mg X-ray source.

tical Surface Analysis by Briggs and Seah[14]. These results are discussed in detail in section 4.5.

4.4 Photoelectrochemistry

4.4.1 Photocurrent Spectroscopy

Tin oxide electrodes coated with CdS, RuS_2 and copper sulfide particles, in a three electrode system using a pH 12 electrolyte solution consisting of Na_2SO_3, were tested for photocurrent activity using applied voltages between -0.3 and 0.3 V and light with a wavelength of 450 nm. No photocurrent response has been observed from tin oxide coated with cadmium sulfide, ruthenium sulfide or copper sulfide particles prepared by the oleylamine method.

4.5 Discussion

The measured band gap of the CdS nanoparticles was found to be 2.41 eV. As the bulk band gap of CdS is 2.42 eV, it is clear that no size quantisation effects are observed. This occurs because the diameter of the particles (7.4 $\pm$ 0.9 nm as determined from TEM images) is more than double the Bohr radius of CdS (3 nm)[15]. The ruthenium sulfide nanoparticles are quantum confined as the band gap of the particles (1.4 eV) are greater than the bulk gap of the material (1.3 eV)[2]. The bulk band gaps of Cu_2S and CuS are 1.21 and 2 eV respectively[3;4], therefore the copper sulfide particles must be quantum confined as the measured band gap was 2.56 eV. Correlating the band gap, E*, to the particle size of ruthenium sulfide and copper sulfide particles using the effective mass model of quantum confinement[16;17] according to equation 1.11 has proved to be difficult due to the lack of data on

the effective masses of electrons and holes for these materials. A broad size distribution was observed for copper sulfide particles whereas ruthenium sulfide and cadmium sulfide particles displayed narrow size distributions. This could be due to small copper sulfide particles forming aggregates of random sizes and the TEM images only displaying these aggregates.

The energy dispersive X-ray analysis spectra displayed in Fig.4.5 demonstrate the presence of Cd and S in the CdS sample, Ru and S in the RuS_2 sample and Cu and S in the copper sulfide sample.

It can be seen from the X-ray powder diffraction pattern of the CdS particles illustrated in Fig.4.6a, that the cadmium sulfide particle are crystalline. The powder X-ray diffraction patterns displayed in Fig.4.6b and c indicate that the ruthenium sulfide and copper sulfide particles are probably amorphous,however, it should be noted that owing to it being difficult to prepare large amounts of these nanoparticles, the failure to measure a diffraction pattern could simply reflect the low concentrations used.

The X-ray photoelectron spectra of the copper sulfide measured using X-rays from Al and Mg sources, Figs.4.7 and 4.8, show the presence of copper, iodine, carbon, nitrogen and oxygen. The N1s peak occurring at a binding energy of 399 eV in all the XPS spectra indicates the presence of an amine in the sample. Therefore oleylamine is present in the copper sulfide particles. A decrease in the oxygen peak after etching with argon ions is observed due to less oxygen being trapped in the sample. The quantity of iodine from the CuI precursor present in the sample is shown to decrease after etching by a drop in the $I3d\frac{5}{2}$ and $I3d\frac{3}{2}$ peaks. This suggests that the iodide ions are mainly

found on the surface of the particles hinting at an excess of copper at the surface. The oxidation state of copper in the sample can be determined by the position and nature of the Cu2p peaks at approximately 930-940 and 950-960 eV. The presence of peaks at 933 and 935 eV with shake up features in the spectrum acquired using a Mg source before ion etching can be attributed to a mix of Cu (I) and Cu (II) species. After etching only a peak at 933 eV is observed indicating the presence of Cu (I). It should be noted that it is difficult to differentiate between Cu (I) and Cu (0), however the Auger peak at a binding energy of 340 keV in the spectrum acquired using a Mg source, suggests the presence of Cu (I). The spectra measured using the Al source confirm these results. The Auger peak for Iodine is shifted 233 eV higher in binding energy in the spectra acquired using the Al source compared to the spectra measured using a Mg source. The same effect is seen in the copper Auger peak. These results indicate that the surface of the particles was partially oxidised after the preparation of the particles as the copper atoms in the center of the particles are in the +1 oxidation state and copper (I) and copper (II) are present on the surface of the particles. The X-ray photoelectron spectra do not show the presence of sulfur in the sample, in contrast to the EDAX spectrum of the copper sulfide particles.

The absence of photocurrent from the particles prepared by the oley-lamine method is not due to the particles not being deposited as coatings of ruthenium sulfide and cadmium sulfide are visibly detectable on the surface of tin oxide electrodes, as shown in Fig.4.9. As it is known from the position of the bands of CdS that electrons will inject into the tin oxide electrode in

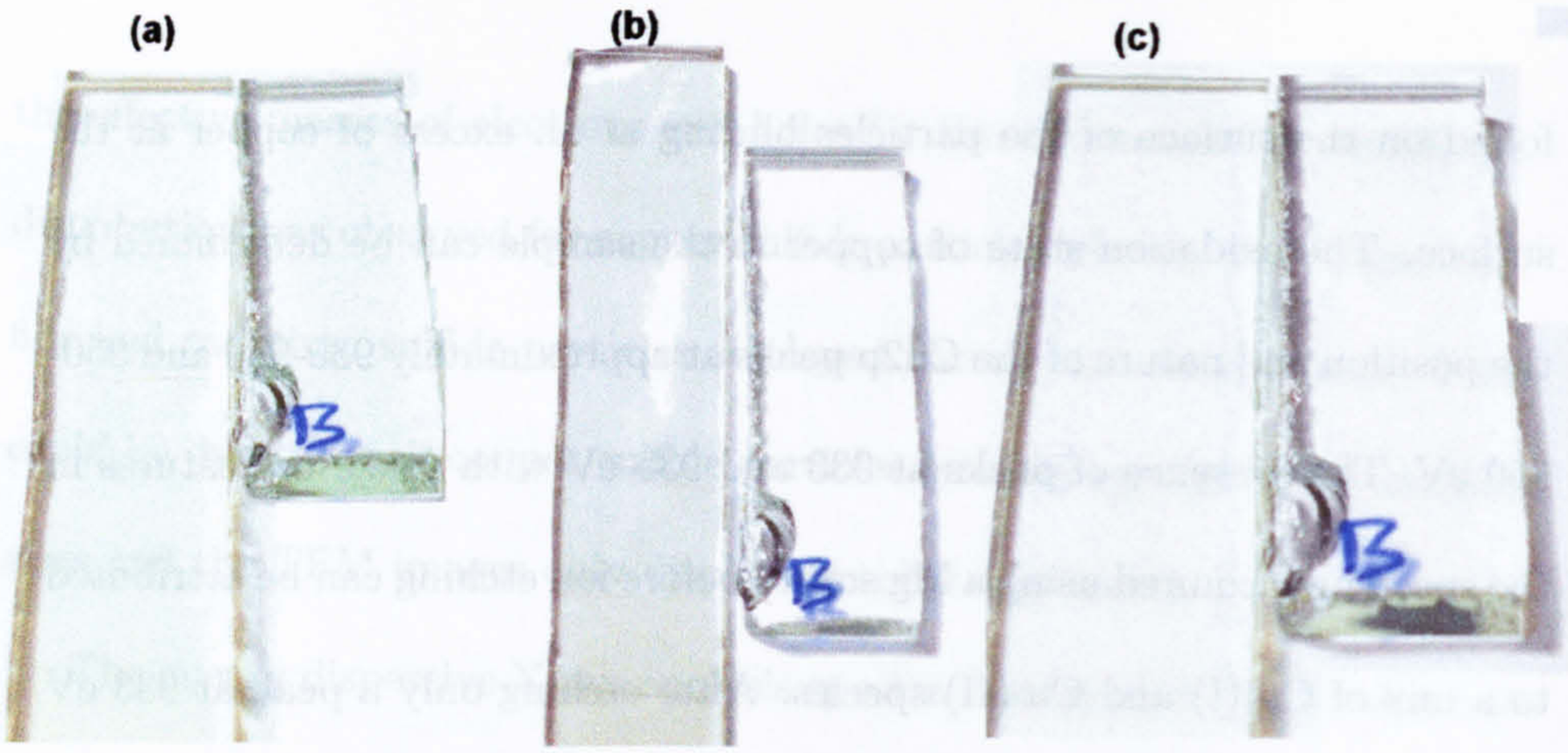

Figure 4.9: Photograph displaying visual comparisons of a) CdS, b) ruthenium sulfide and c) copper sulfide coated tin oxide electrodes with a clean tin oxide electrode, shown to the right of each coated electrode.

the electrolyte employed, it is clear that for the CdS particle, the oleylamine coating on the particles blocks the injection of electrons. The lack of photocurrent in the ruthenium sulfide particles can be explained by electrons from the nanoparticles not being transferred to the tin oxide either because of the long alkyl chain length of the oleylamine coating blocking the transfer or the conduction band of the nanoparticles being lower in energy than the Fermi level of the tin oxide, as shown in Fig.4.10. Copper sulfide particle could exhibit an absence of photocurrent due to the above reasons or the lack of particles deposited on the surface of the tin oxide electrode, as there is no visual evidence of deposition. Oleylamine probably does not effectively coat the large copper sulfide particles that were observed, as the preparation of the particles was carried out using the capping agent as the solvent and high quantities of capping agent typically result in small particles. This ex-

poses the surface of the copper sulfide particles to oxidation processes which may result in a CuO layer being formed on the particle surface. This CuO layer could prevent photocurrent from being observed. The amine capping agent may not produce hole trapping surface states, therefore, the direct recombination of an excited electron and a hole may prevent the observation of photocurrent for cadmium sulfide, ruthenium sulfide and copper sulfide.

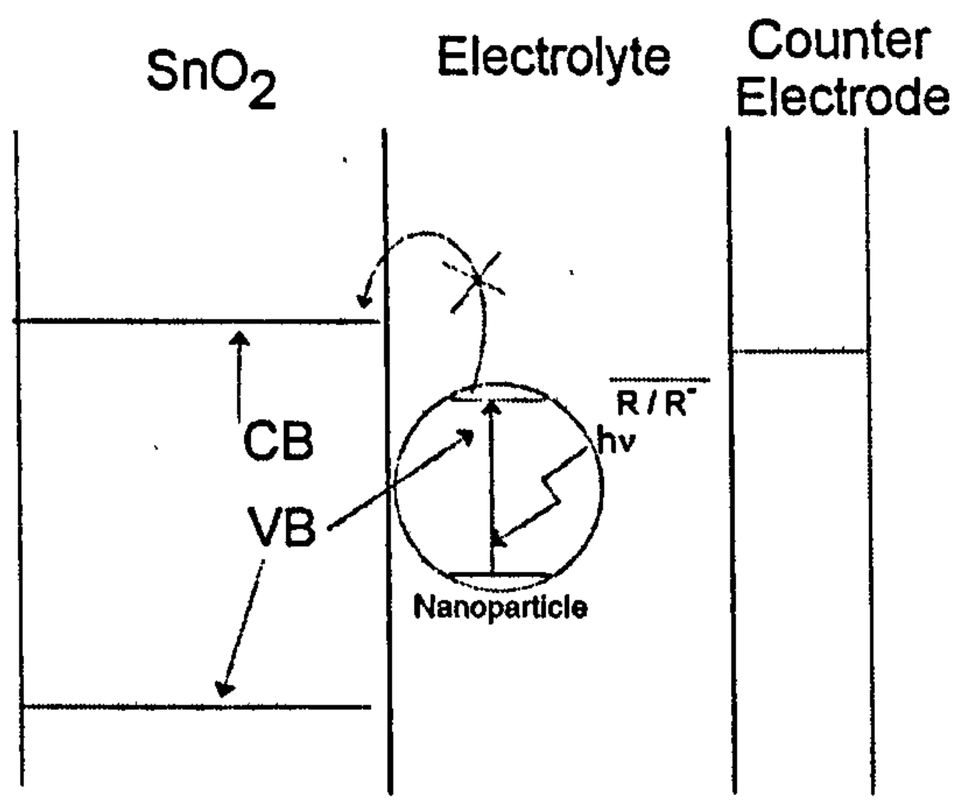

Figure 4.10: Schematic of the electron transfer process that is blocked if the conduction band of the nanoparticle is lower than the Fermi level of the tin oxide electrode.

4.6 Summary

Cadmium sulfide, ruthenium sulfide and copper sulfide particles have been prepared using the oleylamine method. The amorphous ruthenium sulfide and copper sulfide particles show size quantisation effects. Bulk optical prop-

erties are displayed from the crystalline cadmium sulfide particles. However no photocurrent has been observed from these particles when deposited on tin oxide glass electrodes. These particles are not ideal sensitisers for a solar cell as their band gaps are too large and size control using this method is difficult.

References

[1] Joo, J.; Na, H. B.; Yu, T.; Yu, J. H.; Kim, Y. W.; Wu, F. X.; Zhang, J. Z.; Hyeon, T. *J. Am. Chem. Soc.* **2003**, *125*(36), 11100–11105.

[2] Ashokkumar, M.; Kudo, A.; Saito, N.; Sakata, T. *Chem. Phys. Lett.* **1994**, *229*, 383 – 388.

[3] Klimov, V.; Bolivar, P. H.; Kurz, H.; Karavanskii, V.; Krasovskii, V.; Korkishko, Y. *Appl. Phys. Lett.* **1995**, *67*, 653.

[4] Artemyev, M. V.; Gurin, V. S.; Yumashev, K. V.; Prokoshin, P. V.; Maljarevich, A. M. *J. Appl. Phys.* **1996**, *80*, 7028.

[5] Gurunathan, K.; Murali, K. R.; Subramanian, V.; Rangarajan, N.; Lakshmanan, A. S. *Mater. Res. Bull.* **1995**, *30*(12), 1579–1582.

[6] Hara, K.; Sayama, K.; Arakawa, H. *Chem. Lett.* **1998**, page 387.

[7] Jobic, H.; Clugnet, G.; Lacroix, M.; Yuan, S.; Mirodatos, C.; Breysse, M. *J. Am. Chem. Soc.* **1993**, *115*, 3654–3657.

[8] Passaretti, J. D.; Dwight, K.; Wold, A.; J., C. W.; R., C. R. *Inorg. Chem.* **1981**, *20*, 2631–2634.

[9] Hirai, T.; Nomura, Y.; Komasawi, I. *J. Nanoparticle Res.* **2003**, *5*, 61–67.

[10] Lu, Q.; Gao, F.; Zhao, D. *Nanotech.* **2002**, *13*, 741–745.

[11] Lu, Q.; Gao, F.; Zhao, D. *Nano Lett.* **2002**, *2*(7), 725–728.

[12] Haram, S. K.; Mahadeshwar, A. R.; G., D. S. *J. Phys. Chem.* **1996**, *100*, 5868–5873.

[13] Kore, R. H.; Kulkarni, J. S.; K., H. S. *Chem. Mater.* **2001**, *13*, 1789–1793.

[14] Briggs, D.; Seah, M. P. *Practical Surface analysis, Vol. 1:Auger and X-ray photoelectron Spectroscopy;* Wiley: New York, second edition ed., 1990.

[15] Nanda, K. K.; Sarangi, S. N.; Sahu, S. N. *J. Phys. D;Appl. Phys.* **1999**, *32*, 2306.

[16] Pesika, N. S.; Hu, Z. S.; Stebe, K. J.; Searson, P. C. *J. Phys. Chem. B* **2002**, *106*(28), 6985–6990.

[17] Brus. *J. Chem. Phys.* **1984**, *80*(9), 4406–4409.

Chapter 5

CdSe

5.1 Introduction

Cadmium selenide has a bulk band gap of 1.71 eV[1]. Nanoparticles of CdSe have been widely studied as a replacement for dyes in dye sensitised solar cells, since cadmium selenide is known to absorb light of higher energy than its band gap efficiently and the absorption spectrum covers most of the visible spectrum[2;3]. Cadmium selenide nanoparticles have been prepared by a variety of methods. Optical and photoelectrochemical properties of these particles have also been reported.

5.1.1 Methods of Preparing CdSe

Chemical Bath Deposition Techniques

Thin films of CdSe nanoparticles have been prepared by chemical bath deposition techniques. Gorer and Hodes[4] prepared CdSe particles on glass sub-

strates by placing the substrate in an aqueous solution containing $CdSO_4$, potassium nitriloacetate and Na_2SeSO_3 with an excess of Na_2SO_3. The dimensions of the product were temperature dependent. Particles with an average diameter of 4 nm, as measured from TEM images, and a band gap of 2.2 eV were produced when a deposition temperature of 10 °C was used. If the deposition temperature was increased to 40 °C, particles with an average diameter of 5 nm, as measured using TEM, and a band gap of 2.07 eV were observed. Lifshitz *et al.*[5] studied the photoluminescence of CdSe particles deposited on glass substrates using the same method as Gorer and Hodes[4]. The photoluminescence spectra of the CdSe particles prepared by Lifshitz *et al.*[5] displayed a red-IR emission band at 1.43 eV for particles with an average diameter of 6 nm, as measured by TEM. The presence of an emission band with a lower energy than the band gap is likely due to the recombination of an electron with a hole trapped in a surface state arising from incomplete surface passivation of the particles by the capping agent, nitriloacetate. The synthesis of CdSe particles on a substrate outlined by Gorer and Hodes[4] was employed by Shen *et al.*[6] to prepare nanocrystalline TiO_2 electrodes coated with CdSe nanoparticles with an average size of 6 nm, as calculated from the X-ray diffraction peaks using the Debye-Scherrer equation. Photosensitisation of the TiO_2 electrodes was observed by Shen *et al.*[7] using photocurrent spectroscopy and a band gap of 2.1 eV was reported. Pejova *et al.*[8;9] deposited CdSe on glass and polyester substrates from a chemical bath consisting of an aqueous solution of $CdNO_3$, ammonia buffer solution and Na_2SeSO_3. Particles with an average radius of 2.6 nm, as calculated from

the X-ray diffraction peaks using the Debye-Scherrer equation, and a band gap of 2.08 eV were observed by Pejova *et al.*[8]. The following mechanism was proposed for the formation of the CdSe particles by Pejova *et al.*[8]:

$$\begin{aligned}
NH_3 + H_2O &\rightleftharpoons NH_4^+ + OH^- \\
Cd^{2+} + 4NH_3 &\rightleftharpoons [Cd(NH_3)_4]^{2+} \\
SeSO_3^{2-} + H_2O &\rightleftharpoons H_2Se + SO_4^{2-} \qquad (5.1) \\
H_2Se + OH^- &\rightleftharpoons H_2O + HSe^- \\
HSe^- + OH^- &\rightleftharpoons H_2O + HSe^{2-} \\
Cd^{2+} + Se^{2-} &\rightleftharpoons CdSe
\end{aligned}$$

CdSe nanoparticles were deposited on a conducting glass substrate coated with colloidal TiO_2 by Fang *et al.*[10] using a chemical bath containing cadmium acetate, triethanolamine, ammonia and sodium selenosulfate with an excess of sodium sulfite. This resulted in TiO_2 films coated with CdSe particles of less than 7 nm in diameter, as measured by atomic force microscopy (AFM), and with a band gap of 610 nm. Fang *et al.*[10] recorded the photocurrent spectrum of TiO_2 electrodes coated with CdSe particles.

Solution Methods

A number of simple chemical methods to prepare CdSe nanoparticles have been reported. Yochelis and Hodes[11] studied the synthesis of CdSe particles from an aqueous mixture of $CdSO_4$ and sodium seleno sulfate. This method produced particles with an average size of 3.1 nm, as measured using TEM, that displayed lattice fringes matching those of $CdSO_3$ or CdSe. Yochelis and

Hodes[11] suggested two possible reaction pathways; the hydrolysis of $SeSO_3^{2-}$ to HSe^- (equation 5.2) or complex formation between $SeSO_3^{2-}$ and $CdSO_3$ followed by decomposition of the complex (equation 5.3).

$$SeSO_3^{2-} + OH^- \rightarrow HSe^- + SO_4^{2-}$$

$$CdSO_3 + HSe^- \rightarrow CdSe + HSO_3^- \qquad (5.2)$$

$$SO_3Cd + Se - SO_3^{2-} \rightarrow SO_3Cd - Se - SO_3^{2-}$$

$$SO_3Cd - Se - SO_3^{2-} + OH^- \rightarrow CdSe + SO_4^{2-} + HSO_3^- \qquad (5.3)$$

CdSe particles stabilised with mercaptoacetic acid and coated with poly (diallyldimethyl-ammonium chloride) (PDDA) or poly (sodium-p-styrene sulfonate) (PSS) polyelectrolytes were prepared by Zhang *et al.*[12] by refluxing an aqueous solution of cadmium acetate, mercaptoacetic acid and Na_2SeSO_3 followed by dropping the resulting solution of 2 nm CdSe particles into a PDDA or PSS solution. The size of the particles was measured by TEM. The photoluminescence spectra displayed a sharp excitonic emission peak at 475 nm and a broad emission peak from trap states at 585 nm. The photoluminescence was enhanced with addition of PDDA to the particles. This result demonstrates that the hole trapping surface state formed if a thiol is used as the stabiliser, which partially blocks the recombination of an electron and a hole in an exciton, is prevented from trapping hole by the addition of PDDA, resulting in the enhancement of the photoluminescence. Ma *et al.*[13] prepared CdSe particles capped with polyvinyl alcohol (PVA) by stirring an aqueous solution of $CdCl_2$, PVA and sodium selenosulfate. These particles

were deposited on a glass substrate by evaporating the solvent. This resulted in particles with an average diameter of 4.3 nm, as measured from TEM images, and a band gap of 2.19 eV[13]. A synthesis involving the mixing of an aqueous solution of selenourea with sodium sulfite to keep the solution stable with an aqueous solution of $CdCl_2$ with a complexing agent was employed by Yamamoto *et al.*[14] in order to precipitate CdSe particles. This resulted in particles of 0.7 μm in diameter, as measured by SEM, and a band gap of 1.79 eV. Sondi *et al.*[15] prepared CdSe particles coated with aminodextran by mixing an aqueous solution containing $CdCl_2$ and aminodextran with an aqueous Na_2Se or selenourea solution. This resulted in particles of an average diameter between 2 nm and 4 nm, with the small particles occurring when a large concentration of aminodextran was used and large particles being formed when a small concentration of aminodextran was employed[15].

CdSe particles were prepared in solution by Rogach *et al.*[16] by injecting an aqueous solution of NaHSe into a solution of $Cd(ClO_4)_2 \cdot 6H_2O$ and a stabiliser, such as 2-mercaptoethanol, 1-thioglycerol or thioglycolic acid, in water and then refluxing the mixture for several hours. Particles of diameters between 1.4 and 2.2 nm were prepared if 2-mercaptoethanol or 1-thioglycerol was used as the stabiliser. If the stabiliser used was thioglycolic acid, the size of the particles was found to be between 2.1 and 3.2 nm[16]. The size of the particles was measured by TEM. Bäumle *et al.*[17] modified the technique used by Rogach *et al.*[16] by changing the stabiliser used to glutathione. This produced particles of 2 nm in diameter, as measured by TEM, with a peak in the fluorescence spectrum at 533 nm. An increase in the intensity of

the fluorescence peak was observed by Bäumle *et al.*[17] if the particles were modified with streptavidin, probably due to the improved surface passivation of the hole trapping surface states by streptavidin compared to glutathione.

Sonochemical Techniques

Ultrasound techniques have been applied to the preparation of CdSe nanoparticles by Zheng *et al.*[18], Zhu *et al.*[19], Ge *et al.*[20], Mastai *et al.*[21] and Li *et al.*[22]. Li *et al.* synthesised CdSe nanoparticles by exposing a mixture of $Cd(Ac)_2{\cdot}2H_2O$ and selenium in dimethyl sulfoxide to ultrasound under a H_2 / argon atmosphere. This resulted in CdSe nanoparticles with a mean diameter of 7-10 nm, as measured from TEM images, that aggregated into spherical nanoclusters that averaged 40 nm in diameter and had a band gap of 1.83 eV[22]. Using X-ray diffraction the particles were shown to have a hexagonal structure. The particles are thought to form according to a free radical mechanism:

$$(CH_3)_2SO \rightarrow {}^{\bullet}CH_3SO + {}^{\bullet}CH_3 \tag{5.4}$$

$$H_2O \rightarrow {}^{\bullet}H + {}^{\bullet}HO$$

The decomposition of excited molecules, $^*H_2$, formed by the absorption of ultrasound by the H_2 / argon atmosphere, is triggered by the radicals and the resulting $H^{\bullet}$ radical then reacts with Se to form H_2Se, as shown:

$${}^{\bullet}CH_3 + {}^*H_2 \rightarrow CH_4 + H^{\bullet} \tag{5.5}$$

$${}^{\bullet}HO + {}^*H_2 \rightarrow H_2O + H^{\bullet} \tag{5.6}$$

$$Se + 2H^{\bullet} \rightarrow H_2Se \tag{5.7}$$

Finally, the CdSe particles form by the reaction of H_2Se with Cd^{2+}[22]. Ge *et al.*[20], Zhu *et al.*[19], Mastai *et al.*[21] and Zheng *et al.*[18] prepared CdSe by sonicating basic aqueous solutions of Na_2SeO_3 or Na_2SeSO_4 and cadmium sources, along with different additives. Ge *et al.*[20] proposed the following mechanism for the formation of CdSe particles from the sonication of an aqueous mixture of $Cd(NO_3)_2$, ammonia, Na_2SeO_3 and N_2H_4:

$$\begin{aligned} 3SeO_3^{2-} + 3N_2H_4 &\rightarrow 3Se + 3N_2 + 3H_2O + 6OH^- \\ 3Se + 6OH^- &\rightarrow 2Se^{2-} + SeO_3^{2-} + 3H_2O \qquad (5.8) \\ 2Se^{2-} + 2Cd(NH_3)_4^{2+} &\rightarrow 2CdSe + 8NH_3 \end{aligned}$$

CdSe particles with diameters between 20 and 50 nm, as measured by TEM, were formed by this method and using X-ray diffraction, were found to be amorphous . Ge *et al.*[20] observed a narrow exciton emission peak in the luminescence spectrum of the particles at 556 nm. Mastai *et al.*[21] employed a method involving the deposition of CdSe particles by exposing an aqueous solution of $CdSO_4$, potassium nitrilotriacetate and Na_2SeSO_3 at pH 8-10 to alternating current and ultrasound pulses. This resulted in particles with an average size of 4 nm, as measured by TEM, and a band gap of 2.10 eV found using diffuse reflection spectroscopy[21]. CdSe hollow spheres were prepared by Zhu *et al.*[19] by exposing an aqueous solution of $CdCl_2$, ammonia or triethylamine, and Na_2SeSO_3 to ultrasound. The mechanism proposed by Zhu *et al.*[19] for the synthesis of CdSe and the formation of the hollow sphere

structure is outlined in the following equations and Fig.5.1:

$$H_2O \rightarrow H^{\bullet} + OH^{\bullet} \tag{5.9}$$

$$2H^{\bullet} + SeSO_3^{2-} \rightarrow Se^{2-} + 2H^{+} + SO_3^{2-} \tag{5.10}$$

$$Cd(OH)_2 + Se^{2-} \rightarrow CdSe + 2OH^{-} \tag{5.11}$$

The $Cd(OH)_2$ is formed as particles from the reaction of $CdCl_2$ solution with ammonia and acts as a template for the production of CdSe hollow sphere assemblies. Zhu *et al.*[19] determined the band gap of the CdSe in these structures to be 2.7 eV from the UV-Visible spectrum. This demonstrated that the particles were quantum confined. TEM showed that hollow spheres with an average diameter of 120 nm and consisting of 5 nm diameter spherical particles were formed.

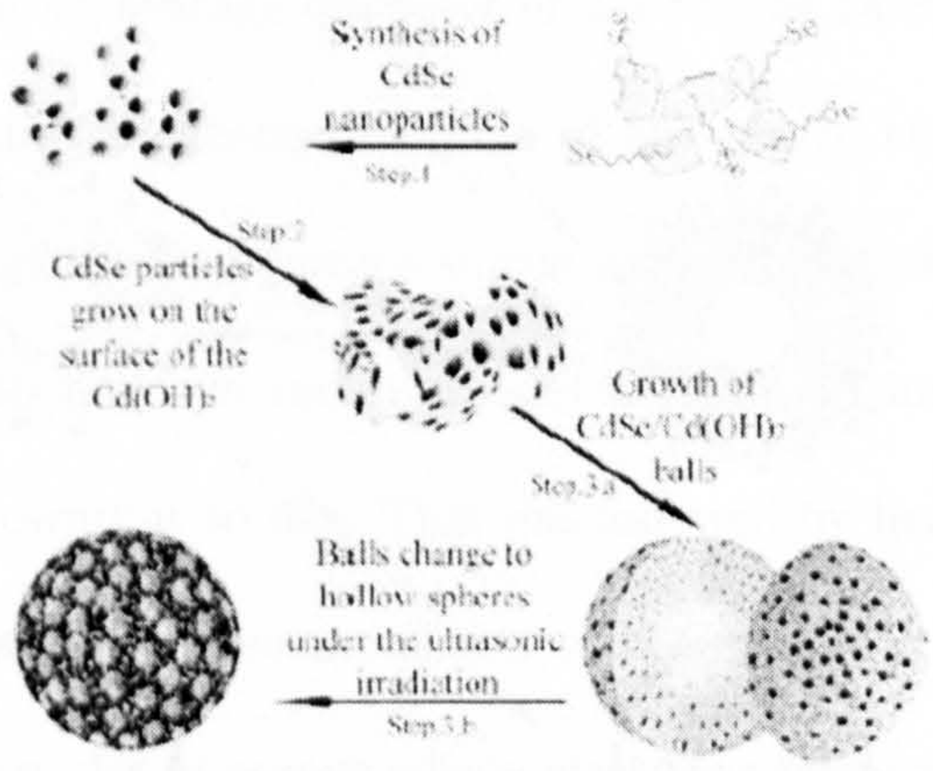

Figure 5.1: Proposed mechanism for the formation of CdSe hollow spheres[19].

Synthesis in Microemulsions

Zheng *et al.*[18] utilised the ability of sodium dodecyl sulfate (SDS) to form vesicles under defined conditions, to prepare CdSe hollow spheres by a reaction on a template surface. The spheres were synthesised by exposing an aqueous solution of SDS and $CdCl_2$ to ultrasound followed by the addition of Na_2SeSO_3 and further sonication. The mechanism proposed by Zheng *et al.*[18] for the formation of the hollow spheres is shown in Fig.5.2. From Zheng's observations of TEM data and UV-Visible spectra, the spheres were found to be approximately 100-200 nm in diameter, composed of CdSe nanoparticles with an average diameter of 3-4 nm, as measured using TEM, and had a

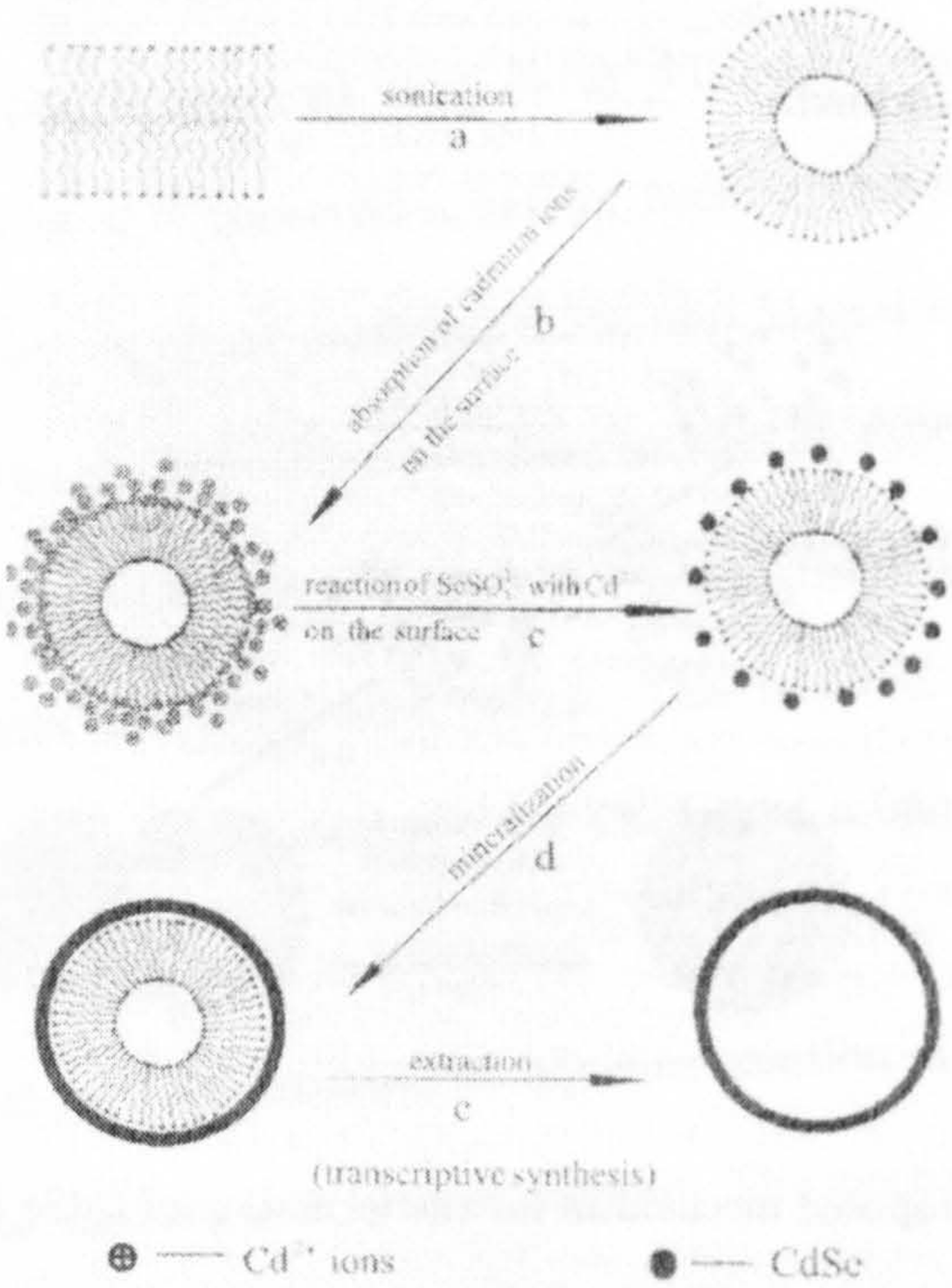

Figure 5.2: Schematic of the formation of CdSe hollow spheres[18].

band gap of 2.01 eV, indicating that quantum confinement occurs[18].

Conversion of a Precursor Adsorbed on a Substrate to CdSe

Cadmium selenide particles have been prepared by reacting H_2Se gas with Cd^{2+} ions in porous films or polymer matrices. Wark *et al.*[23] prepared CdSe in silica films by impregnating a preformed silica film with a solution of cadmium acetate in methanol and then exposing the films to H_2Se. A solution that could be used to form a silica film was prepared by Wark *et al.*[23] by adding HCl to an ethanolic tetraethyl orthosilicate solution, followed by the addition of $C_{16}H_{33}(OCH_2CH_2)_{10}OH$ and cadmium acetate and finally allowing the solution to age for 2 hours. Films were then prepared by spreading the viscous solution on a quartz slide or a silicon wafer, followed by calcination of the films at 623 K. The films were then exposed to H_2Se to produces CdSe particles with an average diameter of 2.5 nm, as calculated according to equation 1.12, and an absorption edge of 557 nm in the films[23]. Belogorokhov *et al.*[24] synthesised porous silicon embedded with CdSe particles by incorporating an aqueous cadmium acetate solution into a porous silicon matrix and allowing it to dry. This was followed by heating the sample to 310 °C resulting in the decomposition of the cadmium acetate to form CdO. The CdSe particles in porous silicon were then formed by exposing the system to H_2Se. Belogorokhov *et al.*[24] observed a photoluminescence peak at 1.79 eV, implying that quantum confinement occurs and it was assumed that CdSe clusters corresponding to the porous silica pore size of 3-5 nm were formed. An increase in photoluminescence peak intensity was observed

after exposure of the porous silica coated with CdSe particles to laser irradiation for 60 minutes. This could be due to an annealing of defects in the CdSe particles. CdSe nanoparticles have been prepared in a polymer matrix by Haggata *et al.*[25]. This method involved the preparation of an adduct of a 2-pyridyl polybutane polymer with dimethyl cadmium[26] and subsequent exposure of this adduct to H_2Se, as displayed in Fig.5.3. Haggata *et al.*[25] observed that an increase in the reaction temperature from -68 °C to 60 °C resulted in the CdSe particles growing from an average diameter of 2.3 nm to an average diameter of 3.6 nm, as determined using TEM. A corresponding

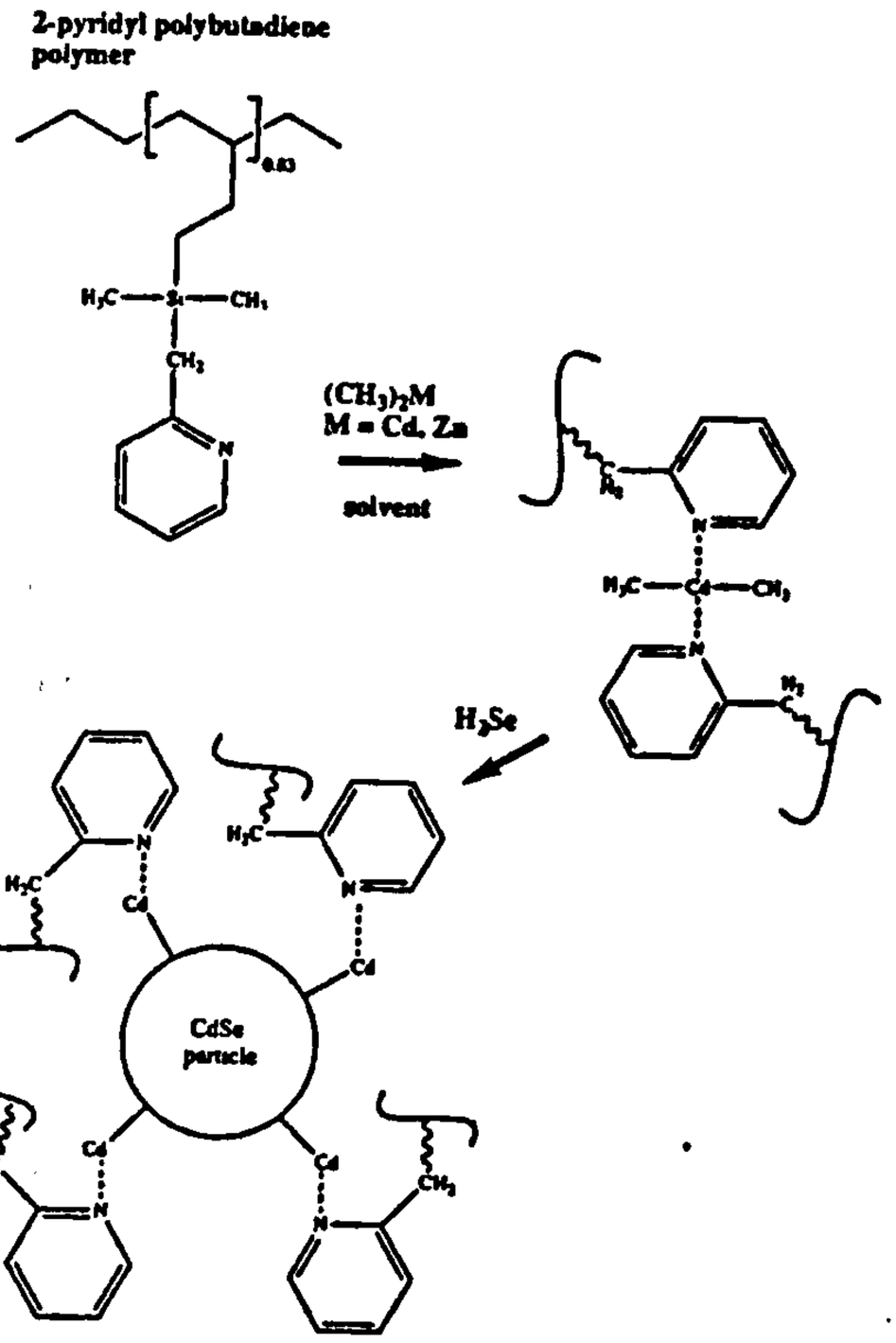

Figure 5.3: Schematic of the formation of CdSe in a 2-pyridylpolybutane polymer.

decrease in the band gap of the particles from 2.72 eV to 2.15 eV was seen by Haggata *et al.*[25].

Microwave Heating Techniques

Palchik *et al.*[27] and Rogach *et al.*[28] prepared CdSe nanoparticles using microwave assisted methods. Cadmium acetate and Se in ethylene glycol were exposed to microwave radiation for 1 hour by Palchik *et al.*[27], resulting in CdSe particles of average diameter 350 nm consisting of CdSe grains with an average diameter of 6-7 nm, as measured by TEM images. The band gap of the particles was found to be 1.93 eV by UV-Visible spectroscopy and photoluminescence. Rogach *et al.*[28] prepared CdSe particles with an average diameter of 4.0 nm, as determined using TEM, by irradiating an aqueous solution of cadmium perchlorate, sodium citrate and N,N-dimethylselenourea with microwaves. In absorbance spectroscopy a band edge of 590 nm was observed[28].

Solvothermal Methods

Gautam *et al.*[29] and Liu *et al.*[30] have prepared CdSe nanoparticles by solvothermal routes. A reaction mixture of cadmium stearate, selenium, tetralin and dodecanethiol in toluene was heated in an autoclave to 250 °C for 5 hours in order to produce CdSe nanoparticles with a mean diameter of 3.0 nm, as measured by TEM[29]. An absorption peak at approximately 510 nm was observed in the UV-Visible absorption spectrum, proving that the particles prepared by Gautam *et al.*[29] were quantum confined. Liu *et al.*[30] synthesised

CdSe by heating $Cd(NO_3)_2 \cdot 4H_2O$, Se and $N_2H_4 \cdot H_2O$ in ethylenediamine at 140 °C in an autoclave for 10 hours. The reaction was proposed to proceed according to the following equation:

$$2Cd^{2+} + N_2H_4 \cdot H_2O + 2Se + 4OH^- \rightarrow 2CdSe \downarrow + N_2 \uparrow + 5H_2O \qquad (5.12)$$

CdSe nanorods of diameters of 10-15 nm and lengths of 100 nm and CdSe nanoparticles of diameters of 100 nm, as measured using TEM, were produced by Liu *et al.*[30] by changing the ratio of Cd^{2+} to Se atoms from 1:1 for the nanorods and 1:2 for the particles. The nanorods were found to have a wurtzite structure, while the nanoparticles had a zinc blend structure. These structures were found by Liu *et al.*[30] using X-ray diffraction.

Preparation By Thermal Evaporation

Thermal evaporation techniques have been employed to prepare CdSe thin films by Baban *et al.*[31] and Nesheva *et al.*[32]. Baban heated CdSe polycrystalline powder to 900-1050 K under vacuum in the presence of a glass substrate[31]. This resulted in polycrystalline thin films of thicknesses, depending on growth time and temperature, between 0.1 and 1.8 μm, as measured from AFM images. The films were composed of crystallites of wurtzite structure of size between 20 and 100 nm. Baban[31] determined band gaps of 1.65 to 1.75 eV for films of thickness between 1.73 and 0.72 μm. A similar method of preparation was used by Nesheva *et al.*[32]. However the deposition of CdSe was alternated with the deposition of a matrix material such as SiO, GeS_2 or ZnSe. Nesheva *et al.*[32] determined the band gap of the CdSe particles

embedded in the matrices to be between 1.95 and 2.0 eV, corresponding to excitonic peaks in the absorption spectra at 635 nm and 620 nm.

Preparation in Micellar and Reverse Micellar Systems

Cadmium selenide particles have been prepared in microemulsions by Kasuya *et al.*[33] and Majetich *et al.*[3]. Kasuya *et al.*[33] dispersed cadmium nitrilotriacetate in decylamine and then further mixed this solution with aqueous Na_2SeSO_3 to yield a system containing micelles. When toluene was added to this solution, the surfactant was transferred to the toluene and transformed in to reverse micelles. Kasuya *et al.*[33] propose that the formation of CdSe nanoparticles occurs in the toluene phase. The resultant particles have an excitonic peak in the absorption spectrum at 415 nm and an average diameter of 1.5 nm (as calculated using equation 1.12), indicating that the particles are quantum confined. Cadmium selenide nanoparticles were synthesised by Majetich *et al.*[3] by the addition of cadmium perchlorate and trimethylsilylselenium solutions to a microemulsion of heptane, water and AOT. The resulting particles were then terminally capped by the addition of butanethiolate, phenylthiolate, thio-2-naphtholate, acetonitrile, pyridine or quinoline in heptane. The particles were 3.5 nm in diameter, as measured by TEM, and the change in surface ligand was found by Majetich *et al.*[3] to affect the recombination of an electron and hole in a trapped or surface state. It was shown that particles coated with thiols exhibit significant luminescence due to the recombination of an electron with a trapped hole, whereas particles coated with amines display luminescence properties consistent with the direct

recombination of an electron and a hole. This leads to the conclusion that the hole trapping surface states are either due to the thiol capping agents passivating the surface states less effectively than the amine capping agents.

Electrodeposition Techniques

Choi *et al.*[34] and Ruach-Nir *et al.*[35] prepared CdSe nanoparticles by electrodeposition. Ruach-Nir *et al.*[35] used a solution of $Cd(ClO_4)_2 \cdot 6H_2O$ and Se in dimethyl sulfoxide, a mechanically strained gold cathode and a graphite anode and performed the electrodeposition of CdSe under constant current. This resulted in particles of decreasing size as the strain on the gold electrode was increased. An increase in band gap from 2.04 eV for particles produced using a gold electrode under no strain to 2.2 eV for particles produced using a gold electrode under compressive strain[35]. Choi *et al.*[34] used a three electrode system employing a gold working electrode coated with a self-assembled monolayer of thiolated β-cyclodextrin, a platinum wire as a counter electrode and an Ag|AgCl|3 mol dm^{-3} KCl reference electrode in an electrolyte containing SeO_2 and $CdSO_4$ in order to deposit CdSe particles at -0.7 V. The CdSe particles produced were observed to have a diameter of 150 nm, as measured using SEM. A photocurrent was measured for these particles on a electrode.

Photochemical Methods

Photochemical methods of preparing CdSe nanoparticles have been reported by Zhu *et al.*[36], Zhao *et al.*[37] and Yan *et al.*[37]. Zhu *et al.*[36] exposed an aque-

ous solution of $CdCl_2$, nitrilotriacetic acid and Na_2SeSO_3, adjusted to pH 11, to light of wavelength 420-250 nm from a 300 W high pressure indium lamp. This resulted in particles with an average diameter of 7 nm, as calculated from the X-ray diffraction peaks using the Debye-Scherrer equation, and a band gap of 1.82 eV. Zhu *et al.*[36] proposed that the particles form according to the following equations:

$$\begin{aligned} SO_3^{2-} + h\nu &\rightarrow SO_3^{-} + e \\ SeSO_3^{2-} + e &\rightarrow Se^{-} + SO_3^{2-} \\ Se^{-} + e &\rightarrow Se^{2-} \\ Cd^{2+} + Se^{2-} &\rightarrow CdSe \end{aligned} \tag{5.13}$$

A similar method to the above synthesis was employed by Zhao *et al.*[37] to prepare CdSe particles with dimensions of 60 nm to 70 nm, as measured by TEM, and an emission peak in the photoluminescence spectrum at 680 nm. These particles were made by irradiating an aqueous solution of $CdCl_2$, nitrilotriacetic acid and Na_2SeSO_3, adjusted to pH 11, with UV light from a high pressure mercury lamp. Yan *et al.*[38] synthesised CdSe nanoparticles by exposing an aqueous solution of cadmium acetate, sodium sulfite, cetyltrimethylammonium bromide ($C_{16}TAB$) and Se to light from a high pressure mercury lamp. The particles produced were found to be 2.5-4.0 nm in diameter, as measured from TEM images, with band gaps between 1.83 eV and 1.93 eV. According to Yan *et al.*[38] the particles were formed according

to the equations shown below:

$$\begin{aligned} SO_3^{2-} + h\nu &\rightarrow SO_3^{-} + e \\ Se + e &\rightarrow Se^{-} \\ Se^{-} + e &\rightarrow Se^{2-} \end{aligned} \tag{5.14}$$

$$Cd^{2+} + Se^{2-} \rightarrow CdSe$$

Preparation by Injection Of Hot Reagents

In 1993 Murray *et al.*[2] reported a hot injection method for preparing CdSe nanoparticles. This synthesis involved first degassing trioctylphosphine oxide (TOPO) in the reaction vessel at 200 °C under vacuum, flushing with argon and then maintaining the system at 300 °C under an argon atmosphere. Dimethyl cadmium was then dissolved in trioctyl phosphine (TOP). In a separate vessel a trioctyl phosphine selenide (TOPSe) solution in TOP was prepared by reacting Se powder with TOP. The TOPSe solution was then mixed with the dimethyl cadmium solution, added to the reaction vessel and the heat was removed, causing a reduction in the temperature of the system to approximately 180 °C. The temperature was then raised to 260 °C and samples were removed after various growth times, producing a number of samples of CdSe nanoparticles with different sizes from one reaction. Murray *et al.*[2] prepared TOP/TOPO capped CdSe particles with average diameters between 1.2 nm, for short growth times, and 11.5 nm, for long growth times, as measured using TEM. The particles produced had a narrow size distribution and showed sharp absorption features which displayed an increased

absorption edge wavelength with particle size. Murray *et al.*[2] proved that the particles were crystalline by powder X-ray diffraction. CdSe and CdS particles were synthesised by this method, using bis(trimethylsilyl) selenide or bis(trimethylsilyl) sulfide in place of the phosphine chalcogenide precursor initially used. CdSe particles capped with pyridine were prepared by Murray *et al.*[2] by a repetitive procedure of heating a mixture of TOPO/TOP-capped CdSe particles and pyridine to 60 °C, followed by flocculation of the particle by the addition of hexane. This method and variations thereof have been widely studied. Kuno *et al.*[39] have studied the luminescence of CdSe particles passivated by 4-picoline, 4-(trifluoromethyl) thiophenol and tris(2-ethylhexyl) phosphate prepared by the surface modification of particles synthesised using the above method. The surface of these particle was characterised by proton NMR and P^{31} NMR experiments. An increase in emissions from deep traps was observed upon exchange of tris(2-ethylhexyl) phosphate ligands with either the 4-picoline or 4-(trifluoromethyl) thiophenol capping agents, implying that tris(2-ethylhexyl) phosphate is more successful at passivating the surface states which trap holes. The addition of hexyl-phosphonic acid to the TOPO solvent before the start of the reaction was discovered, by Peng *et al.*[40], to slow the growth of the particles and enable the production of CdSe nanorods with dimensions of 3.6 nm by 6.6 nm, as measured from TEM images. Landes *et al.*[41] added a quenching step to the method used by Murray *et al.*[2] by adding nanoparticle/TOPO solution to room temperature hexane to produce CdSe particles with an average diameter of 1.6 nm. The addition of n-butylamine to a solution of 1.6 nm

CdSe particles, size calculated using equation 1.12, was shown by Landes *et al.*[41] to result in the appearance of a feature in the optical absorption spectrum at 414 nm, while the broad peak at 440 nm observed from the original particle solution decreased in intensity. CdSe particles coated with poly(amidoamine) dendrimers were synthesised by Zhang *et al.*[42] via the surface exchange of the CdSe particles made using the method pioneered by Murray *et al.*[2]. This resulted in particles that were stable to oxidation for 2 months, had an average diameter of 5.5 nm, as measured by TEM, and an absorption onset at approximately 620 nm[42]. Talapin *et al.*[43] found that using an initial solution of hexadecylamine in TOPO in the preparation of CdSe particles from TOPSe and dimethyl cadmium decreased the growth rate of the CdSe particles. Bowen Katari *et al.*[44] prepared CdSe nanoparticles using tributylphosphine (TBP) in place of TOP. Particles with sizes ranging from 1.8 nm to 6.7 nm, as measured using TEM, with a corresponding change in the band gap from 2.5 eV to 1.9 eV were prepared using this method. Using small angle X-ray diffraction, the particles were found to be crystalline. Particles produced by the method used by Bowen Katari *et al.*[44] were deposited on indium tin oxide/p-paraphenylene vinylene (PPV) plates by Colvin *et al.*[45]. The luminescence properties were studied and the electroluminescence of CdSe and PPV were found to be voltage dependent. Ginger *et al.*[46] studied the photoelectrochemical properties of CdSe, with diameters of 2.7 nm and 4.5 nm, as measured by TEM, prepared by the synthesis used by Bowen Katari *et al.*[44], sandwiched between indium tin oxide and aluminium electrodes. Photocurrent spectra displayed peaks at

530 nm and 602 nm for the particles with diameters of 2.7 nm and 4.5 nm respectively and efficiencies of 1-3 % were observed. Peng *et al.*[47] replaced dimethyl cadmium with CdO as the cadmium precursor used in preparation pioneered by Murray *et al.*[2]. This offers the advantage that the dimethyl cadmium which is highly toxic, pyrophoric and unstable at room temperature is eliminated. Using this approach highly monodisperse CdSe particles were produced over a range of sizes. Peng *et al.*[47] observed an absorption peak at 440 nm for the smallest particles that were prepared. A photovoltaic device consisting of CdSe particles produced by a similar method to that used by Peng *et al.*[47] sandwiched between an aluminium cathode and an anode consisting of indium tin oxide coated with a blend of poly(3,4-ethylene dioxythiophene) with poly(styrene sulfonate) was prepared by Sun *et al.*[48]. A short circuit external quantum efficiency of 45 % was observed under illumination with light of wavelength 480 nm. Qu *et al.*[49] employed a similar method of preparing CdSe to Peng *et al.*[47], using CdO, $CdCO_3$ or cadmium acetate as the cadmium precursor and TOPO, stearic acid or mixtures of TOPO with stearic acid, lauric acid, dodecylamine or a phosphonic acid as the solvent. Cadmium acetate was found to be the most versatile precursor. Qu *et al.*[49] observed that small particles in the size range of 1.5 nm to 8 nm, as measured from TEM images, are easily prepared in TOPO or a mixture of TOPO and a phosphonic acid, while particles in the size range of 8 nm to 25 nm are best synthesised in stearic acid. Aldana *et al.*[50] prepared CdSe particles according to the method used by Peng *et al.*[47], but using cadmium acetate as the cadmium precursor and TOPO as the solvent. The

resultant particles were heated in methanolic solution of a thiol in order to produce thiol coated CdSe particles. From studies of the effects of time on the absorption spectrum, these particles were found to be photochemically unstable. Using NMR and UV-Visible absorption spectroscopy as methods of determining the decomposition, Aldana *et al.*[50] suggested three processes involved in this instability. Zhelev *et al.*[51] observed an enhancement in the photoluminescence of CdSe nanoparticles from exposure of the particles to UV-irradiation over time. These particles were produced by the method outlined by Qu *et al.*[49] using cadmium acetate as the cadmium precursor and TOPO as the solvent.

Preparation Using a Single Source Precursor

Cadmium selenide nanoparticles have been prepared from the thermal decomposition of a single source precursor by O'Brien *et al.*[52–55]. These precursors include bis[methyl(n-hexyl)diselenocarbamato]cadmium[52;54], methyl diethyldiselenocarbamato cadmium[53] and cadmium imino-bis(diisopropylphosphine selenide)[55]. The preparation of these complexes are complicated[56–59]. CdSe particles with average diameters between 4.8 and 6.4 nm, as measured using TEM, and band gaps between 1.96 and 2.18 eV have been reported using this method.

Synthetic Method Using bis(trimethylsilyl)selenide as the Selenide source

Ptatschek *et al.*[60] produced CdSe nanoparticles by first synthesising a complex of a cadmium precursor with 3-aminopropyltriethoxysilane (AMEO) by refluxing an ethanolic solution of these compounds. This complex was then exposed to bis(trimethylsilyl)selenide which resulted in AMEO-capped CdSe nanocrystals with an average diameter of 1.6 nm, as measured using TEM. These particles were spin coated on to glass slides an were observed to have an peak in the optical absorption spectrum at 410 nm indicating size quantisation. Ptatschek *et al.*[60] observed an increase in size to an average diameter of 3 nm, as measured by TEM, if 2-butoxyethanol replaced ethanol as the solvent. In the above method CdSe particles are formed from a simple room temperature reaction of a cadmium precursor and bis(trimethylsilyl)selenide.

This chapter will study the preparation of CdSe particles by this method using $Cd(ClO_4)_2$ in place of the complex of Cd with AMEO, 3-mercaptopropionic acid as a capping agent and THF as the solvent. The particles will be deposited on tin oxide glass electrodes in situ. This method will be studied as this preparation offers a simple synthetic route to CdSe coated electrodes and similar syntheses using the same cadmium precursor and capping agent have produced CdS coated electrodes that exhibited photocurrent. The CdSe coated electrodes and solutions of the particles will be characterised by UV-Vis spectroscopy, TEM and photoelectrochemical techniques.

5.2 Preparation of Nanoparticles

Electrodes precleaned in a 5 mol dm^{-3} KOH bath for 2 hours, were placed in a 250 ml conical flask. 50 ml of THF containing 5 x 10^{-5} moles of $Cd(ClO_4)_2$ and 3.8 x 10^{-6} moles of 3-mercaptopropionic acid was then added to the conical flask. The reaction mixture was placed in a dry box and stirred for 5 minutes. 12.5 μl of bis(trimethylsilyl)selenide was added and the mixture was stirred for a set period of time. After this time, a drop of the reaction mixture was placed on a TEM grid, the UV-Vis spectrum of the solution was measured and the electrodes were removed from the solution, washed with THF and dried. Reaction times of 2 minutes and 1 hour were used.

5.3 Characterisation

5.3.1 UV-Vis Spectroscopy

The UV-Visible absorption spectra of cadmium selenide nanoparticles prepared using reaction times of 2 minutes and 1 hour are shown in Fig. 5.4. A non-zero base line was observed in the UV-Visible spectra due to the CdSe particles scattering light. Table 5.1 displays the band gaps estimated from the absorption edge in the UV-Visible spectra of the CdSe nanoparticles.

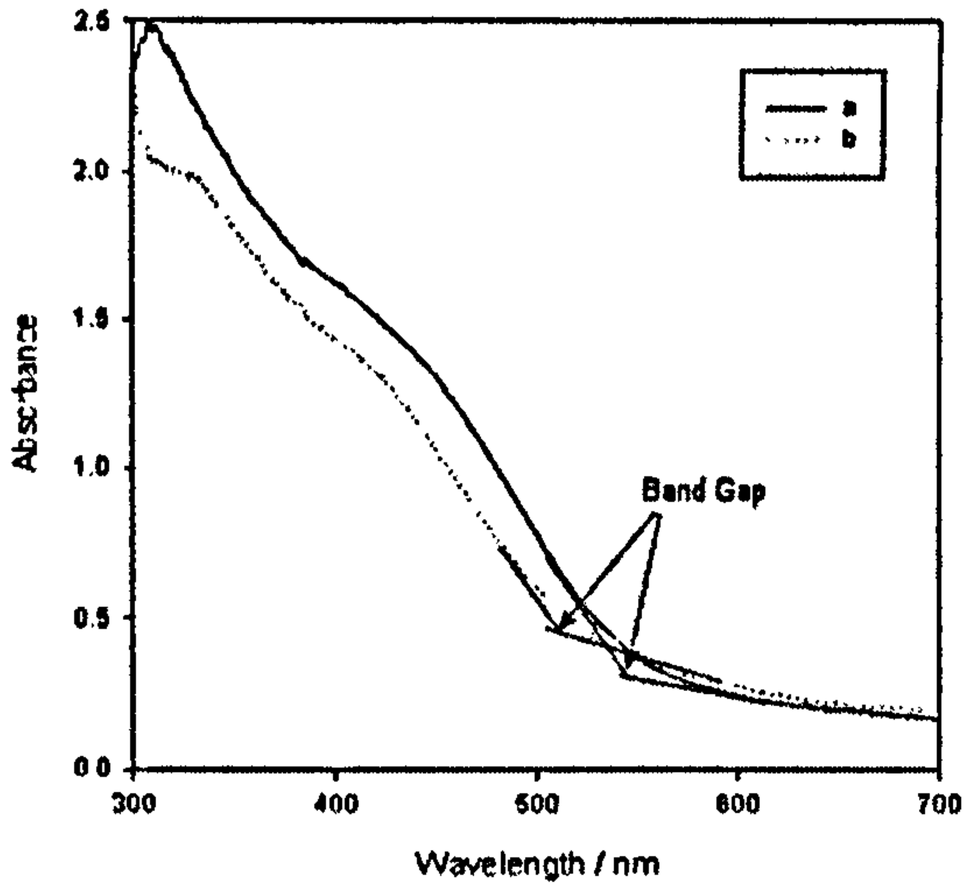

Figure 5.4: UV-Vis spectra of CdSe nanoparticles after a reaction time of a) 2 minutes and b) 1 hour.

Reaction Time	Absorption edge / nm	Estimated Band Gap /eV
2 minutes	545	2.27
1 hour	513	2.41

Table 5.1: Estimated band gaps of CdSe particles.

5.3.2 Transmission Electron Microscopy

Fig. 5.5 illustrates example TEM images of CdSe nanoparticles after reaction times of 2 minutes and 1 hour. The average particle size of the samples are listed in Table 5.2. These sizes were calculated by statistical analysis of the size distributions shown in Fig.5.6 found by measuring the number of particles indicated in the table. Fig.5.7 displays the energy dispersive X-ray analysis spectra of the CdSe nanoparticles after reaction times of 2 minutes and 1 hour.

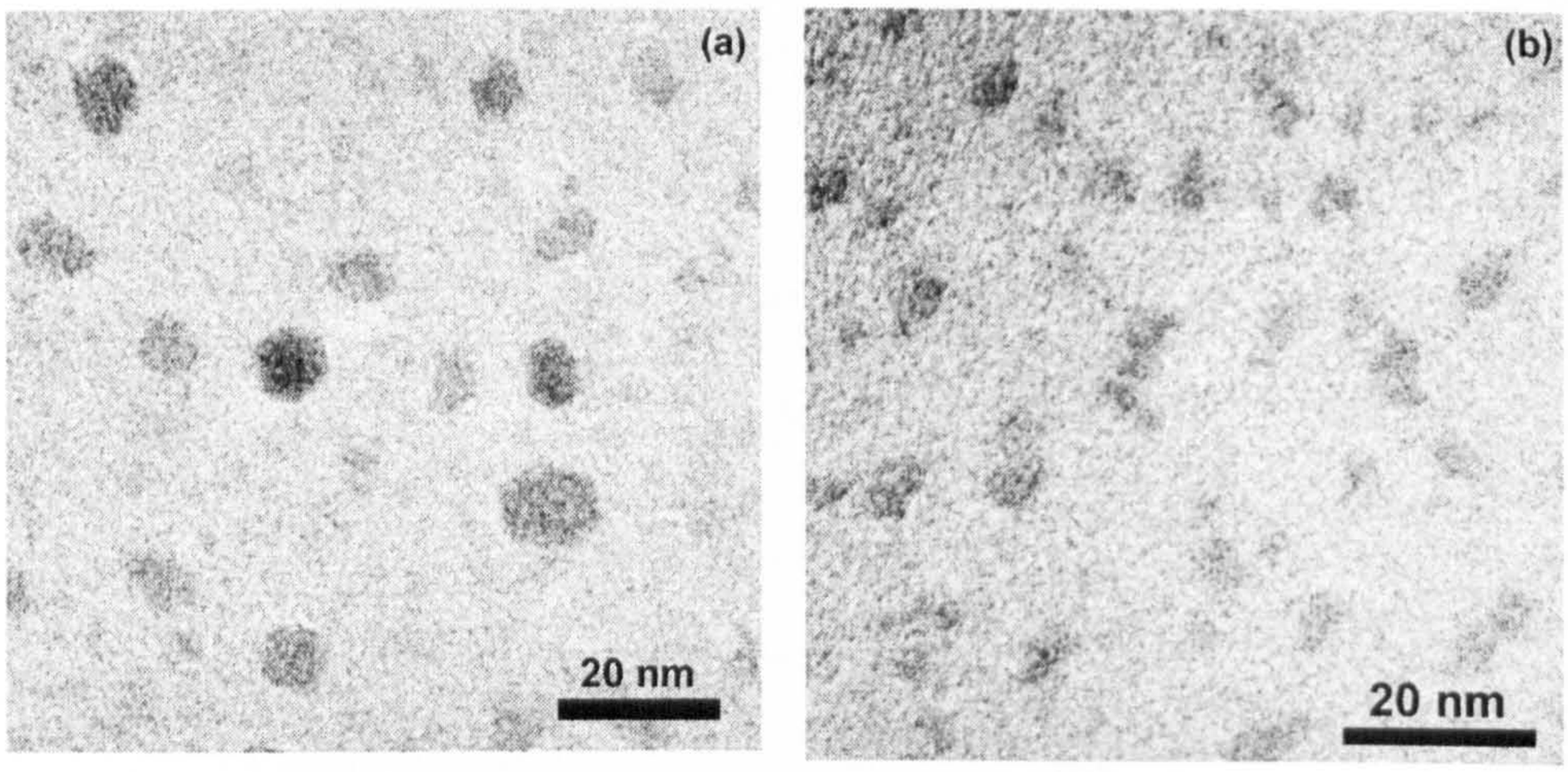

Figure 5.5: TEM images of CdSe nanoparticles after a reaction time of a) 2 minutes and b) 1 hour.

Reaction Time	Particle diameter / nm	sample size
2 minutes	6.1 ± 1.7	356
1 hour	5.3 ± 1.5	432

Table 5.2: Average particle diameter of CdSe nanoparticles after a reaction time of 2 minutes and 1 hour with the respective number of measurements used in the statistical analysis.

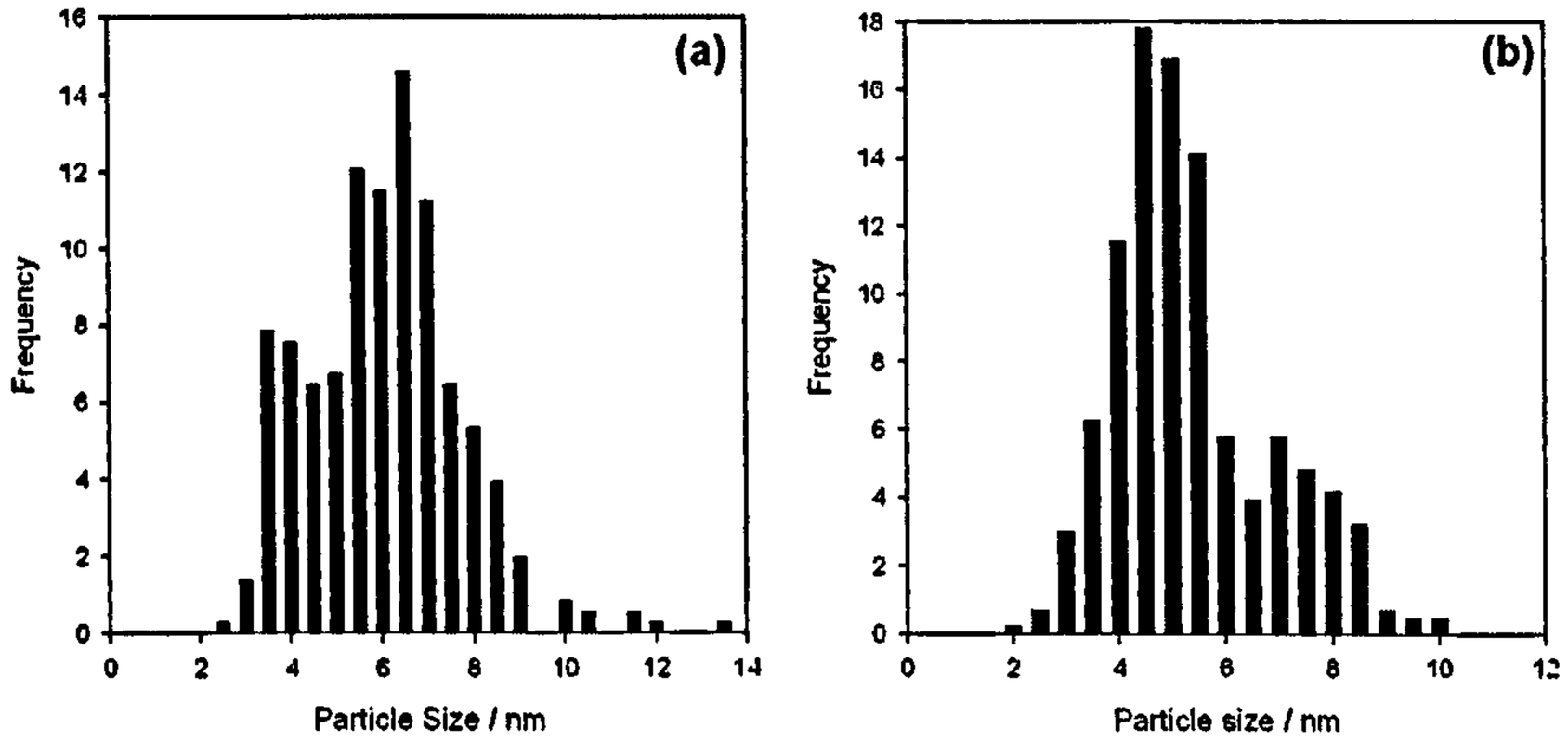

Figure 5.6: Size distributions of CdSe nanoparticles after a reaction time of a) 2 minutes and b) 1 hour.

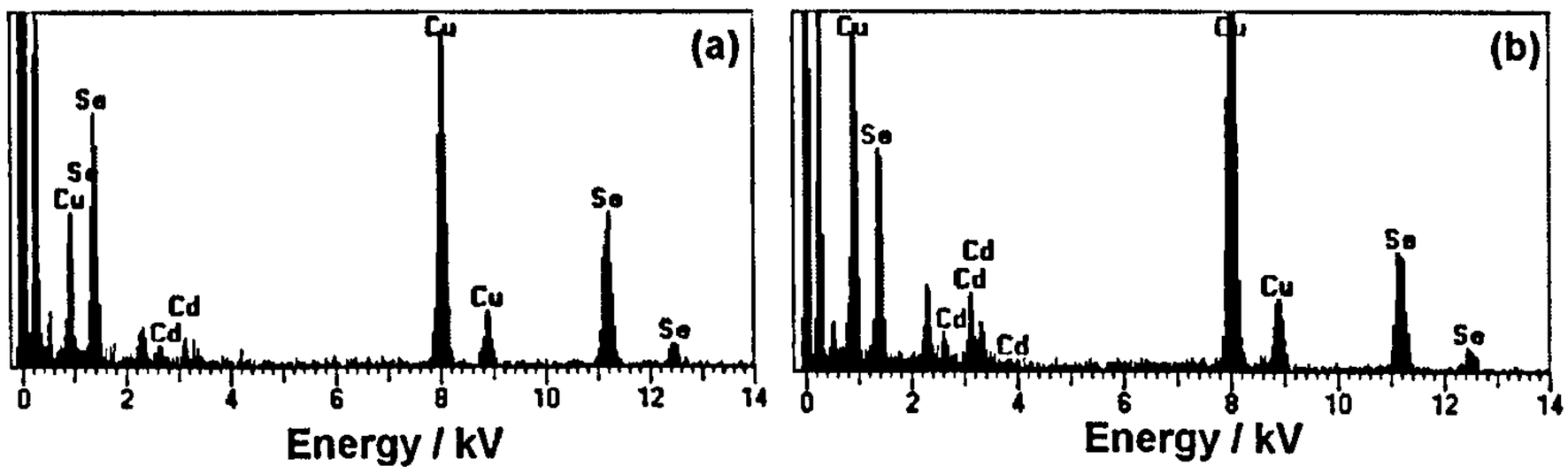

Figure 5.7: Energy dispersive X-ray analysis spectra of CdSe nanoparticles after a reaction time of a) 2 minutes and b) 1 hour.

5.4 Photoelectrochemistry

5.4.1 Photocurrent Spectroscopy

The photocurrent spectra of CdSe nanoparticles after reaction times of 2 minutes and 1 hour are illustrated in Fig.5.8. These spectra were measured at a potential of 0V vs Ag|AgCl|3 mol dm^{-3} KCl. CdSe particles grown for 2 minutes and 1 hour were found to have band gaps of 2.39 eV (517 nm) and

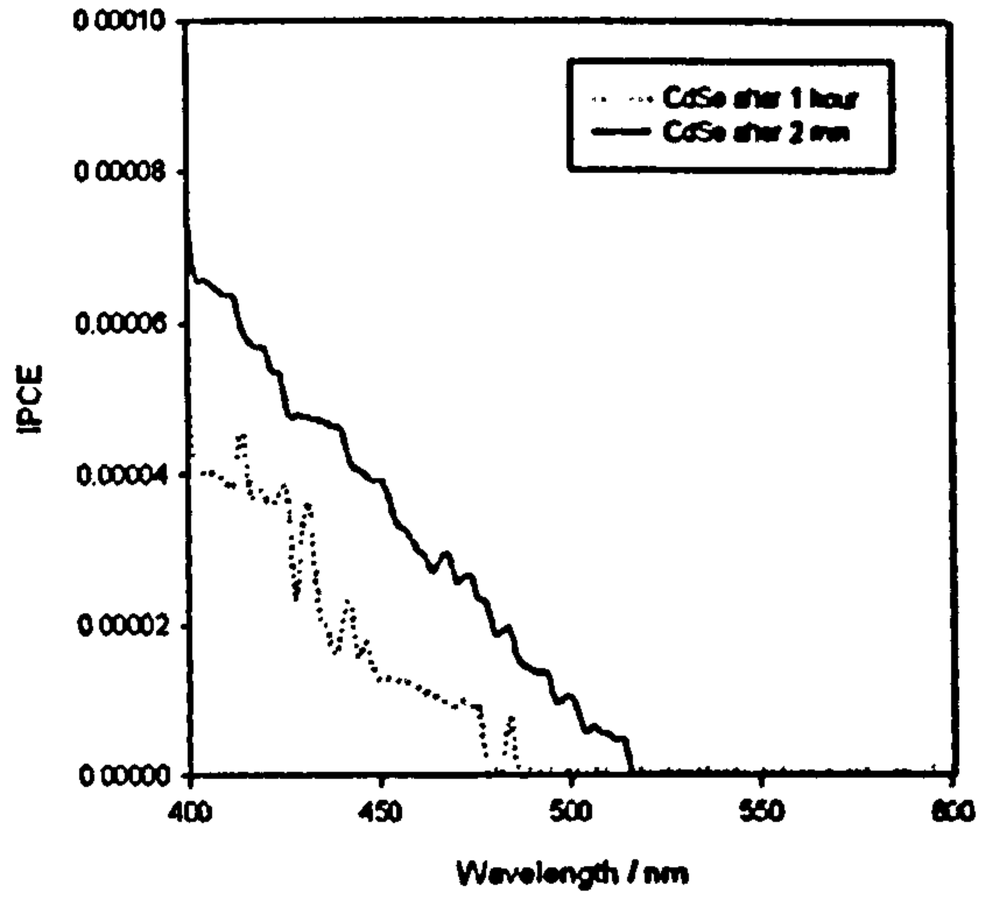

Figure 5.8: Photocurrent spectra of CdSe nanoparticles after a reaction time of a) 2 minutes and b) 1 hour obtained at 0 V vs. Ag|AgCl|3 mol dm^{-3} KCl and using monochramatic light chopped at 17 Hz.

2.59 eV (478 nm) respectively. An incident photon to electron conversion efficiency of less than 0.01 % was observed.

5.5 Discussion

It can be seen from the UV-Visible spectra that the CdSe particles grown for 2 minutes have a smaller band gap than the CdSe particles grown for 1 hour. This result indicates that the particles are decreasing in size as the growth time is increased, as shown by the relationship of the band gap of the material to the size of the particles displayed in equation.1.11. As errors are introduced in the band gaps found in the UV-Visible spectra by the scattering of light by the particles, the effective mass model of quantum confinement is

applied to the band gaps found using photocurrent spectroscopy in order to estimate the dependence of the band gap on the size of the semiconductor particles.

A decrease in particle size from 6.1 ± 1.7 to 5.3 ± 1.5 nm was observed as the growth time was increased from 2 minutes to 1 hour in the TEM images. For the preparation of CdSe particles, by mixing Cd^{2+} and a Se source in solution, it is expected that particles will grow with increasing reaction time as the reagents form CdSe on the surface of the nuclei. However, the reagent mixture changes in colour from orange to yellow with increasing reaction time, which indicates that the particle size decreases with increasing reaction time from the qualitative analysis of equation 1.11. The presence of Cd and Se in the samples were confirmed by EDAX indicating that no chemical change occurs within the particle as the particles decrease in size. Therefore it is probable that there is a slow decomposition or dissolution occurring at the surface of the CdSe particles in THF solution after the initial formation of the particles.

The band gap of the CdSe can be related to the particle size by equation 1.11 using the effective mass model of quantum confinement. The effective masses of electrons and holes in CdSe have been calculated to be 0.13 and 0.45 respectively[61], by Dimmock and Wheeler[62] using the effective mass approximation theory of Dresselhaus[63]. The high frequency relative dielectric constant of CdSe is 5.8[16]. Fig.5.9 illustrates the band gap of CdSe as a function of particle size, using a bulk band gap of 1.71 eV. From the band gaps of the particles grown for 2 minutes and the particles grown for 1 hour mea-

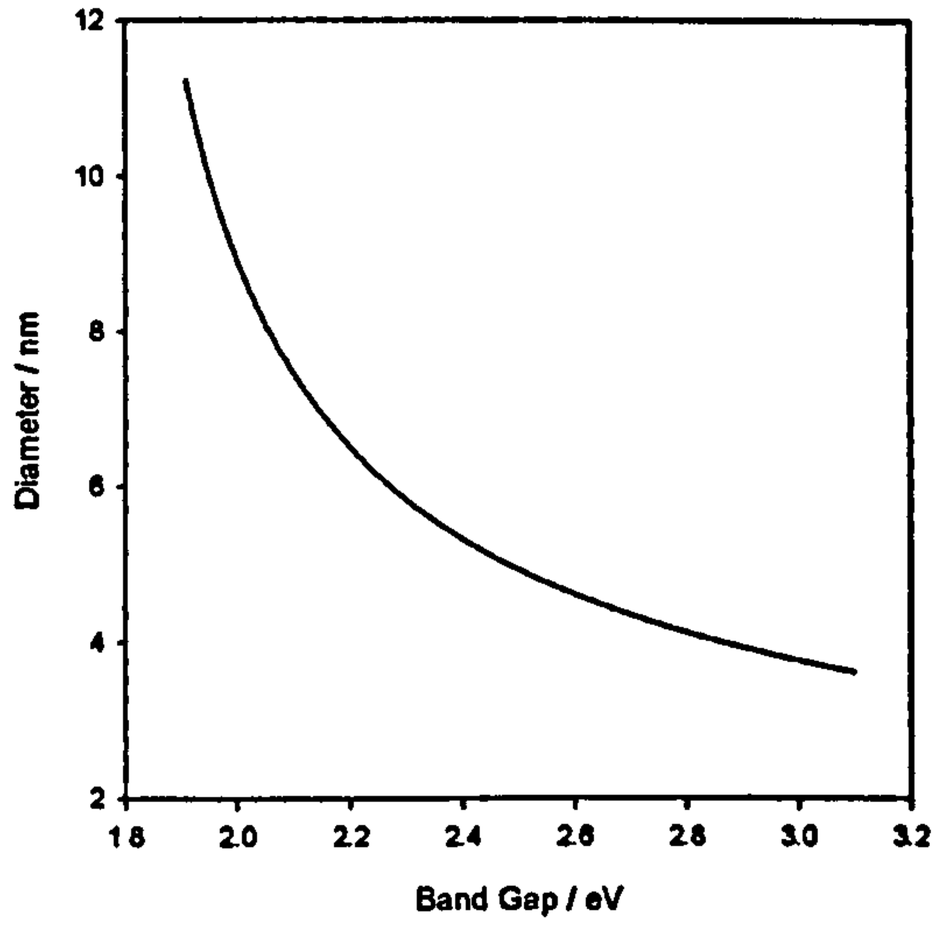

Figure 5.9: Band gap of CdSe particles as a function of calculated CdSe particle diameter.

sured by photocurrent spectroscopy (2.39 and 2.59 eV respectively), average particle diameters of 5.3 nm and 4.6 nm respectively have been calculated using equation 1.11. Particle sizes of 6.0 and 5.3 nm have been found from the band gaps for particles grown for 2 minutes and 1 hour (2.27 eV and 2.41 eV respectively) found using UV-Vis absorption spectroscopy. These sizes are within the error margins of the sizes measured using TEM.

Very low efficiencies were observed in the photocurrent spectra. As the electrodes were not highly coloured, this is most likely to be due to poor deposition of the particles on the electrode surface. Alternatively the conduction bands of the particles and electrodes could be very close to each other in energy, limiting the electron transfer from the particle to the electrode or the mechanisms for the loss of an electron resulting from the photonic excitation of CdSe, illustrated in Fig.5.10, occur at a similar rate to that for the transfer

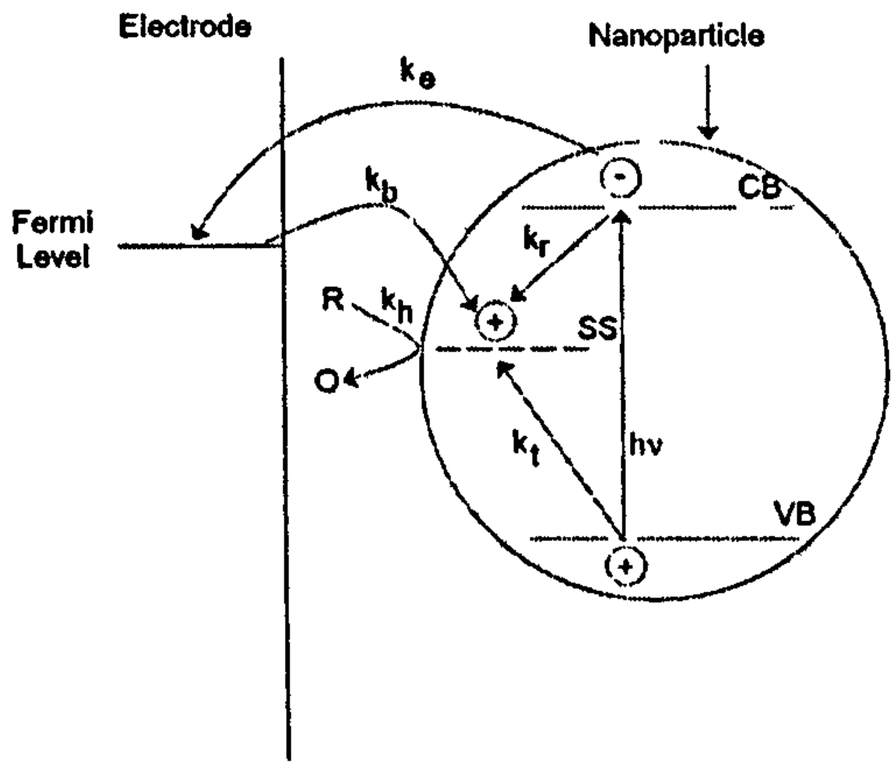

Figure 5.10: A schematic of the charge transfer processes occurring in CdSe coated electrode in electrolyte system. SS = a surface state, R = reduced form of the electrolyte hole scavenger, O = oxidised form of the electrolyte hole scavenger, k_t, k_r, k_e, k_h and k_b = the rate constants of trapping a hole in the surface state, recombination, electron transfer, hole transfer and back electron transfer respectively.

of the electron to the electrode, thus limiting the observed photocurrent.

Due to the low efficiencies observed in the photocurrent spectra and the decomposition of the particles in the growth solution, CdSe particles prepared using this method are not ideal sensitisers for use in solar cells.

5.6 Summary

CdSe nanoparticles have been prepared using bis(trimethylsilyl)selenide. These particles appear to be unstable in the as-prepared solution and exhibit only a small amount of photocurrent when exposed to light.

References

[1] Strehlow, W. H.; Cook, E. L. *J. Phys. Chem. Ref. Data* **1973**, *2*(1), 163 – 185.

[2] Murray, C. B.; Norris, D. J.; Bawendi, M. G. *J. Am. Chem. Soc.* **1993**, *115*, 8706.

[3] Majetich, S. A.; Carter, A. C. *J. Phys. Chem.* **1993**, *97*, 8727.

[4] Gorer, S.; Hodes, G. *J. Phys. Chem.* **1994**, *98*(20), 5338–5346.

[5] Lifshitz, E.; Dag, I.; Litvitn, I. D.; Hodes, G. *J. Phys. Chem. B* **1998**, *102*, 9245.

[6] Shen, Q.; Toyoda, T. *Jap. J. Appl. Phys.* **2004**, *43*, 2946.

[7] Shen, Q.; Arae, D.; Toyoda, T. *J. Photochem. Photobio. A* **2004**, *164*, 75.

[8] Pejova, B.; Tanusevski, A.; Grozdanov, I. *J. Solid State Chem.* **2003**, *172*, 381.

[9] Pejova, B.; Grozdanov, I. *Mater. Lett.* **2004**, *58*, 666.

[10] Fang, J.; Wu, J.; Lu, X.; Shen, Y.; Lu, Z. *Chem. Phys. Lett.* **1997**, *270*, 145.

[11] Yochelis, S.; Hodes, G. *Chem. Mater.* **2004**, *16*, 2740.

[12] Zhang, S.; Yu, J.; Li, X.; Tian, W. *Nanotech.* **2004**, *15*, 1108.

[13] Ma, X.-D.; Qian, X.-F.; Yin, J.; Xi, H.-A.; Zhu, Z.-K. *J. Coll. Inter. Sci.* **2002**, *252*, 77.

[14] Yamamoto, O.; Sasamoto, T. *J. Mater. Res.* **1998**, *13*, 3394.

[15] Sondi, I.; Siiman, O.; Matijeic. *J. Coll. Inter. Sci.* **2004**, *275*, 503.

[16] Rogach, A. L.; Kornowski, A.; Gao, M. Y.; Eychmuller, A.; Weller, H. *J. Phys. Chem. B* **1999**, *103*(16), 3065–3069.

[17] Baumle, M.; Stamou, D.; Segura, J.-M.; Hovius, R.; Vogel, H. *Langmuir* **2004**, *20*, 3828.

[18] Zheng, X.; Xie, Y.; Zhu, L.; Jiang, X.; Yan, A. *Ultrasonics Sonochemistry* **2002**, *9*, 311.

[19] Zhu, J.-J.; Xu, S.; Wang, H.; Zhu, J.-M.; Chen, H.-Y. *Adv. Mater.* **2003**, *15*, 156.

[20] Ge, J.-P.; Li, Y.-D.; Yang, G.-Q. *Chem. Commun.* **2002**, page 1826.

[21] Mastai, Y.; Polsky, R.; Koltypin, Y.; Gedanken, A.; Hodes, G. *J. Am. Chem. Soc.* **1999**, *121*(43), 10047–10052.

[22] Li, H.-L.; Zhu, Y.-C.; Chen, S.-G.; Palchik, O.; Xeng, J.-P.; Koltypin, Y.; Gofer, Y.; Gednken, A. *J. Solid State Chem.* **2003**, *172*, 102.

[23] Wark, M.; Wellmann, H.; Rathousky, J. *Thin Solid Films* **2004**, *458*, 20.

[24] Belogorokhov, A. I.; Belogorokhova, L. I.; Perez-Rodriguez, A.; Morante, J. R.; Gavrilov, S. *Appl. Phys. Lett.* **1998**, *73*, 2766.

[25] Haggata, S. W.; ColeHamilton, D. J.; Fryer, J. R. *J. Mater. Chem.* **1997**, *7*(10), 1969–1975.

[26] Haggata, S. W.; Li, C.; Cole-Hamilton, D. J.; Fryer, J. R. *J. Mater. Chem.* **1996**, *6*, 1771.

[27] Palchik, O.; Kerner, R.; Gedanken, A.; Weiss, A. M.; Slifkin, M. A.; Palchik, V. *J. Mater. Chem.* **2001**, *11*, 874.

[28] Rogach, A. L.; Nagesha, D.; Ostrander, J. W.; Giersig, M.; Kotov, N. A. *Chem. Mater.* **2000**, *12*, 2676.

[29] Gautam, U. K.; Rajamthi, M.; Meldrum, F.; Morgan, P.; Seshdri, R. *Chem. Commun.* **2001**, page 629.

[30] Liu, Y.; Xu, Y.; Li, J.-P.; Zhang, B.; Wu, D.; Sun, Y.-H. *Chem. Lett.* **2004**, *33*, 1162.

[31] Baban, C.; Rusu, G. I. *Appl. Surf. Sci.* **2003**, *211*, 6.

[32] Nesheva, D.; Hofmeister, H.; Levi, Z.; Aneva, Z. *Vacuum* **2002**, *65*, 109.

[33] Kayusa, A. *Nature Materials* **2004**, *3*, 99.

[34] Choi, S.-H.; Woo, D.-H.; Myung, N.; Kang, H.; Park, S.-M. *J. Electrochem. Soc.* **2001**, *148*, C569.

[35] Ruach-Nir, I.; Wagner, H. D.; Rubenstein, I.; Hodes, G. *Adv. Funct. Mater.* **2003**, *13*, 159.

[36] Zhu, J.-J.; Liao, X.; Zhao, X.; Wang, J. *Mater. Lett.* **2001**, *47*, 339.

[37] Zhao, W.-B.; Zhu, J.-J.; Chen, H.-Y. *J. Cryst. Growth* **2003**, *252*, 587.

[38] Yan, Y.-L.; Li, Y.; Qian, X.-F.; Yin, J.; Zhu, Z.-K. *Mater. Sci. Eng. B* **2003**, *103*, 202.

[39] Kuno, M.; Lee, J. K.; Dabbousi, B. O.; Mikulec, F. V.; Bawendi, M. G. *Journal of Chemical Physics* **1997**, *106*(23), 9869–9882.

[40] Peng, X. G.; Manna, L.; Yang, W. D.; Wickham, J.; Scher, E.; Kadavanich, A.; Alivisatos, A. P. *Nature* **2000**, *404*(6773), 59–61.

[41] Landes, C.; Braun, M.; Burda, C.; El-Sayed, M. A. *Nano Lett.* **2001**, *1*, 667.

[42] Zhang, C.; O'Brien, S.; Balogh, L. *J. Phys. Chem. B* **2002**, *106*, 10316.

[43] Talapin, D. V.; Rogach, A. L.; Kornowski, A.; Haase, M.; Weller, H. *Nano Lett.* **2001**, *1*(4), 207–211.

[44] Katari, J. E. B.; Colvin, V. L.; Alivisatos, A. P. *J. Phys. Chem.* **1994**, *98*(15), 4109–4117.

[45] Colvin, V. L.; Schlamp, M. C.; Alivisatos, A. P. *Nature* **1994**, *370*(6488), 354–357.

[46] Ginger, D. S.; Greenham, N. C. *J. Appl. Phys.* **2000**, *87*, 1361.

[47] Peng, Z. A.; Peng, X. *J. Am. Chem. Soc.* **2001**, *123*, 183.

[48] Sun, B. nd Marx, E.; Greenham, N. C. *Nano Lett.* **2003**, *3*, 961.

[49] Qu, L. H.; Peng, Z. A.; Peng, X. G. *Nano Lett.* **2001**, *1*(6), 333–337.

[50] Aldana, J.; Wang, Y. A.; Peng, X. G. *J. Am. Chem. Soc.* **2001**, *123*(36), 8844–8850.

[51] Zhelev, Z.; Jose, R.; Nagase, T.; Ohba, H.; Bakalova, R.; Ishikawa, M.; Baba, Y. *J. Photochem. Photobio. B* **2004**, *75*, 99.

[52] Trindade, T.; Obrien, P. *J. Mater. Chem.* **1996**, *6*(3), 343–347.

[53] Trindade, T.; Obrien, P. *Adv. Mater.* **1996**, *8*(2), 161.

[54] Ludolph, B.; Malik, M. A.; O'Brien, P.; Revaprasadu, N. *Chem. Commun.* **1998**, (17), 1849–1850.

[55] Crouch, D. J.; O'Brien, P.; Malik, M. A.; Skabara, P. J.; Wright, S. P. *Chem. Commun.* **2003**, page 1454.

[56] Abrahams, I.; Malik, A.; Motevalli, M.; Obrien, P. *J. Organomet. Chem.* **1994**, *465*(1-2), 73–77.

[57] Obrien, P.; Walsh, J. R.; Jones, A. C.; Rushworth, S. A. *Polyhedron* **1990**, *9*(12), 1483–1485.

[58] Hursthouse, M. B.; Malik, M. A.; Motevalli, M.; Obrien, P. *Polyhedron* **1992**, *11*(1), 45–48.

[59] Hurhouse, M. B.; Malik, M. A.; Mottevalli, M.; O'Brien, P. *J. Mater. Chem.* **1992**, *2*, 949.

[60] Ptatchek, V.; Schreder, B.; Herz, K.; Hilbert, U.; Ossau, W.; Schottner, G.; Raha1user, O.; Bischof, T.; Lermann, G.; Materny, A.; Kiefer, W.;

Bacher, G.; Forchel, A.; Su, D.; Giersig, M.; Mu1ller, G.; Spanhel, L. *J. Phys. Chem. B* **1997**, *101*, 8898.

[61] Kroger, F. A. *J. Phys. Chem. Solids* **1965**, *26*, 1707.

[62] Dimmock, J. O.; Wheeler, R. G. *J. Appl. Phys.* **1961**, *32*, 2271.

[63] Dresselhaus, G. *J. Phys. Chem. Solids* **1956**, *1*, 15.

Chapter 6

Lead Sulfide

6.1 Introduction

Lead sulfide has a bulk band gap of 0.41 eV[1] and a Bohr radius of 18 nm. This means that PbS particles exhibit size quantisation effects over a large range of sizes, the smallest particles theoretically exhibiting a band edge of less than 800 nm in the absorption spectrum. Therefore small, well-defined PbS particles are candidates for sensitisers in solar cells. Methods to prepare PbS that have been employed previously are discussed below.

6.1.1 Synthetic Methods for the Preparation of Lead Sulfide

Film Techniques

Yang *et al.*[2] and Plass *et al.*[3] prepared PbS nanoparticles on TiO_2 electrodes by dipping a porous substrate, conducting tin oxide glass electrodes coated

with a mesoporous film of TiO_2 formed according to the procedure outlined in section 2.1, into an aqueous solution of lead nitrate, followed by immersion in to an aqueous solution of Na_2S. This process could be repeated a number of times to increase the size of the lead sulfide particles. Yang *et al.*[2] formed particles with average diameters of 2.94, 3.99 and 4.76 nm, as calculated using equation 1.12, by increasing the number of the times the deposition process was carried out. Yang *et al.*[2] observed photodegradation of the PbS coated electrode and showed that this could be minimised by coating the lead sulfide particles with a thiol layer. A solid state cell consisting of a TiO_2 coated tin oxide electrode coated with PbS particles produced by the technique outlined above and an organic charge transport material connected to a gold contact was synthesised by Plass *et al.*[3]. The organic charge transport material used was spiro-OMeTAD. The IPCE spectrum of these systems displayed a maximum value of 45 % at a wavelength of 420 nm.

Bakueva *et al.*[4] prepared PbS nanoparticles capped with a combination of thioglycerol and dithioglycerol by adding an aqueous solution of Na_2S to an aqueous solution containing the capping agent and lead acetate. A change in the absorption edge from 1000 to 1330 nm, corresponding to a change particle diameter from 2.7 to 4.0 nm, as calculated using equation 1.12, was observed by Bakueva *et al.*[4] upon changing the ratio of Pb to S from 1:0.3 to 1:0.7.

Syntheses Involving The Thermal Decomposition of a Sulfur Containing Compound

Lead sulfide nanoparticles have been prepared by the decomposition of thiourea or thioacetamide in the presence of a lead precursor. Zhou *et al.*[5] added a dimethyl sulfoxide solution of thioacetamide to a dimethyl sulfoxide solution of lead acetate and polydithiafulvene and stirred the resulting mixture vigorously for 6 hours in order to produce lead sulfide particles capped with polydithiafulvene. The particles displayed an absorption onset at 725 nm and an average particle diameter of 4 nm, as measured by TEM, was observed. A solution of lead acetate and thioacetamide in ethylenediamine was heated slowly to 60 °C by Chen *et al.*[6] in order to synthesise lead sulfide nanorods of average diameter 75 nm and lengths between 150 and 700 nm, as measured using TEM. Chen *et al.*[6] proposed the following mechanism for the reaction:

$$\begin{aligned} CH_3CSNH_2 + 2OH^- &\rightarrow NH_3 + CH_3COO^- + HS^- \\ HS^- + OH^- &\rightarrow H_2O + S^{2-} \\ Pb^{2+} + S^{2-} &\rightarrow PbS \end{aligned} \tag{6.1}$$

Lead sulfide crystals were prepared by Ma *et al.*[7] by heating an aqueous solution of acetic acid, lead acetate and thioacetamide to 80 °C for five hours. Ma *et al.*[7] observed, using TEM, that the crystals had eight symmetric arms with two adjacent corners being 2 μm apart. Lifshitz *et al.*[8] synthesised lead sulfide nanoparticles embedded in a polymer film by spreading a solution of polyacrylamide, lead nitrate and thiourea on a glass substrate and then

heated the substrate to 375 K for 12 hours. Particles of average diameter 2.1 and 0.8 nm, as measured by TEM, were prepared by controlling the concentration of the precursors and a substantial blue shift in the absorption spectra was observed. Films of PbS nanoparticles were grown on glass, quartz and silicon substrates by Joshi *et al.*[9] by immersing the substrate in a stirred alkaline aqueous solution of thiourea and lead acetate. Particles of various sizes with different band gaps were observed depending on the temperature and pH of the bath as outlined, in Table.6.1. Kang *et al.*[10] prepared PbS

pH	Temperature / °C	size / nm	Band Gap /eV
9.25	20	12	2.32
9.25	35	14	2.15
9.75	20	15	2.05
9.75	35	19	1.80
10.25	20	17	1.95
10.25	35	23	1.52

Table 6.1: Band gaps and sizes of PbS particles as prepared by Joshi *et al.*[9].

nanoparticles in a TiO_2/glycerol matrix by first stirring an aqueous solution of lead acetate, ethanol, acetic acid, titanium isopropoxide, glycerol and thiourea for 24 hours, then evaporating 70 % of the solvent and finally spin coating the viscous sol on to a glass substrate followed by annealing at 160 °C. The resultant PbS clusters had an average size of 10 nm and were embedded in a TiO_2-glycerol matrix. The following mechanism was suggested by Kang *et al.*[10] for the formation of PbS nanoparticles, from the TiO_2/glycerol matrix

precursor containing Pb^{2+} and thiourea.

$$NH_2CSNH_2 + 2H_2O \rightarrow H_2S + CO_2 + 2NH_3 \qquad (6.2)$$

$$Pb^{2+} + H_2S \rightarrow PbS + 2H^+$$

These sizes were measured from TEM images.

Solution Precipitation

H_2S has been used in order to synthesise lead sulfide particles. Lu *et al.*[11] produced PbS nanoparticles by injecting H_2S gas in to an ethanolic solution of $Pb(ClO_4)_2$ and hydroxypropyl cellulose. Thin films of the hydroxypropyl cellulose coated PbS particles were then dip coated onto fused silica glass. These particles were found to be crystalline and have an average size of 4.7 nm, as measured by TEM. The addition of H_2S gas to an ethanolic solution of lead acetate and dodecylthiol was used to prepare lead sulfide nanoparticles by Gurin *et al.*[12]. This resulted in particles with sizes in the 1 - 5 nm range, as measured from AFM images. Kyprianidou-Leodidou *et al.*[13] bubbled H_2S gas through water to produce H_2S solution and then added this solution to an aqueous solution of polyethylene oxide, lead acetate and sodium dodecyl sulfate in order to produce PbS nanoparticles. It was found that by changing the molar ratio of sodium dodecyl sulfate to lead acetate from 0.0034 to 0.347, the size of the particles decreased from 24 nm to 4 nm, as measured by TEM. Nanocrystalline PbS was synthesised by Mukherjee *et al.*[14] by adding H_2S gas to aqueous solutions containing different amounts of polyacrylamide and $PbNO_3$. This resulted in particles with decreasing average diameters of

18 nm, 16.8 nm and 9.9 nm, as measured by TEM, with corresponding band gaps of 1.03, 1.14 and 1.49 eV respectively as the concentration of $PbNO_3$ was increased. Lu *et al.*[15], Fernee *et al.*[16;17] and Bakkers *et al.*[18] prepared PbS particles by injecting H_2S gas into an aqueous solution of polyvinyl alcohol and a lead precursor. Particles with an average diameter of 3.3 nm, as measured by TEM, were synthesised using $Pb(ClO_4)_2$ as the lead source. Lu *et al.*[15] dip coated such particles onto a fused silica substrate. These particles were found to exhibit three sharp peaks at 592, 391 and 294 nm indicating that the particles are quantum confined. Bakkers *et al.*[18] deposited PbS particles with a diameter of 6.5 nm, as measured by TEM, on a gold electrode and studied the photoelectrochemical properties of the particles. PbS particles with an average diameter of 3 nm, as measured using TEM, were prepared using lead acetate as the lead precursor by Fernee *et al.*[16;17]. These particles were then surface passivated by adding a solution of sodium hexametaphosphate and $CdCl_2$. A slight blue shift on passivation of the PbS was observed and a broad emission was recorded from the surface passivated particles. PbS particles capped with 4-aminothiophenol were prepared by mixing solutions of 4-aminothiophenol and lead acetate in methanol at - 88 °C, followed by the addition of Na_2S in methanol and subsequent warming of the system to -20 °C by Torimoto *et al.*[19]. This resulted in particles with an average particle size of 2.8 nm, as measured from TEM images, and an unresolved absorption edge at about 600-700 nm indicating that the particles are quantum confined.

Joo *et al.*[20] prepared lead sulfide particles by mixing a $PbCl_2$ in oleylamine

solution with a sulfur in oleylamine solution at 90 °C and then aging the mixture at 220 °C. This resulted in nearly cubic particles with an average size of 13 nm, as measured by TEM. Lattice fringes were observed in the TEM images indicating that the particles were crystalline. Joo *et al.*[20] also found that the particle size could be controlled by changing the ratio of $PbCl_2$ to sulfur in the reaction mixture.

Conversion of a Precursor Adsorbed on a Substrate to PbS

Jiang *et al.*[21] synthesised PbS particles on a gold substrate by dipping the substrate into an ethanolic solution of 11-mercaptoundecanoic acid followed by immersion of the substrate in a $Pb(NO_3)_2$ solution and finally exposure of the system to H_2S gas. This resulted in an orderly arrangement of PbS particles with an average diameter of 3.2 nm, as measured by scanning tunnelling microscopy (STM), on a 11-mercaptoundecanoic acid self assembled monolayer on a gold substrate. Nabok *et al.*[22] exposed spin coated films of 1-, 4-, 8-, 11-, 15-, 18-, 22-, and 25-octahexyl phthalocyaninato lead to H_2S gas in order to produce lead sulfide particles, with an average diameter of 2.24 nm, as calculated from the 1.91 eV band gap measured by UV-Vis spectroscopy using equation 1.12, in a phthalocyanine film.

A polymer film of alternating layers of polydiallyldimethylammonium chloride and polystyrene sulfonate was immersed in an aqueous solution of $Pb(NO_3)_2$, then exposed to H_2S gas and this reaction was then repeated in order to form PbS particles. This method was outlined by Dutta *et al.*[23] and produced particles with a broad range of sizes between 1 and 10 nm, as

measured by TEM.

Hydrothermal and Solvothermal Methods

Hydrothermal techniques have been used by Wang *et al.*[24], An *et al.*[25] and Jiang *et al.*[26] in order to produce lead sulfide nanoparticles. Wang *et al.*[24] synthesised PbS particles of sizes between 50-80 nm, as measured using TEM, by heating an aqueous solution of $PbCl_2$ and thioacetamide in an autoclave at 120 °C for 18 hours. PbS particles of sizes 50-80 nm, as measured using TEM, were prepared by An *et al.*[25] by heating a mixture of lead and sulfur in water in an autoclave at 180 °C for 10-14 hours. The particles were found to be crystalline and exhibited an emission peak at 646 nm in the photoluminescence spectrum. An *et al.*[25] postulated that the mechanism of the formation of PbS particles occurs according to the equations displayed below:

$$\begin{aligned} Pb + 2H_2O &\rightarrow Pb(OH)_2 + H_2\uparrow \\ H_2 + S &\rightarrow S^{2-} + 2H^+ \\ Pb(OH)_2 + S^{2-} + 2H^+ &\rightarrow PbS + 2H_2O \end{aligned} \tag{6.3}$$

Jiang *et al.*[26] heated an aqueous solution containing lead acetate, $Na_2S_2O_3$ and $C_{17}H_{33}COOK$ in an autoclave at 180 °C for 24 hours in order to produce uniform cubic PbS crystals with an edge length of 22.6 nm, as measured by TEM. Equation 6.4 shows the reaction mechanism proposed by Jiang *et al.*[26].

$$\begin{aligned} 2Pb(OOCCH_3)_2 \cdot 2H_2O + 3S_2O_3^{2-} \rightarrow\ & 2PbS + 4HOOCCH_3 + 4SO_3^{2-} + 2H^+ \\ & + H_2O \end{aligned} \tag{6.4}$$

An autoclave containing a solution of lead acetate and ethylenediamine in water with a solution of carbon disulfide in toluene on top was heated to 140-160 °C for 12 hours by Mo *et al.*[27]. This resulted in crystalline lead sulfide nanorods with diameters of 30-160 nm, as measured by TEM, and lengths of up to several micrometers. Mo *et al.*[27] suggested that this solvothermal production of PbS nanorods occurs according to the following mechanism:

$$\begin{aligned} H_2NCH_2CH_2NH_2 + CS_2 &\rightarrow H_2NCH_2CH_2NHCSSH \\ n(H_2NCH_2CH_2NHCSSH) &\rightarrow [-HNCH_2CH_2NHCS-]n + nH_2S\uparrow \\ Pb^{2+} + H_2S &\rightarrow PbS\downarrow + 2H^+ \end{aligned} \tag{6.5}$$

A Mechanochemical Technique

Balaz *et al.*[28] prepared crystalline PbS particles with an average diameter of 18 nm, as calculated from the X-ray diffraction peaks using the Debye-Scherrer equation, by milling a mixture of lead acetate and Na_2S under an argon atmosphere.

Ultrasonic Techniques

Lead sulfide nanoparticles were synthesised by Zhu *et al.*[29] using a sonochemical method. This method involved the sonication of a solution of lead acetate and sulfur in ethylenediamine. Zhu *et al.*[29] reported rectangular PbS particles with average dimensions of 15 x 20 nm, as measured by TEM, and determined that the presence of ethylenediamine was vital to the formation of the particles prepared using this method. In order to prepare PbS particles, Zhao *et al.*[30] exposed solutions of lead acetate and thiourea in ethanol, wa-

ter, ethylene glycol or polyethylene glycol either to ultrasound or microwave irradiation. Table.6.2 summarises the sizes of particles produced, in the various solvents, by the two procedures. These sizes were measured by TEM.

Method	solvent	size / nm
Microwave	ethanol	150-200
Microwave	water	30-50
Microwave	ethylene glycol	15-35
Microwave	polyethylene glycol	100-150
Ultrasound	ethanol	10-15
Ultrasound	water	80-100
Ultrasound	ethylene glycol	100-150
Ultrasound	polyethylene glycol	20-30

Table 6.2: Sizes of PbS particles as prepared by Zhao *et al.*[30].

Zhao *et al.*[30] observed a band gap of 3.49 eV for PbS particles prepared in polyethylene glycol under ultrasound irradiation.

Microwave Heating Methods

Lead sulfide nanocrystals have been prepared by exposing a solution of lead acetate, sulfur and NaOH in ethanol or polyethylene glycol to microwaves by Ding *et al.*[31;32]. PbS particles with average sizes of 10 nm and 15-20 nm, as measured by TEM images, were observed by synthesis in ethanol and polyethylene glycol respectively. Ding *et al.*[32] speculated that the synthesis

in an ethanol solvent occurred due to heating, according to the equations:

$$\begin{aligned} 4S + 6NaOH &\rightarrow 2Na_2S + Na_2S_2O_3 + 3H_2O \\ Na_2S + Pb^{2+} &\rightarrow PbS + 2Na^{+} \end{aligned} \tag{6.6}$$

The following equations were suggested by Ding *et al.*[31] for the formation of PbS in polyethylene glycol under microwave heating.

$$\begin{aligned} Pb^{2+} &\rightarrow Pb \\ Pb + S &\rightarrow PbS \end{aligned} \tag{6.7}$$

In this case, Pb^{2+} was reduced to Pb using polyethylene glycol as a reducing agent, followed by direct combination of Pb and S to form the particles.

Synthesis In Microemulsions

Chen *et al.*[33] synthesised PbS by first dissolving lead acetate and hexanethiol in methanol, then adding toluene and water, separation of the toluene phase and addition of Na_2S to the toluene phase. This resulted in particles with average diameters of 2.53 to 3.98 nm, as measured by TEM, and absorption edges in the region 600-800 nm. The size could be varied by controlling the concentration of hexanethiol used. Chen *et al.*[34] mixed an ethanol-water solution of pyridinium di-n-hexadecyldithiophosphate and Na_2S with an aqueous solution of lead acetate by in order to prepare dialkyldithiophosphate coated PbS nanoparticles. It was demonstrated that dialkyldithiophosphate coated PbS nanoparticles were more soluble in organic solvents than non-coated PbS particles. Buckner *et al.*[35], Chakraborty and Moulik[36] and Ogawa *et al.*[37] synthesised PbS nanoparticles by mixing a sodium dioctyl sulfosuccinate

(AOT) in heptane solution containing an aqueous lead acetate or $Pb(NO_3)_2$ or lead perchlorate solution with an AOT in heptane solution containing an aqueous Na_2S solution. PbS particles capped with $Pb(OH)_2$ and ZnS were prepared by Buckner *et al.*[35] by using the above method with either excess lead acetate or excess Na_2S and $Zn(NO_3)_2$ respectively. An emission maximum at 800 nm was observed in the luminescence spectra. Chakraborty and Moulik[36] prepared PbS nanoparticles with an average size of 2-4 nm, as obtained from dynamic light scattering (DLS) measurements, and a band gap of 3-4 eV using this method and $Pb(NO_3)_2$ as the lead source. PbS particles prepared by Ogawa *et al.*[37] using the above method, were deposited on gold substrates coated with a hexanedithiol self-assembled monolayer, by immersing the substrate in a heptane solution containing the aforementioned particles. It was found that PbS particles were oxidised at 0.25 V vs a saturated calomel electrode and reduced at -1.1 V vs a saturated calomel electrode. Wang and Yang[38] produced PbS particles in a poly(vinyl butyral) matrix by dip-coating a poly(vinyl butyral) film containing a $Pb(AOT)_2$ complex on to a glass substrate and then exposing the film to H_2S gas. Nanorods with average dimensions of 2.2 x 0.1 μm, as measured using TEM, and an absorption edge at approximately 1.57 eV were observed by Wang and Yang[38]. Khiew *et al.*[39] mixed a solution containing 32 % nonionic surfactant (food grade sucrose fatty acid ester), 52 % 1-butanol in cyclohexane solution and 16 % aqueous solution of lead nitrate with a similar solution containing Na_2S instead of lead nitrate and prepared PbS nanoparticles with diameters between 3 and 8 nm, as measured using TEM, and a band gap of 2.05 nm in a

biodegradable microemulsion medium. Wang *et al.*[40] added a sulfur-toluene solution to a solution of lead acetate, sodium lauryl sulfate and ethylenediamine and exposed the system to ultrasound irradiation in order to synthesise PbS particles in an ultrasound induced microemulsion. These particles were found to be in the range of 8-13 nm in size, as measured by TEM, and had a crystalline structure. Zhang *et al.*[41] prepared PbS nanoparticles capped with polyoxyethylene (9) dodecylether ($C_{12}E_9$) by adding a microemulsion containing a Na_2S aqueous solution, cyclohexane and $C_{12}E_9$ drop wise to a similar microemulsion in which the Na_2S aqueous solution was replaced with a lead nitrate aqueous solution. This resulted in crystalline particles with an average diameter of 20 nm, as measured by TEM, the outer 5 nm of which can be attributed to the capping agent and a band gap of 700 nm. A mixture of an aqueous lead nitrate solution, aqueous Na_2S solution and a hexane solution of hexanol and sodium dodecyl sulfate was placed in an autoclave and heated to 120 °C for 12 hours by Xiang *et al.*[42]. This resulted in polycrystalline nanowires with average diameters between 20 and 40 nm, as measured by TEM, and lengths up to several micrometers. Changqi *et al.*[43] exposed a microemulsion consisting of an aqueous solution of lead acetate, CS_2 in kerosene, octyl phenyl poly(ethylene oxide)-10, octyl phenyl poly(ethylene oxide)-4 and isopropanol to γ radiation in order to produce nanocrystalline PbS nanoparticles with an average diameter of 5 nm, as measured using TEM, and an absorption band in the UV-Vis spectrum between 450 and 250 nm. The microemulsion acted as a template for the particles and the mechanism of the formation of PbS was discussed by Changqi *et al.*[43] ac-

cording to the following unbalanced equations:

$$\begin{aligned} H_2O &\xrightarrow{\gamma} e^-_{aq} + H^\bullet + OH^\bullet + H_2O_2 \\ CS_2 + e^-_{aq} &\rightarrow S^- + CS^{\bullet -} \\ e^-_{aq} + S^- &\rightarrow S^{2-} \\ Pb^{2+} + S^{2-} &\rightarrow PbS \end{aligned} \tag{6.8}$$

Electrodeposition Techniques

Nanda *et al.*[44–46] prepared lead sulfide nanocrystalline films on a conducting tin oxide glass substrate by an electrodeposition technique. This method involved the cathodic electrodeposition of the particles on to a indium tin oxide glass electrode from a solution containing lead nitrate and $Na_2S_2O_3$ with a pH of 0.62. A current density of 2 mA / cm^2 was used to prepare films of thickness 60 nm with a crystal size of 20 nm, as measured from AFM images, and a band gap of 2.63 eV.

Photochemical Methods

Ichimura *et al.*[47] exposed an aqueous solution of lead acetate and $Na_2S_2O_3$ to the light from a high pressure mercury arc-lamp by in order to produce PbS particles on the surface of a substrate immersed in the solution. The particle size was estimated to be 50 nm, as calculated from the X-ray diffraction peaks using the Debye-Scherrer equation, and films with a thickness of 1 μm, as measured using SEM, were deposited on a glass substrate. Ichimura *et al.*[47]

explained the mechanism of this synthesis by the following equations:

$$\begin{aligned} S_2O_3^{2-} + h\nu &\rightarrow S + SO_3^{2-} \\ S_2O_3^{2-} + h\nu &\rightarrow e^- + S_2O_3^- \\ Pb^{2+} + S + 2e^- &\rightarrow PbS \end{aligned} \tag{6.9}$$

Preparation by Injection Of Hot Reagents

Stable, monodisperse semiconductor particles have been prepared by a 'hot injection' technique pioneered by Murray *et al.*[48] and discussed in section. 5.1.1. Due to the quality of the particles produced by this method, it has been adapted by a number of people in order to prepare nanoparticles of different semiconductors. Peng *et al.*[49;50] replaced the dimethyl cadmium used by Murray *et al.*[48] with cadmium acetate, $CdCO_3$ or CdO as dimethylcadmium decomposes in hot TOPO. Murray *et al.*[51] prepared PbSe nanocrystals over a range of sizes between 3.5 and 15 nm, as measured by TEM, by replacing the dimethyl cadmium used in their original method with lead oleate produced from the *in-situ* reaction of lead acetate with oleic acid, adding diphenyl ether to the TOPO solvent and reducing the temperature to 150 °C. The injection of sulfur in octadecene solution into a mixture of CdO, oleic acid and octadecene that had been heated to 300 °C and allowed to cool to 250 °C was used by Yu *et al.*[52;53] in order to synthesise oleic acid capped CdS particles as an adapted version of the preparation reported by Murray *et al.*[48]. Yu *et al.*[54] used PbO instead of CdO and TOPSe in place of the sulfur in octadecene solution in the previously mentioned synthesis in order to pre-

pare PbSe nanoparticles with average diameter 5.9 nm, as measured using TEM. PbS nanoparticles coated with an oleate ligand were synthesised by Hines and Scholes[55;56] by replacing the TOPSe used by Yu *et al.*[54] in order to produce PbSe particles with bis(trimethylsilyl)sulfide. These methods result in particles that are capped with a long chain molecule which would limit the electron transfer from a particle deposited on TiO_2 coated tin oxide glass electrode to the electrode. The capping agent was exchanged from a TOPO or oleate ligand to a pyridine ligand by Murray *et al.*[48] and Yu *et al.*[52] by repeatedly dissolving the as-prepared particles in pyridine at 80 °C. A decrease in particle size between the as-prepared particles and the pyridine exchanged particles was observed by Murray *et al.*[48] in the TEM images. An increase in electroluminscence intensity between PbS particles capped with oleate ligands and PbS capped with octylamine formed by the surface exchange of the oleate cap on the as-prepared particles with octyl amine was observed by Bakueva *et al.*[56]

This chapter will discuss the preparation of PbS nanoparticles using a method similar to the one outlined by Yu *et al.*[54] and subsequent surface exchange of the capping agent with pyridine according to the method used by Murray *et al.*[48]. The characteristics and photoelectrochemical properties of the particles before and after exchange of the capping agent with pyridine are also discussed.

6.2 Preparation of Nanoparticles

6.2.1 Particle Preparation

0.26 g of sulfur was dissolved in 3 ml of tri-octylphosphine (TOP). 0.89 g of PbO and 16 ml of 1-octadecene were placed in a three-necked round-bottomed flask and the reaction system was assembled as illustrated in Fig.6.1. The system was degassed under vacuum at 100 °C for 1 hour,

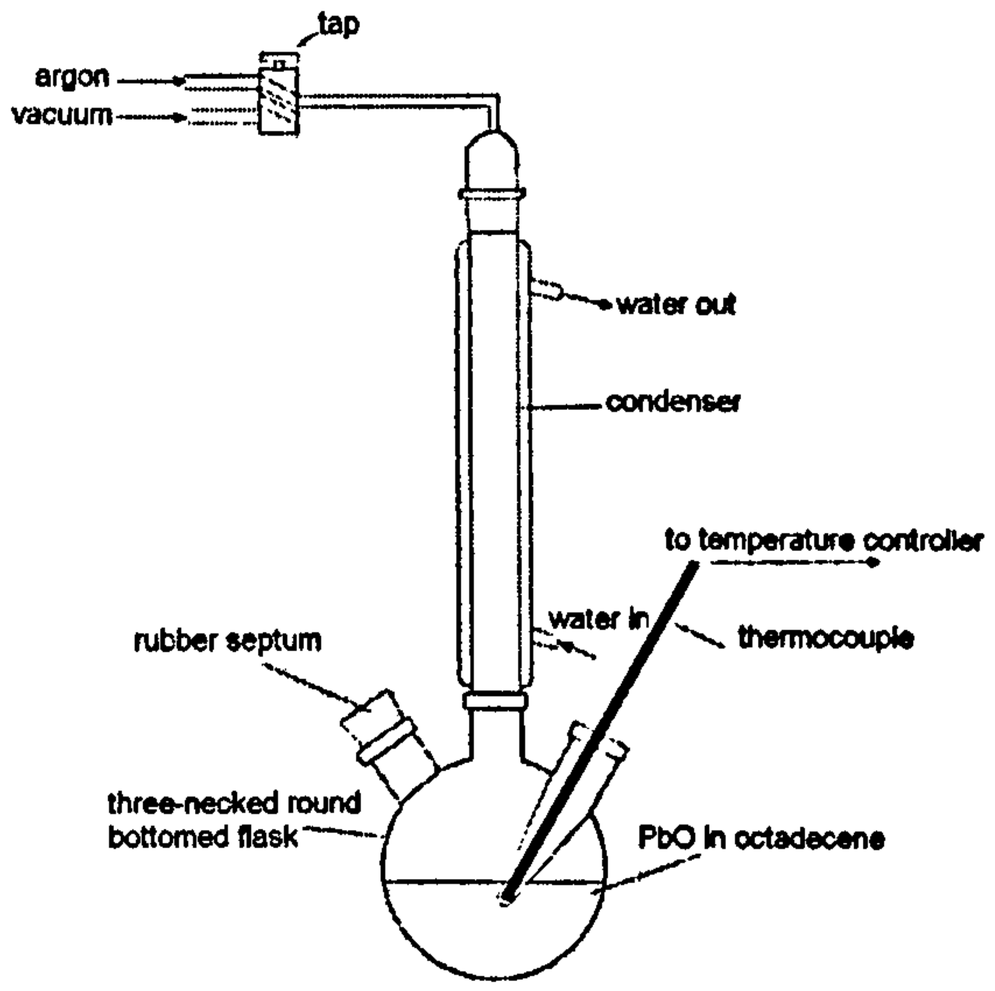

Figure 6.1: Apparatus used in the preparation of lead sulfide nanoparticles.

followed by the introduction of an argon atmosphere. This degassing was carried out twice. 2.7 ml of oleic acid was added to the round-bottomed flask under argon and the system was heated to 150 °C until the lead oxide had dissolved. The flask was removed from the heat and solution was vigorously stirred, while the sulfur in TOP solution was rapidly injected. The particles were then grown at 120 °C. The reaction was quenched by adding the particles to cold chloroform after a set length of time from that of injection.

The lead sulfide particles were purified by the addition of methanol and subsequent centrifugation for 30 minutes at 8000 rpm. After the solvent was removed, the particles were redispersed in chloroform. The particles were prepared using growth times of 2.5, 5, 7.5 and 10 minutes.

6.2.2 Pyridine Exchange

15 mg of PbS nanoparticles prepared using a growth time of 5 minutes and 2 ml of pyridine were placed in a round bottomed flask connected to a condenser fitted with a switch between a vacuum pump and an argon line. The system was degassed under vacuum at room temperature for 50 minutes and then an argon atmosphere was introduced. The flask was heated to 70 °C overnight and then allowed to cool.

6.2.3 Deposition on substrates

Conducting tin oxide glass electrodes and TiO_2 coated electrodes were heated to 140°C. Pyridine exchanged particles in pyridine or non-exchanged particles in chloroform were then dropped on the substrates.

6.3 Characterisation

6.3.1 UV-Vis Spectroscopy

The UV-Visible absorption spectra of the lead sulfide particles prepared over a range of growth times is shown in Fig.6.2. Table.6.3 displays the estimated band gaps of these particles from different growth times. Fig.6.3 displays

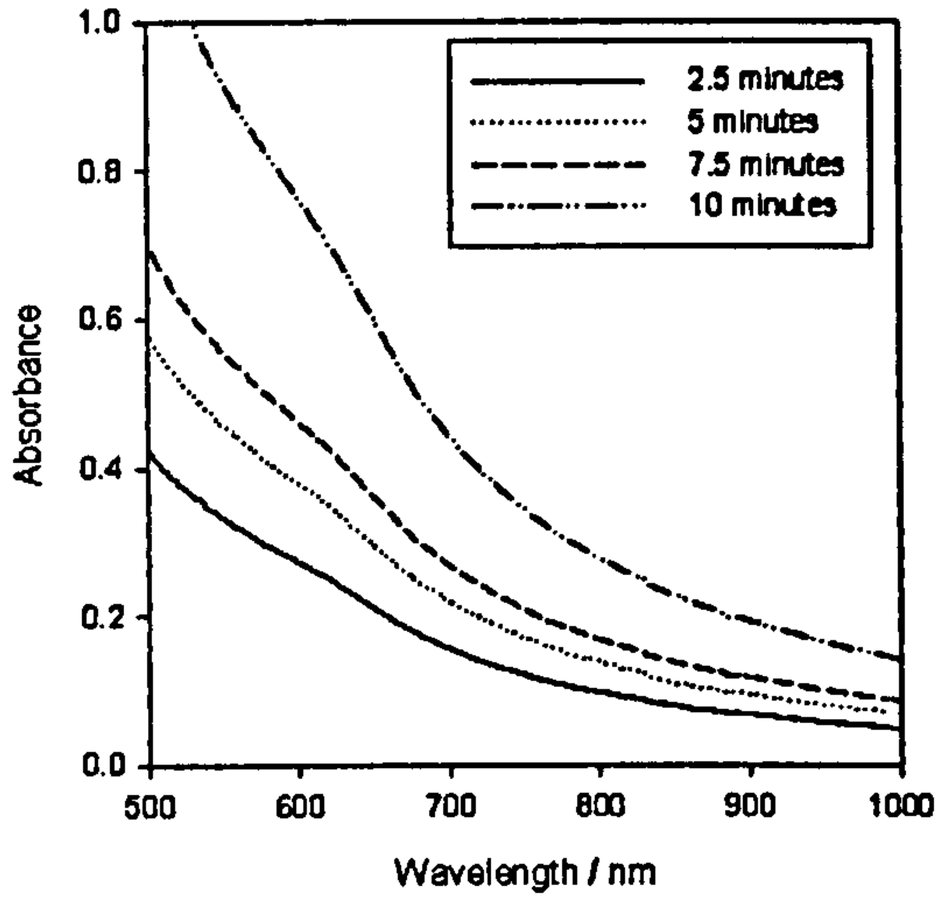

Figure 6.2: UV-Vis Spectra of PbS nanoparticles grown for 2.5, 5, 7.5 and 10 minutes.

Type of Particles	Absorption edge / nm	Estimated Band Gap /eV
2.5 minutes	737	1.68
5 minutes	746	1.66
7.5 minutes	754	1.64
10 minutes	763	1.63

Table 6.3: Estimated band gaps of PbS particles frown for 2.5, 5, 7.5 and 10 minutes.

the UV-Visible absorption spectra of pyridine exchanged and non-exchanged PbS particles that had been grown for 5 minutes. The estimated band gaps of the non-exchanged and pyridine exchanged versions of the PbS particles produced after a growth time of 5 minutes are indicated in Table.6.4

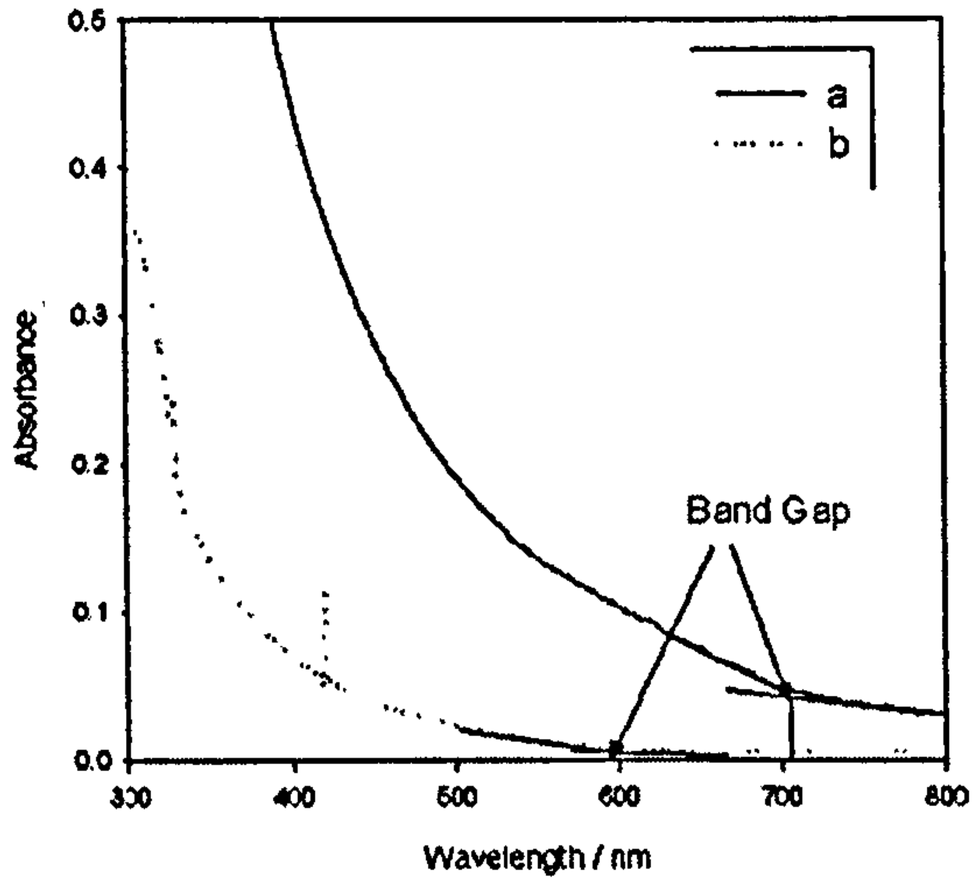

Figure 6.3: UV-Vis Spectra of a) non-exchanged and b) pyridine exchanged PbS nanoparticles.

Type of Particles	Absorption edge / nm	Estimated Band Gap /eV
non-exchanged PbS particles	700	1.77
pyridine exchanged PbS particles	595	2.08

Table 6.4: Estimated band gaps of non-exchanged and pyridine exchanged PbS particles grown for 5 minutes.

6.3.2 Transmission Electron Microscopy

Example TEM images of pyridine exchanged and non-exchanged lead sulfide nanoparticles grown for 5 minutes are shown in Fig.6.4. The size distributions of the particles, displayed in Fig.6.5, were used to calculate the average particle sizes of pyridine exchanged and non-exchanged PbS particles from the measurement of a number of the particles as shown in Table.6.5.

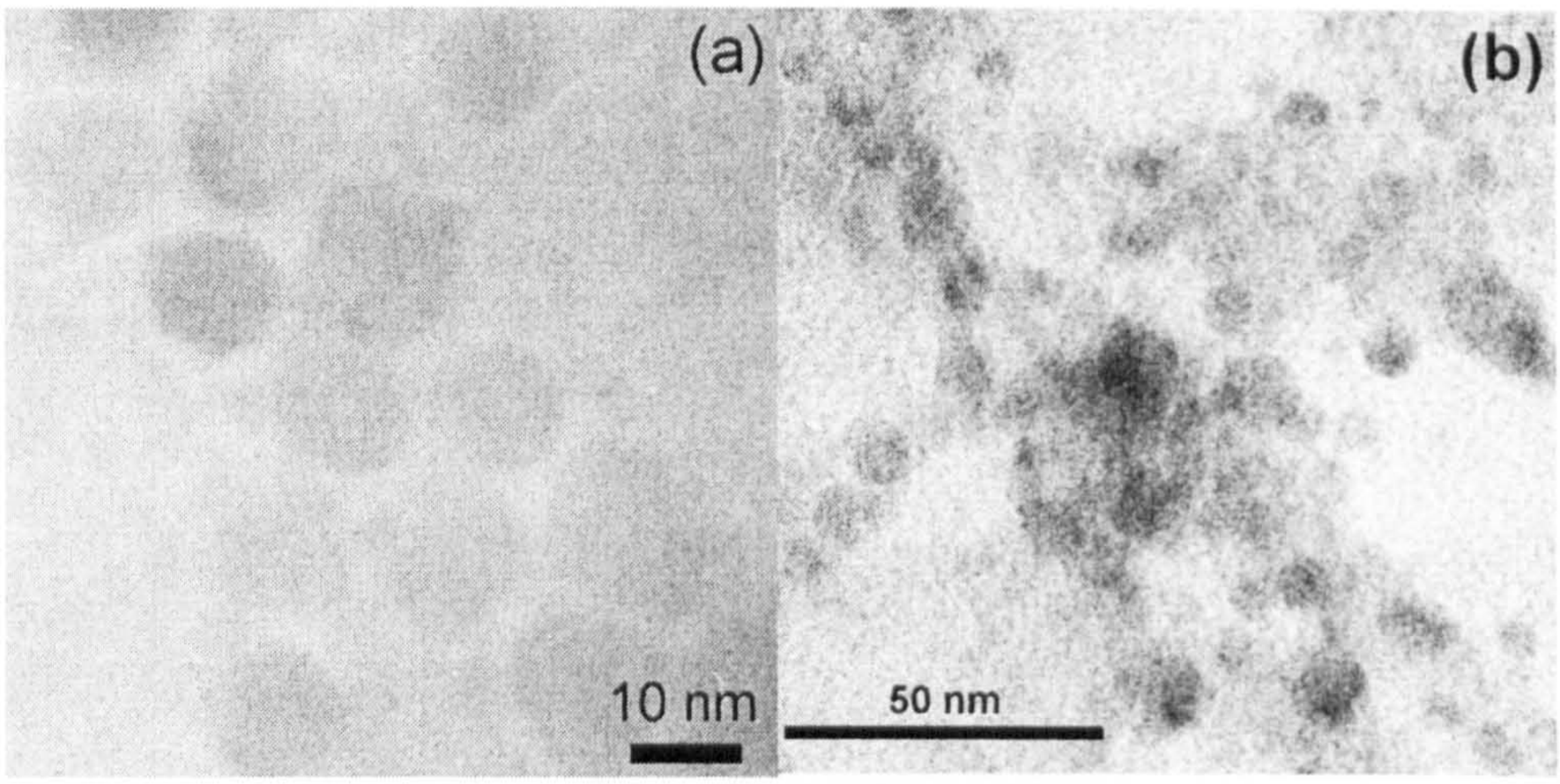

Figure 6.4: TEM images of a) non-exchanged and b) pyridine exchanged PbS nanoparticles.

Type of Particles	Particle diameter / nm	sample size
non-exchanged PbS particles	12.3 ± 1.3	149
pyridine exchanged PbS particles	7.2 ± 1.6	250

Table 6.5: Average particle diameter of PbS nanoparticles grown for 5 minutes before and after pyridine exchange with the respective number of measurements used in the statistical analysis.

Fig.6.6 shows the energy dispersive x-ray analysis spectra of the particles on TEM grids.

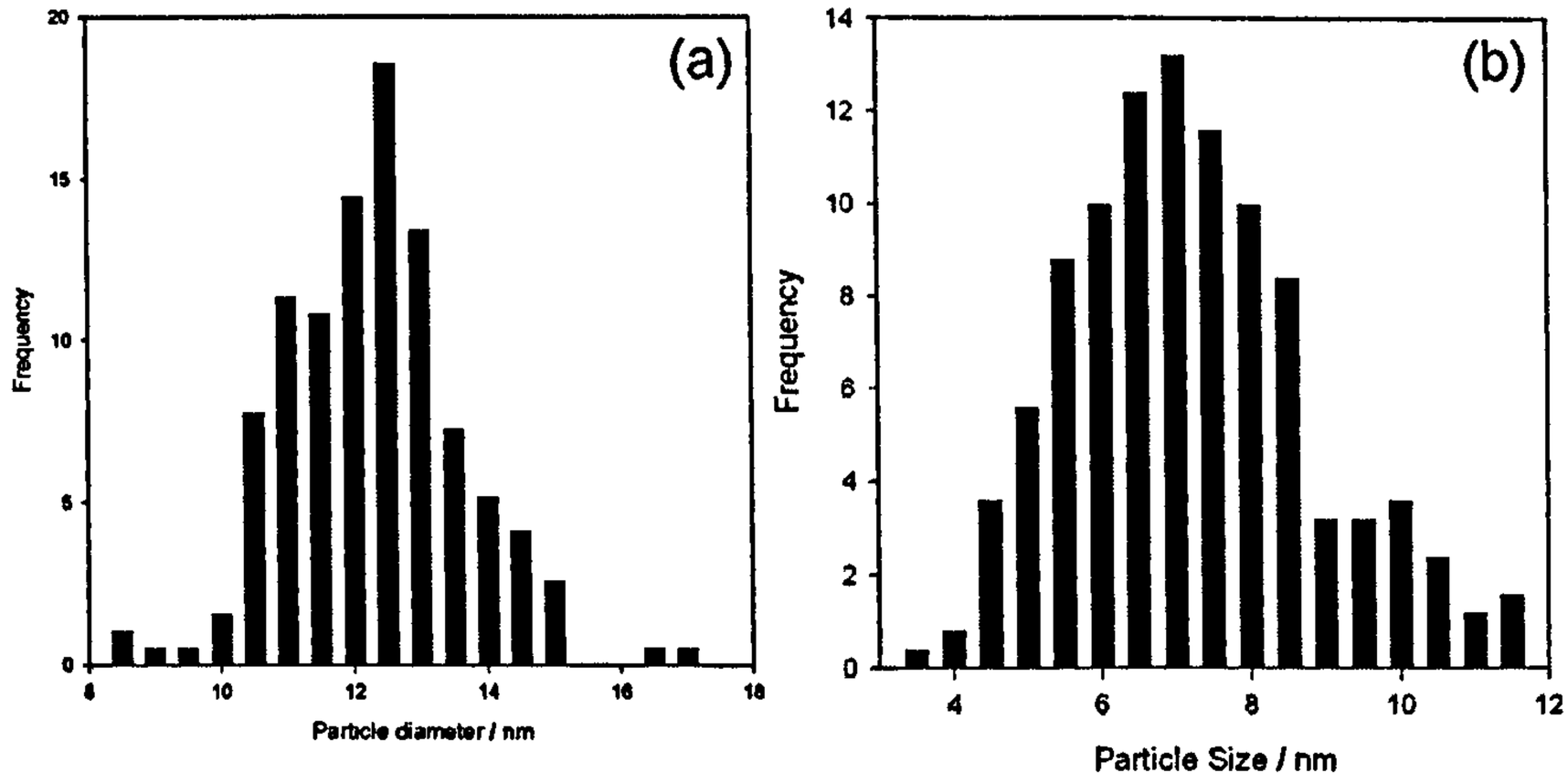

Figure 6.5: Size distributions of a) non-exchanged and b) pyridine exchanged PbS nanoparticles.

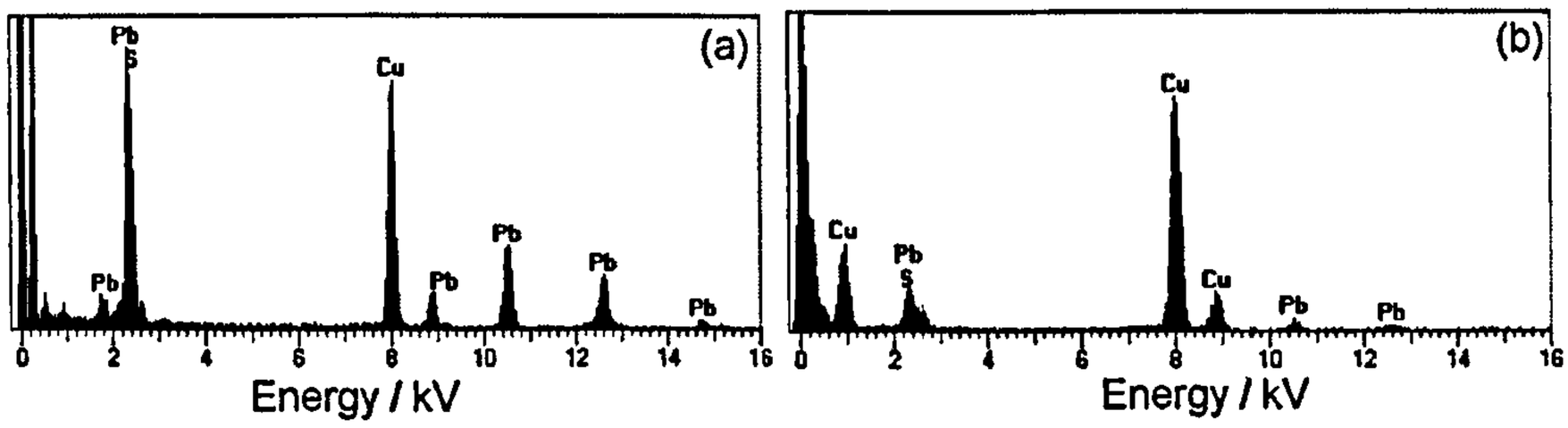

Figure 6.6: EDAX Spectra of a) non-exchanged and b) pyridine exchanged PbS nanoparticles.

6.3.3 Scanning Electron Microscopy

SEM images of pyridine exchanged and non-exchanged PbS nanoparticles on conducting tin oxide glass electrodes and TiO_2 coated electrodes are shown in Fig.6.7 a and b and Fig.6.8 a and b. The dark areas in Fig.6.7a represent an area coated with PbS particles while the light areas correspond to uncoated tin oxide.

The exposed tin oxide is displayed inside the white oval in Fig.6.8a.

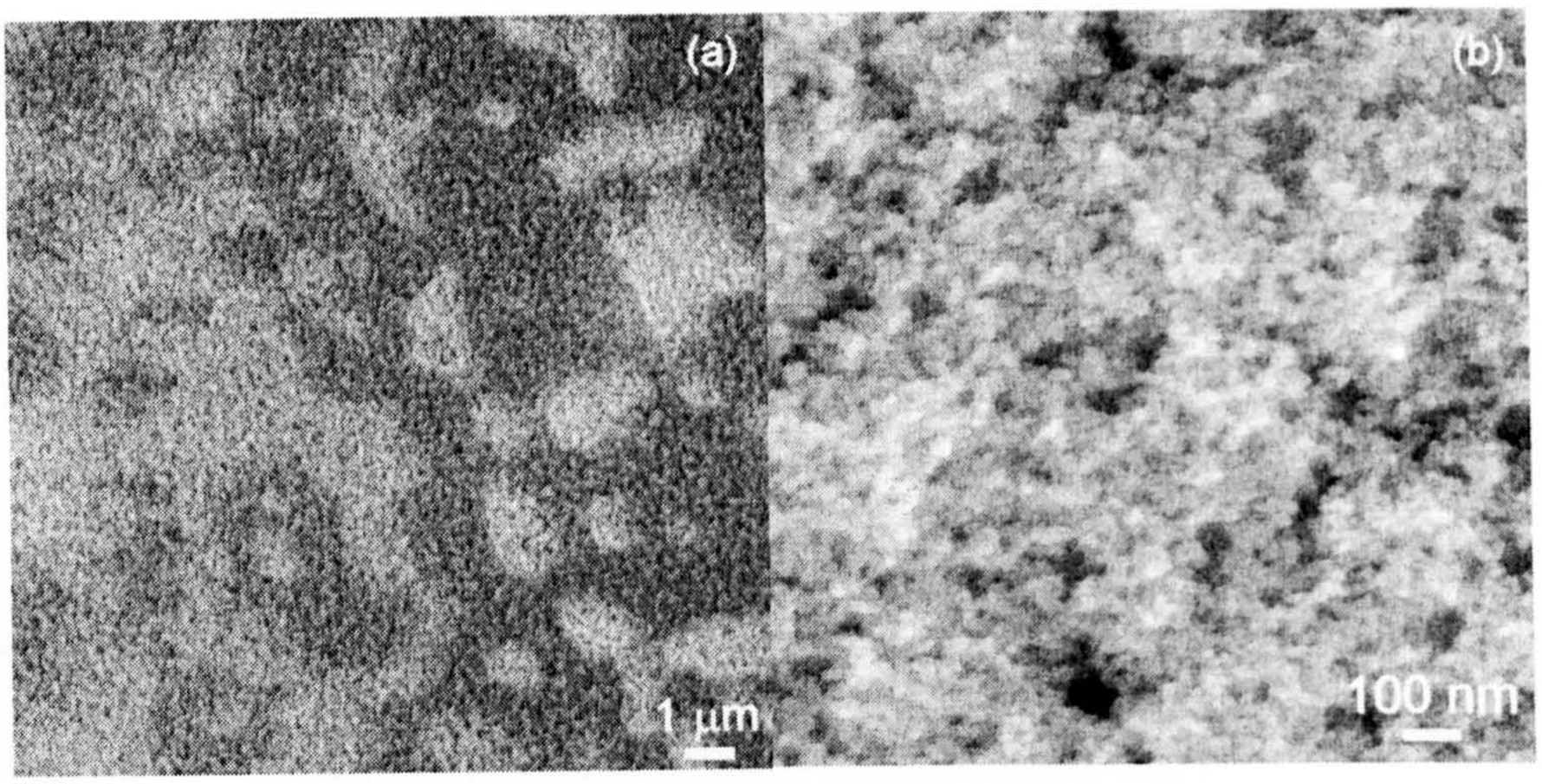

Figure 6.7: SEM images of non-exchanged PbS nanoparticles on a) tin oxide glass electrode and b) TiO_2 coated tin oxide glass electrode.

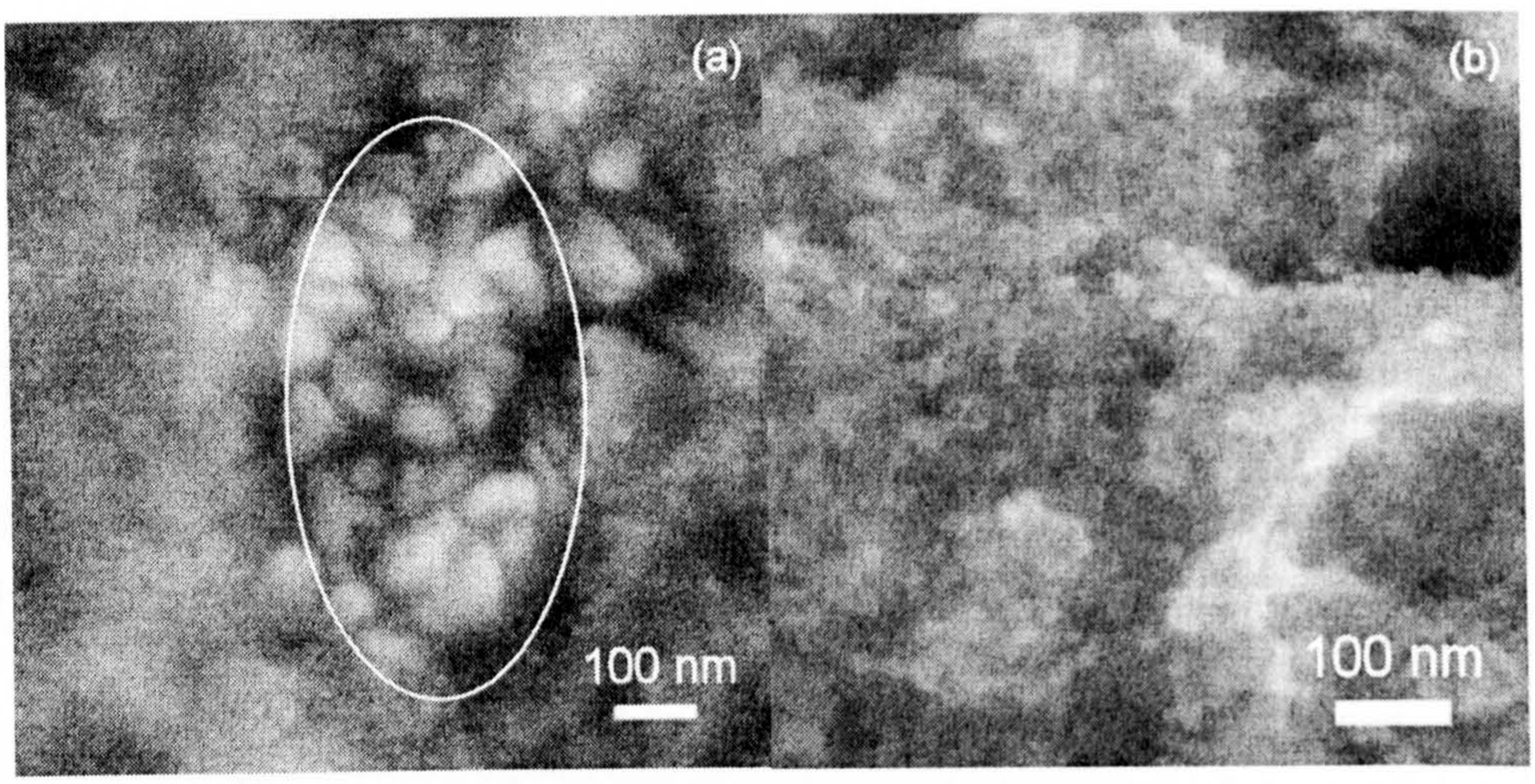

Figure 6.8: SEM images of pyridine exchanged PbS nanoparticles on a) tin oxide glass electrode and b) TiO_2 coated tin oxide glass electrode.

6.3.4 Powder X-Ray Diffraction

Fig.6.9 displays the powder X-ray diffraction pattern of lead sulfide particles grown for 5 minutes. This shows no evidence of crystallinity in the particles.

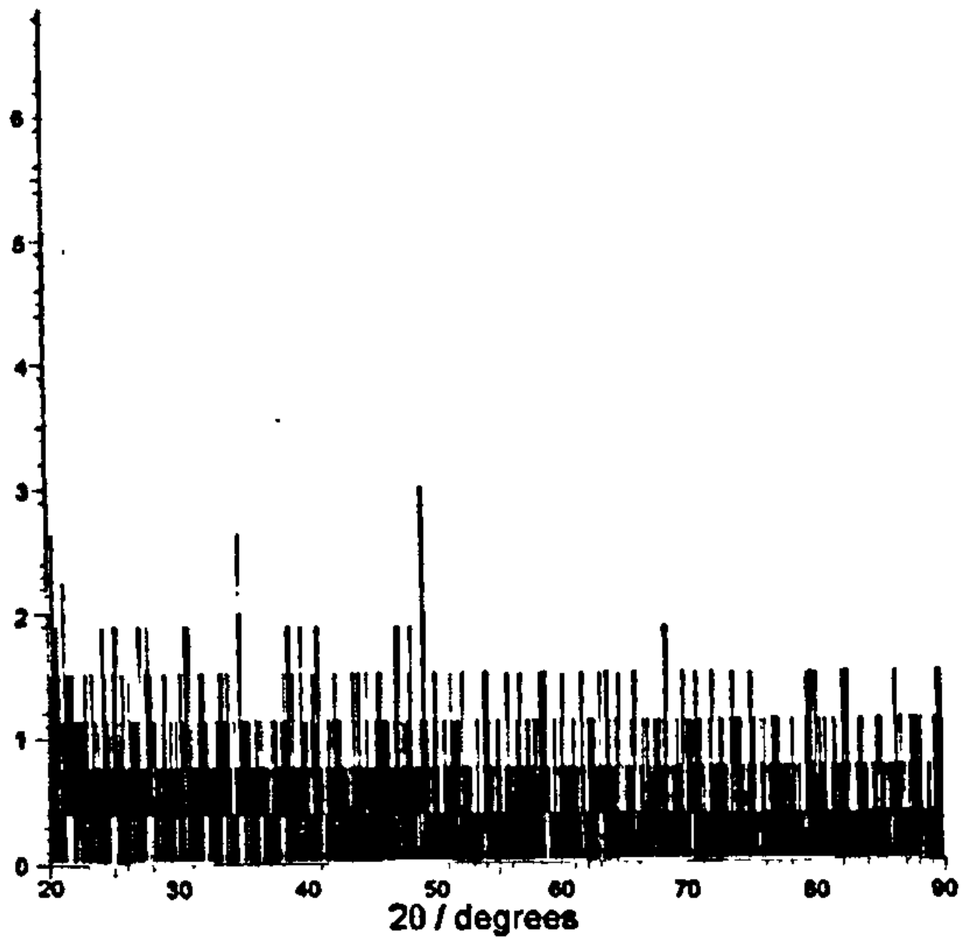

Figure 6.9: Powder X-ray diffraction pattern of non-exchanged PbS particles that were grown for 5 minutes.

6.4 Photoelectrochemistry

6.4.1 Photocurrent-Potential Curves

Current *vs.* potential curves of TiO_2 coated electrodes sensitised with pyridine exchanged and non-exchanged PbS nanoparticles exposed to chopped light are displayed in Fig.6.10 and show an onset in photocurrent at approximately -0.6V.

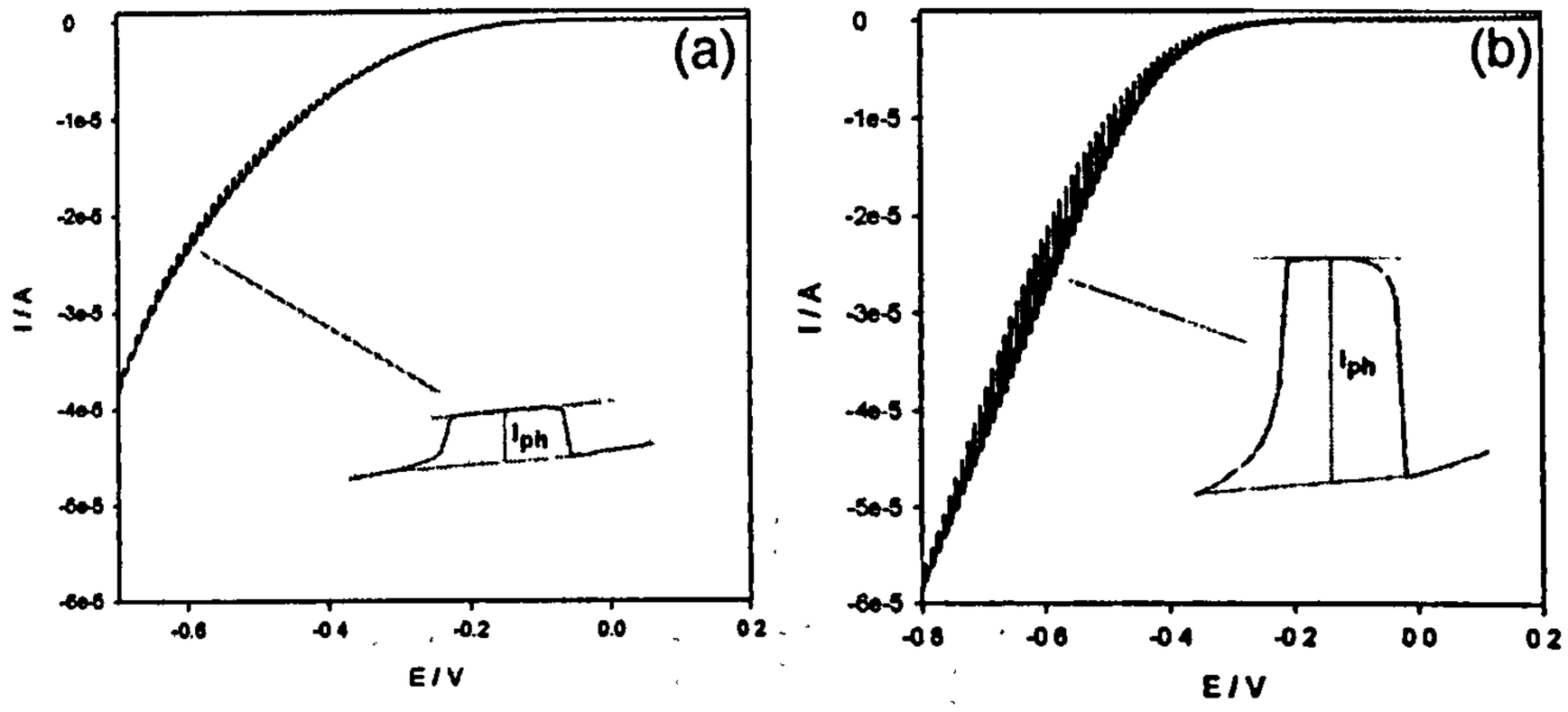

Figure 6.10: I-V curves of a) non-exchanged and b) pyridine exchanged PbS nanoparticles on TiO_2 coated tin oxide electrodes in a Na_2SO_3 electrolyte buffered at pH 12 exposed to light from a Xenon arc lamp chopped at 0.1 Hz. i_{ph} = photocurrent.

From the peak heights of the photocurrent transients, defined as i_{ph} in Fig.6.10, and the position of the peaks, it is possible to plot graphs of photocurrent versus potential for non-exchanged PbS and pyridine-capped particles as shown in Fig. 6.11. Fig.6.11 clearly displays a peak at -0.6 V for both samples. Pyridine-capped PbS particles display enhanced photocurrent compared to the non-exchanged particles.

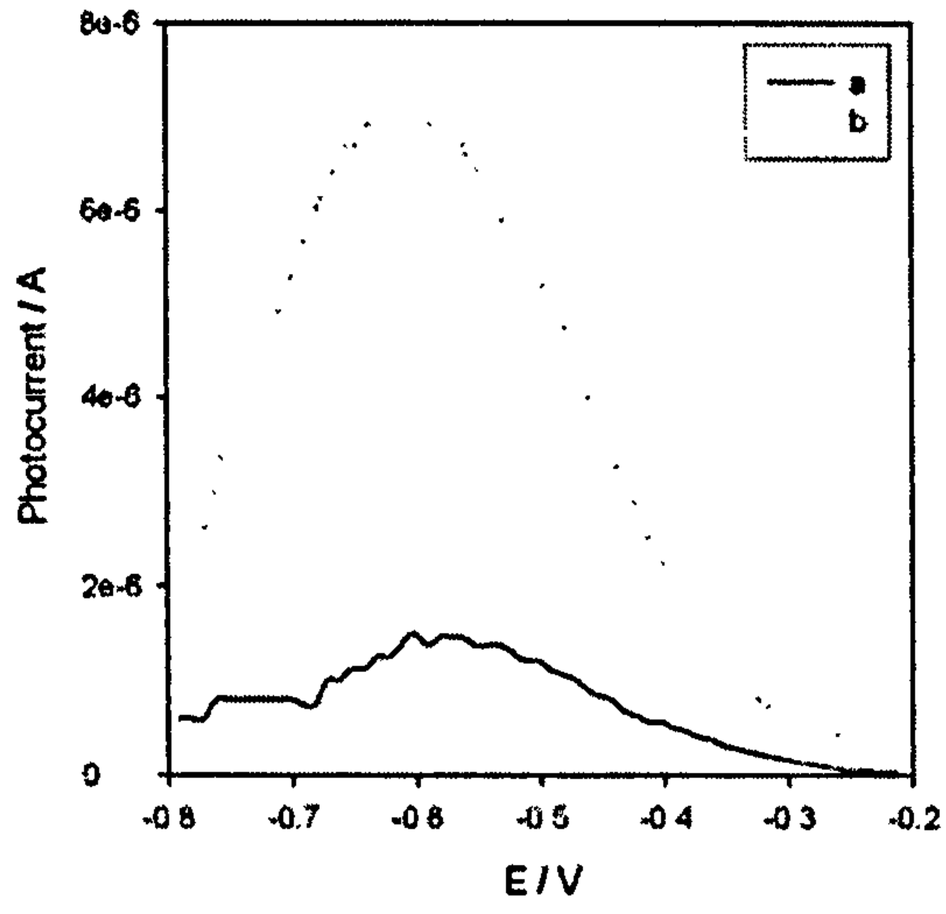

Figure 6.11: The dependence of photocurrent, measured from the photocurrent transient peak heights in Fig.6.10, on applied potential for a) non-exchanged and b) pyridine exchanged PbS nanoparticles on TiO_2 coated tin oxide electrodes in a Na_2SO_3 electrolyte buffered at pH 12 exposed to light from a Xenon arc lamp chopped at 0.1 Hz.

6.4.2 Photocurrent Spectroscopy

A potential of -0.6 V vs. Ag|AgCl|3 mol dm^{-3} KCl was used in the photocurrent experiments due to the position of a maximum peak height of a phototransient in the current-potential curves. Fig.6.12 shows the IPCE spectra of the pyridine exchanged and non-exchanged PbS nanoparticles deposited on TiO_2 coated electrodes. Band gaps of 2.03 eV (611 nm) and 2.41 eV (515 nm) were observed for PbS particles and pyridine exchanged PbS particles respectively.

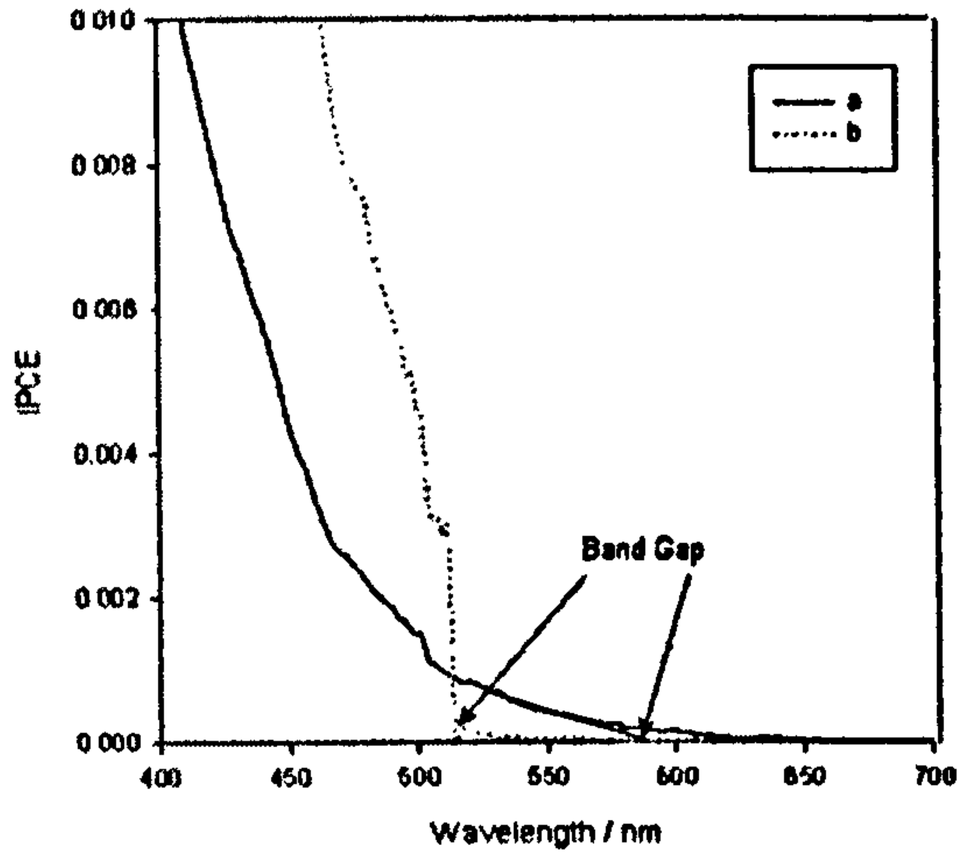

Figure 6.12: Photocurrent spectra of a) non-exchanged and b) pyridine exchanged PbS nanoparticles obtained at -0.6 V vs. Ag|AgCl|3 mol dm^{-3} KCl and using monochromatic light chopped at 0.5 Hz.

6.5 Discussion

The UV-Vis spectra of the particle produced after growth times of 2.5 and 10 minutes display a small decrease in the band gap from 1.68 eV to 1.63 eV. Due to the error in the baseline caused by light scattering from the particles, it is difficult to tell if the observed decrease in estimated band gap with increased time is due to an increase in the particle size or the errors in the estimation. It can be seen that there is a difference in the estimated band gaps of the particles grown for 5 minutes in Fig.6.2 and the particles before the surface exchange with pyridine in Fig.6.3. This could be due to slight differences in the concentrations of the materials used in the preparation, the temperature of the system, the rate of quenching of the sample, the exact growth time of the particles or a combination of the above. The observed

increase in band gap from 1.77 eV to 2.08 eV in the PbS particles before pyridine exchange and after pyridine exchange respectively indicates a decrease in size upon surface exchange with pyridine corresponding to partial dissolution of the PbS particles in pyridine due to the higher solubility of PbS in pyridine.

From the size distributions in Fig.6.5, it is clear that the particles produced by this method exhibit a high degree of monodispersity. A decrease in particle size from 12.3 ± 1.3 to 7.2 ± 1.6 nm was observed after exchanging the capping agent with pyridine. This is consistent with the result reported by Murray *et. al*[48] for exchanging the TOPO cap on CdSe particles with pyridine. The presence of both Pb and S in the particles is confirmed in the EDAX spectra in Fig.6.6.

Photocurrent is not seen for lead sulfide particles on tin oxide electrodes as the particles deposit in patches on the tin oxide surface, as shown in Figs.6.7a and 6.8a, resulting in not enough particles being present in order to measure a photocurrent response. As the particles are not chemically bonded to the surface of the electrode and the particles are soluble in the solvent used in the solution, when another drop of the particles in solution comes in to contact with the electrodes, the particles on the electrode redissolve and the particles reform in patches on the surface of the electrode as the solvent evaporates. It should be noted that washing the electrodes with water does not remove the particles as the particles are not soluble in water. Figs.6.7b and 6.8b display the pores in the TiO_2 film are nearly all filled with PbS particles.

From the I-V curves shown in Fig.6.10 and the dependence of photocur-

rent on applied potential displayed in Fig.6.11, it is clear that, compared to the non-exchanged PbS particles, the pyridine capped PbS particles exhibit enhanced photocurrent. This is probably due to the pyridine-capped particles either being closer to the TiO_2 surface than the non-exchanged PbS particles, which are capped with an oleate group, or the pyridine on the surface of the particles shift the conduction band of the PbS to higher energies and therefore electron transfer to the TiO_2 is more favourable for the pyridine-capped particles in both cases. The suppression of photocurrent at potentials greater than -0.2 V is likely due to the depletion of charge carriers in the tin oxide electrode to such a point that the Fermi level of tin oxide is lower than that of the counter electrode reducing current flow. The photocurrent spectra shown in Fig.6.12 displays band gaps of 2.03 eV and 2.41 eV for the PbS particles before and after surface exchange with pyridine respectively and an IPCE for these particles on TiO_2 of less than 1 %. A low efficiency could be observed if one or more of the electron loss process, such as recombination of the electron and hole formed in the nanoparticle from exposure to light (k_r) or back electron transfer from the TiO_2 substrate into a surface state of the nanoparticle (k_{ss}) or the hole in the valence band of the nanoparticle (k_h) or to regenerate the electrolyte after it scavenges the hole from the nanoparticle (k_{el}) occurs at a similar or greater rate than the rate of electron transfer from the conduction band of the nanoparticle to the tin oxide electrode across the TiO_2 film. These processes are displayed schematically in Fig.6.13. The effective mass model of quantum confinement can be used in order to estimate the size of the particles from their band

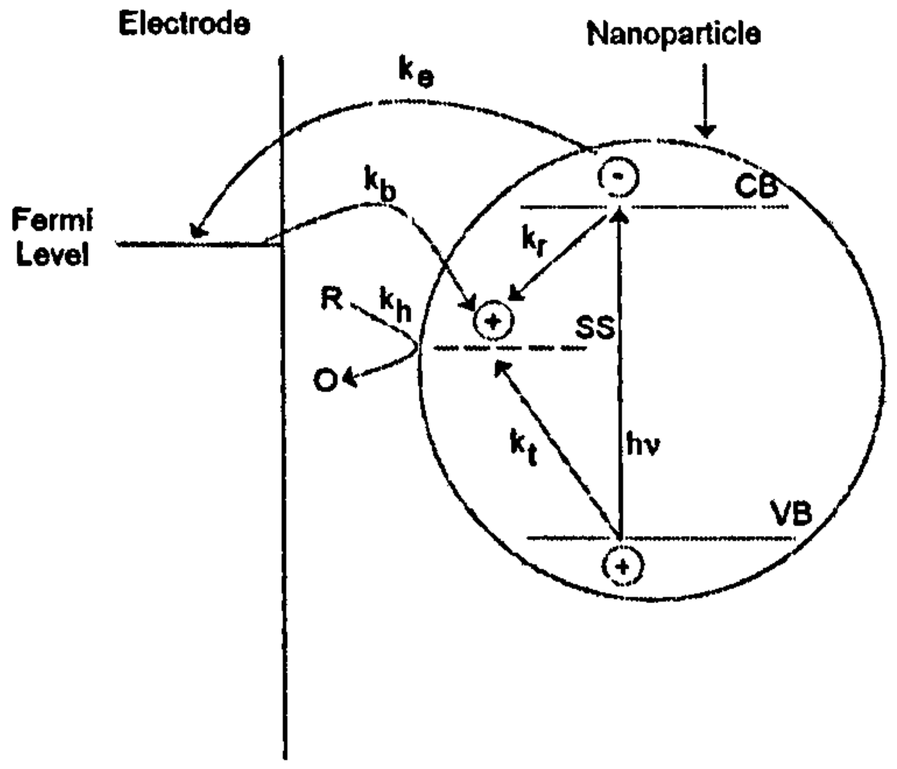

Figure 6.13: Schematic of electron transfer processes involved in the photocurrent experiment.

gaps according to equation.1.11. The effective masses of holes and electrons in PbS were both calculated to be 0.085[1]. The bulk band gap of PbS of 0.41 eV[1] and a high frequency dielectric constant of 17.2[1] were used in order to calculate the particle size from band gaps found using photocurrent spectroscopy. This resulted in the calculated particle sizes of the PbS particles before and after pyridine exchange to be 4.8 and 4.3 nm respectively. There is a significant difference between the calculated and measured particle sizes. This may occur if the particles are not crystalline or spherical or the unit cell structure and dimensions in both the particles and the bulk crystalline semiconductor material are not nearly identical.

6.6 Summary

PbS particles have been prepared by a similar technique to that used by Yu *et al.*[54] to produce PbSe. Exchange of the capping agent with pyridine was found to decrease the particle size. Photocurrent was observed for these particles on TiO_2 coated electrodes. As less than 1 % IPCE was observed, alternative methods of surface exchange and deposition of PbS particles on to a surface may be required in order to see if PbS particles are a possible replacement for the dye in dye sensitised solar cells.

References

[1] Nanda, K. K.; Kruis, F. E.; Fissan, H.; Behera, S. N. *J. Appl. Phys.* **2004**, *95*, 5035.

[2] Yang, S.-M.; Wang, Z.-S.; Huang, C.-H. *Synthetic Metals* **2001**, *123*, 267.

[3] Plass, R.; Pelet, S.; Krueger, J.; Grätzel, M.; Bach, U. *J. Phys. Chem. B* **2002**, *106*(31), 7578–7580.

[4] Bakueva, L.; Gorelikov, I.; Musikhin, S.; Zhao, X. S.; Sargent, E. H. *Adv. Mater.* **2004**, *16*, 926.

[5] Zhou, Y.; Itoh, H.; Uemura, T.; Naka, K.; Chujo, Y. *Langmuir* **2002**, *18*, 5287.

[6] Chen, M.; Xie, Y.; Yao, Z.; Qian, Y.; Zhou, G. *Mater. Res. Bull.* **2002**, *37*, 247.

[7] Ma, Y.; Qi, L.; Ma, J.; Cheng, H. *Cryst. Growth and Design* **2004**, *4*, 351.

[8] Lifshitz, E.; Sirota, M.; Poteanu, H. *J. Cryst. Growth* **1999**, *196*, 126.

[9] Joshi, R. K.; Kanjilal, A.; Sehgal, H. K. *Appl. Surf. Sci.* **2004**, *221*, 43.

[10] Kang, K.; Daneshvar, K.; Tsu, R. *Microelectronics Journal* **2004**, *35*, 629.

[11] Lu, S.; Sohling, U.; Krajewski, T.; Mennig, M.; Schmidt, H. *J. Mater. Sci. Lett.* **1998**, *17*, 2071.

[12] Gurin, V. S. *J. Cryst. Growth* **1998**, *191*, 161.

[13] Kyprianidouleodidou, T.; Caseri, W.; Suter, U. W. *J. Phys. Chem.* **1994**, *98*(36), 8992–8997.

[14] Mukherjee, M.; Datta, A.; Chakravorty, D. *Appl. Phys. Lett.* **1994**, *64*, 1159.

[15] Lu, S. W.; Sohling, U.; Mennig, M.; Schmidt, H. *Nanotech.* **2002**, *13*, 669.

[16] Fernee, M. J.; Watt, A.; Warner, J.; Cooper, S.; Heckenberg, N.; Rubinsztein-Dunlop, H. *Nanotech.* **2003**, *14*, 991.

[17] Fernee, M. J.; Watt, A.; Warner, J.; Heckenberg, N.; Rubinsztein-Dunlop, H. *Nanotech.* **2004**, *15*, 1328.

[18] Bakkers, E. P. A. M.; Kelly, J. J.; Vanmaekelbergh, D. *J. Electroanal. Chem.* **2000**, *482*(1), 48–55.

[19] Torimoto, T.; Sakata, T.; Mori, H.; Yoneyama, H. *J. Phys. Chem.* **1994**, *98*, 3036.

[20] Joo, J.; Na, H. B.; Yu, T.; Yu, J. H.; Kim, Y. W.; Wu, F. X.; Zhang, J. Z.; Hyeon, T. *J. Am. Chem. Soc.* **2003**, *125*(36), 11100–11105.

[21] Jiang, P.; Liu, Z.; Cai, S. *Langmuir* **2002**, *18*, 4495.

[22] Nabok, A. V.; Ray, A. K.; Cook, M. J.; Burnham, P. M.; Iwantono.; Yanuar, H.; Simmonds, M.; Basova, T. V. *IEEE Trans. Nanothechnol.* **2004**, *3*, 388.

[23] Dutta, A. K.; Ho, T.; Zhang, L.; Stroeve, P. *Chem. Mater.* **2000**, *12*, 1042.

[24] Wang, D.; Yu, D.; Mo, M.; Liu, X.; Qian, Y. *Solid State Comm.* **2003**, *125*, 475.

[25] An, C.; Tang, K.; Jin, Y.; Liu, J.; Lv, H.; Qian, Y. *J. Cryst. Growth* **2003**, *253*, 467.

[26] Jiang, Y.; Wu, Y.; Xie, B.; Yuan, S.; Liu, X.; Qian, Y. *J. Cryst. Growth* **2001**, *231*, 248.

[27] Mo, M.; Shao, M.; Hu, H.; Yang, L.; Yu, W.; Qian, Y. *J. Cryst. Growth* **2002**, *244*, 364.

[28] Balaz, P.; Boldizarova, E.; Godocikova, E.; Briancin, J. *Mater. Lett.* **2002**, *57*, 1585.

[29] Zhu, J. J.; Liu, S. W.; Palchik, O.; Koltypin, Y.; Gedanken, A. *J. Solid State Chem.* **2000**, *153*(2), 342–348.

[30] Zhao, Y. and, L. X.; Hong, J. and, Z. J. *Mater. Chem. Phys.* **2004**, *87*, 149.

[31] Ding, T.; Zhu, J.-J. *Mater. Sci. Eng. B* **2003**, *100*, 307.

[32] Ding, T.; Zhang, J-R., L. S.; Zhu, J.-J. *Microelectronic Engineering* **2003**, *66*, 46.

[33] Chen, S.; Truax, L. A.; Sommers, J. M. *Chem. Mater.* **2000**, *12*, 3864.

[34] Chen, S.; Liu, W.; Yu, L. *J. Mater. Res.* **1999**, *14*, 2147.

[35] Buckner, S. W.; Konold, R. L.; Jelliss, P. A. *Chem. Phys. Lett.* **2004**, *394*, 400.

[36] Chakraborty, I.; Moulik, S. P. *J. Nanoparticle Res.* **2004**, *6*, 233.

[37] Ogawa, S.; Hu, K.; Fan, F. F.; Bard, A. J. *J. Phys. Chem. B* **1997**, *101*, 5707.

[38] Wang, S.; Yang, S. *Langmuir* **2000**, *16*, 389.

[39] Khiew, P. S.; Radiman, S.; Huang, N. M.; Ahmad, M. S. *J. Cryst. Growth* **2003**, *254*, 235.

[40] Wang, H.; Zhang, J.; Zhu, J. *J. Cryst. Growth* **2002**, *246*, 161.

[41] Zhang, B.; Li, G.; Zhang, J.; Zhang, Y.; Zhang, L. *Nanotech.* **2003**, *14*, 443.

[42] Xiang, J.; Yu, S.; Liu, B.; Xu, Y.; Gen, X.; Ren, L. *Inorg. Chem. Comm.* **2004**, *7*, 572.

[43] Changqi, X.; Zhicheng, Z.; Hailong, W.; Qiang, Y. *Mater. Sci Eng. B* **2003**, *104*, 5.

[44] Nanda, K. K.; Sahu, S. N.; Soni, R. K.; Tripathy, S. *Phys. Rev. B* **1998**, *58*, 15405.

[45] Nanda, K. K.; Sahu, S. N. *Adv. Mater.* **2001**, *13*, 280.

[46] Nanda, K. K.; Sahu, S. N. *Appl. Phys. Lett.* **2001**, *79*, 2743.

[47] Ichimura, M.; Narita, T.; Masui, K. *Mater. Sci. Eng. B* **2002**, *96*, 296.

[48] Murray, C. B.; Norris, D. J.; Bawendi, M. G. *J. Am. Chem. Soc.* **1993**, *115*, 8706.

[49] Peng, Z. A.; Peng, X. *J. Am. Chem. Soc.* **2001**, *123*, 183.

[50] Qu, L. H.; Peng, Z. A.; Peng, X. G. *Nano Lett.* **2001**, *1*(6), 333–337.

[51] Murray, C. B.; Sun, S. H.; Gaschler, W.; Doyle, H.; Betley, T. A.; Kagan, C. R. *IBM J. Res. Dev.* **2001**, *45*(1), 47–56.

[52] Yu, W. W.; Qu, L. H.; Guo, W. Z.; Peng, X. G. *Chem. Mater.* **2003**, *15*(14), 2854–2860.

[53] Yu, W. W.; Peng, X. *Angew. Chem. Int. Ed.* **2002**, *41*, 2368.

[54] Yu, W. W.; Falkner, J. C.; Shih, B. S. Colvin, V. L. *Chem. Mater.* **2004**, *16*, 3318.

[55] Hine, M. A.; Scholes, G. D. *Adv. Mater.* **2003**, *15*, 1844.

[56] Bakueva, L.; Musikhin, S.; Hine, M. A.; Chang, T. F.; Tzolov, M.; Scholes, G. D.; Sargent, E. H. *Appl. Phys. Lett.* **2003**, *82*, 2895.

Chapter 7

Conclusions

The preparation of several different semiconductor nanoparticles have been carried out and the suitability of these particles for use as sensitisers in solar cells have been discussed. A summary of the results obtained in this thesis is outlined below and several avenues of further research are discussed.

Tin oxide electrodes coated with Bi_2S_3 nanoparticles were prepared *in situ* using an arrested precipitation method. It was found that the size of the particles could be controlled by the concentration of 3-mercaptopropionic acid used. However, the band gap of the particles was determined to be difficult to tune by changing the size of the particles and hence it was concluded that Bi_2S_3 nanoparticles were not ideal for sensitisation of TiO_2 in solar cells.

A general method of preparing metal sulfide nanoparticles, proposed by Joo *et al.*[1], was used to synthesise cadmium sulfide, ruthenium sulfide and copper sulfide nanoparticles. No photocurrent was observed for tin oxide electrodes coated with these particles. As there was visual evidence of successful deposition of cadmium sulfide and ruthenium sulfide nanoparticles

and it is known that electrons from the conduction band of CdS inject into tin oxide, it was concluded that the lack of photocurrent in these samples was most likely due to the long chain length of oleylamine, which is assumed to coat the surface of the particles, blocking the electron transfer. Substitution of the oleylamine capping agent with a smaller stabiliser, such as pyridine, may result in an observable photocurrent. The particles produced by this method in this thesis are not ideal sensitisers for a solar cell as their band gaps are too large. From the experimental details of the oleylamine method, it is clear that the only means of controlling the size of the particles is via the ratio of the heavy metal source to sulfur and that the size and shape of the particles can not be easily predicted from this ratio. Hence, although the oleylamine method can be used to prepare many different metal sulfide particles, it may not be the ideal process to use to prepare sensitisers for solar cells.

CdSe nanoparticles were prepared from the reaction of cadmium perchlorate and bis(trimethylsilyl)selenide and deposited on tin oxide electrodes. A decrease in size with an increase in reaction time was observed and was concluded to be due to the decomposition of quickly formed CdSe particles in solution. It is clear from this and the low levels of photocurrent observed from electrodes coated with these particles, that this method is not suitable for preparing semiconductor nanoparticles.

A 'hot injection' technique, similar to that used by Yu *et al.*[2] to produce PbSe, was used in order to prepare monodisperse PbS nanoparticles. The oleic acid coating on the surface of the particles was exchanged with pyridine,

resulting in pyridine coated particles. A decrease in size was observed upon pyridine exchange, due to the higher solubility of PbS in pyridine. Non-exchanged and pyridine exchanged particles were drop coated on to TiO_2 coated tin oxide electrodes. The pyridine exchanged particles exhibited an enhanced photocurrent compared to the non-exchanged particles, most likely due to pyridine being smaller than oleic acid and therefore electron transfer from PbS to the TiO_2 is easier for the pyridine coated particles. As the size of the particles can be controlled by the reaction time, with particle diameters of up to 36 nm being expected to yield quantum confined properties, and the prepared particles have an average diameter of 12.3 ± 1.3 nm and a band gap of 1.77 eV, it is clear that PbS nanoparticles are potentially ideal for use as a sensitiser in solar cells. However, less than 1 % IPCE was observed for PbS particles deposited on TiO_2 coated tin oxide electrodes, indicating that either the rates of the electron transfer processes in the photocurrent experiment are not ideal for efficient electron transfer from the particles to the TiO_2 or insufficient PbS particles are being deposited. Hence, alternative methods of surface exchange and deposition of PbS particles on to a surface should be investigated. The use of different electrolytes should also be studied in order to maximise the rate at which the hole in the valence band of the nanoparticle is scavenged and therefore reducing the chance of the electron loss processes occurring.

The arrested precipitation and 'hot injection' techniques could be used to prepare Sb_2S_3, Bi_2Se_3, FeS_2, $FeSe_2$ and Cr_2S_3, which may result in ideal semiconductor nanoparticles for the sensitisation of solar cells.

References

[1] Joo, J.; Na, H. B.; Yu, T.; Yu, J. H.; Kim, Y. W.; Wu, F. X.; Zhang, J. Z.; Hyeon, T. *J. Am. Chem. Soc.* **2003**, *125*(36), 11100–11105.

[2] Yu, W. W.; Falkner, J. C.; Shih, B. S. Colvin, V. L. *Chem. Mater.* **2004**, *16*, 3318.